Practical System Implementation for 5G Wireless Communication Systems

by

Weiheng Ni
B.Eng., Beijing University of Posts and Telecommunications, 2013

A Thesis Submitted in Partial Fulfillment of the
Requirements for the Degree of

MASTER OF APPLIED SCIENCE

in the Department of Electrical and Computer Engineering

Practical System Implementation for 5G Wireless Communication Systems

by

Weiheng Ni
B.Eng., Beijing University of Posts and Telecommunications, 2013

Supervisory Committee

Dr. Xiaodai Dong, Supervisor
(Department of Electrical and Computer Engineering)

Dr. Wu-Sheng Lu, Departmental Member
(Department of Electrical and Computer Engineering)

Supervisory Committee

Dr. Xiaodai Dong, Supervisor
(Department of Electrical and Computer Engineering)

Dr. Wu-Sheng Lu, Departmental Member
(Department of Electrical and Computer Engineering)

ABSTRACT

The fifth generation (5G) wireless communications technology will be a paradigm shift which does not only provide an explosive increment on the achievable data rate per cell, but also ideally decreases the costs and energy consumption per data link. The engineering requirements of 5G standard can be intuitively interpreted as highly enhanced spectral efficiency and energy efficiency. This thesis focuses on the practical implementation issues of the massive multiple-input multiple-output (MIMO) and energy harvesting systems. To begin with, massive MIMO, as one of the key technologies of 5G systems, can provide enormous enhancement in spectral efficiency. For a practical massive MIMO system, hybrid processing (precoding/combining), by restricting the number of RF chains to far less than the number of antenna elements, can significantly reduce the implementation cost compared to the full-complexity radio frequency (RF) chain configuration. This thesis designs the hybrid RF and baseband precoders/combiners for multi-stream transmission in the point-to-point (P2P) massive MIMO systems, by directly decomposing the pre-designed digital precoder/combiner of a large dimension. The performance of the matrix decomposition based hybrid processing (MD-HP) scheme is near-optimal compared to the singular value decomposition (SVD) based full-complexity processing.

In addition, the downlink communication of a massive multiuser MIMO (MU-MIMO) system is also investigated, and a low-complexity hybrid block diagonalization (Hy-BD) scheme is developed to approach the performance of the traditional BD method. We aim to harvest the large array gain through the phase-only RF precoding and combining and then BD processing is performed on the equivalent baseband

channel in the massive MU-MIMO scenario. The MD-HP and Hy-BD schemes are examined in both the large Rayleigh fading channels and millimeter wave channels.

On the other hand, energy harvesting is an increasingly attractive and renewable source of power for wireless communications devices, which contributes to the enhancement of the system energy efficiency. This thesis also designs the energy cooperation assisted energy harvesting communication between a practical transmitter and receiver, whose hardware circuits consume non-zero power when active. The energy cooperation save-then-transmit (EC-ST) scheme aims to obtain the optimal active time ratio and energy cooperation power for the maximum throughput under additive white Gaussian channels and the minimum outage probability under block Rayleigh fading channels.

Contents

List of Figures

List of Acronyms

4G: Fourth generation

5G: Fifth generation

LTE-A: Long term evolution-advanced

MISO: Multiple-input single-output

MIMO: Multiple-input multiple-output

MU-MIMO: Multiple user MIMO

SNR: Signal-to-noise ratio

SINR: Signal-to-interference-plus-noise ratio

CSI: Channel state information

SVD: Singular value decomposition

BS/MS: Base station/Mobile station

SDMA: Spatial division multiple access

MMSE: Minimum mean squared error

EGT/EGC: Equal gain transmission/combining

MRC/MRT: Maximum-ratio combining/transmission

ZF: Zero forcing

BD: Block diagonalization

RF: Radio frequency

DPC: Dirty paper coding

MD-HP: Matrix decomposition based hybrid processing

Hy-BD: Hybrid block diagonalization

DFT: Discrete Fourier transform

EC-ST: Energy cooperation save-then-transmit

CS: Compressive sensing

SDP: Semidefinite programming

AoD/AoA: Angles of departure/arrival

ULA: Uniform linear array

SWIPT: Simultaneous wireless information and power transfer

AWGN: Additive white Gaussian noise

ACKNOWLEDGEMENTS

First and foremost, I would like to express my sincere gratitude to my supervisor Professor Xiaodai Dong, who has supported me throughout my research and study in the past two years. As a supervisor, her academic guidance helped me diving into the world of research; as a friend, she helped me drawing the blueprint for my future career. I believe that the best choice I have ever made for my master study was selecting her as my supervisor. I also want to thank Professor Wu-Sheng Lu for lecturing the course Engineering Optimization where he made the fundamentals of optimization really easy to understand, and giving a gorgeous method to solve the matrix decomposition problem in Chapter 2.

My heartfelt gratitude also goes to all members of our research group, with whom I have spent most of my time at University of Victoria. In particular, I would like to thank Le Liang, Leyuan Pan, Yongyu Dai, Lan Xu, Zheng Xu, Wanbo Li, Ping Cheng and Farnoosh Talaei for the inspiring discussions. Moreover, I am grateful to my friend Yi Shi, who enlightened me the first glance of research. In addition, I thank my friends in Beijing University of Posts and Telecommunications: Rao Zhang, Bo Li, Bo Tang, Yanyin Zhu and Guohua Wu for the days we were working together and for the fruits we had obtained.

Finally, I again express my wholehearted gratitude to all my friends, both inside and outside of University of Victoria, who render me a wonderful life. This thesis is dedicated to my family, including my parents, my elder sisters and my grandparents, who have been supporting me with their love throughout my life.

I acknowledge the Natural Sciences and Engineering Research Council of Canada and the University of Victoria Graduate Awards program for providing financial support for my Master Studies.

Weiheng Ni

Chapter 1

Introduction

As the long term evolution-advanced (LTE-A) wireless communication system, embodying 4G, is reaching maturity on the academic research and practical deployment, the blossoming discussions on the new possible 5G standard has captured the attention of the researchers and engineers all over the world [1]. The 5G wireless communications technology will be a paradigm shift which does not only provide an explosive increment on the achievable data rate per cell, but also ideally decreases the costs and energy consumption per data link. Specifically, the network throughput (bps/area) required by the 5G standard is expected to increase by around 1000 times over the current 4G. To achieve such an objective, the multiple-input multiple-output (MIMO) technique, especially at a large scale, is one of the key enabling components to be adopted. As for reducing the energy consumption of data transmission, energy harvesting is an increasingly attractive solution to rely on renewable sources for powering the wireless communications devices.

In the point-to-point communication scenario with multiple antennas employed at both the transmitter and the single user receiver, the signals radiated from the antennas of the transmitter go through multiple propagation paths and finally arrive at the receiver antennas with different delays. In a typical MIMO communication scenario, diversity and multiplexing are the keys to achieve high spectral efficiency for the data links. To begin with, we choose a simple case where a single-antenna transmitter sends one data stream to the multiple-antenna receiver that exploits maximum ratio combining (MRC) to retrieve the transmitted signal. The receive signal-to-noise ratio (SNR) will obtain extra power gain and diversity gain which linearly increase with the receive antenna number and the average channel gains compared to the transmit SNR [27]. The diversity rendered by the multiple antennas, hence, essen-

tially offers a higher spectral efficiency through increasing the receive SNR. Other than the receive diversity, the transmit diversity based on the space-time codes, e.g., the so called Alamouti scheme, also provides a diversity gain by repeatedly sending the transmit symbols through different transmit antennas over different symbol times. Furthermore, multiple data streams transmission is supported by the MIMO technique when both the transmitter and receiver have multiple antennas, namely, spatial multiplexing. Generally, there often exists a mismatch between the number of data streams and the number of transmit/receive antennas, which requires the precoding and combining at the transmitter and receiver respectively. As long as the full channel state information (CSI) is available, by selecting some corresponding right and left singular vectors to construct the precoder and combiner based on the singular value decomposition (SVD), the transmitted streams can be considered to equivalently pass through some parallel channels so that reliable communication with spatial multiplexing is supported by the MIMO technique.

When it comes to the practical communications in the cellular network, a base station (BS) with a number of antennas needs to communicate with multiple users/-mobile stations (MSs), which is so called multiple user MIMO (MU-MIMO) system. Different from the traditional time or frequency division multiple access cellular systems, the MSs in the MU-MIMO system are able to share the same time and frequency resources through spatial division multiple access (SDMA), whose main principle is consistent with the spatial multiplexing of data streams in the point-to-point (P2P) MIMO scenario. However, for a general non-cooperative MU-MIMO system, the MSs cannot share their CSI with others or proceed signal combining together. This essential feature of the MU-MIMO system leads to a disadvantageous result that the signals for others will cause interference to the intended MS. Therefore, the parameter that plays a role on the spectral efficiency should be the signal-to-interference-plus-noise ratios (SINRs) of the MSs. In the downlink communication of the MU-MIMO systems, some linear precoding/combining schemes are commonly utilized, such as minimum mean squared error (MMSE), zero-forcing (ZF) and block diagonalization (BD) schemes [5]-[6] [28]. Note that ZF precoding can only be employed in the MU-MIMO system with single-antenna MSs, which is realized by projecting the data stream of each MS to the null space of others' channels. The BD scheme is a generalization of the ZF which supports the multiple-antenna MSs. Besides, a number of signal processing schemes have been investigated for pursuing the higher spectral efficiency up to the channel capacity recently.

On the other hand, energy harvesting for communication devices has emerged as a prominent research area due to its benefit of powering the devices through alternative energies instead of battery or hardwire power [29], [30]. By employing the piezoelectric, electromagnetic, photo-voltaic or other energy harvesting technologies, external sources, such as kinetic, solar energy and ambient radio waves, can be harvested to power the devices. Thus, energy harvesting becomes an attractive and effective solution for powering the energy-constrained devices and prolonging their lifetime, which essentially enhance the energy efficiency of the wireless communication systems. In addition, energy cooperation allows the devices to intentionally transfer some energy to others to assist communications, which actually extends the feasible region of a performance optimization problem, so that the performance of the energy harvesting wireless communications can substantially be improved by energy cooperation.

This thesis proposes the hybrid precoding schemes in the P2P MIMO and MU-MIMO scenarios when a large scale of antennas are implemented in the system. The hybrid processing schemes take effect based on the limited radio frequency (RF) chain configuration which aims to reduce the hardware implementation costs under the massive MIMO setting. For energy harvesting based communications research, optimization of an energy cooperation assisted energy harvesting wireless communication is studied in this thesis. The rest of this chapter elaborates the motivation for this thesis as well as an overview of the main contributions.

1.1 Motivation

To realize the tremendous capacity target of the 5G wireless communication system, one promising option is to scale up to massive MIMO systems to reap the highly increased spectral efficiency [1]-[2]. In the limit of an infinite number of antennas, the massive MIMO propagation channel becomes quasi-static where the effects of uncorrelated noise and fast fading vanish, and such favorable characteristics enable arbitrary small energy per transmitted bit [2], and the large array gain is rendered by a massive number of antennas at the order of a hundred or more [3]. Moreover, in the massive MU-MIMO systems, some simple linear pre/post-processing (transmit precoding/receive combining) schemes, such ZF and linear MMSE, are able to approach the optimal capacity performance achieved by the dirty paper coding (DPC) as the number of antennas goes to infinity [5]. Conventional pre-processing is performed through modifying the amplitudes and phases of the complex transmit symbols at the

baseband and then upconverted to the passband after passing through RF chains (including the digital-to-analog conversion, signal mixing and power amplifying), which requires that the number of the RF chains is in the range of hundreds, equal to the number of the antenna elements. Post-processing similarly involves a large number of analog receive RF chains and digital baseband operations. This leads to unacceptably high implementation cost and energy consumption.

Recently, enabled by the cost-effective variable phase shifters, a limited number of RF chains have been applied in the MIMO systems [10]-[17]. The analog RF processing provides the high-dimensional phase-only control while the digital baseband processing can be performed in a very low dimension, termed as hybrid processing. Under the limited RF chain constraint, lots of research efforts have been made to design the high-performance and feasible hybrid processing schemes. For instance, [8] implement the hybrid processing to the downlink of the massive MU-MIMO systems with single-antenna users, and the near-optimal capacity performance, compared to the full-complexity systems, is achieved through the ZF baseband precoding combined with the equal gain transmission (EGT) processing in the RF domain. In addition, references [10] and [9] investigate the hybrid processing schemes in the P2P MIMO systems, focusing on the single-stream and multiple-stream communication respectively.

However, it is in general much more difficult to design the hybrid processing based schemes since the number of required precoders/combiners is doubled compared to the conventionally full-complexity processing. It is not clear how to systematically design these processing units. The analog RF precoder/combiner are constrained by the nature of the phase shifters, namely, the amplitudes of all entries of the RF precoder/combiner matrices are constant, which further increases the design difficulty. To efficiently and effectively proceed the hybrid processing scheme design, it is feasible to start from the existing full-complexity processing schemes. As is known to us, the P2P MIMO channel capacity can be achieved by the SVD based processing (the water-filling power allocation is included). Therefore, directly decomposing the pre-designed optimal precoder/combiner of a large dimension could be one option to realize the hybrid processing. [14] presents a hybrid processing by decomposing the optimal precoding/combining matrix via orthogonal matching pursuit with the transmit/receive array response vectors as the basis vectors for the RF precoder/combiner, which requires the information of all propagation paths of the MIMO channel. This thesis is the first to give a general matrix decomposition based hybrid process-

ing design that maximizes the system spectral efficiency, with only the non-convex constant-amplitude constraint for the RF precoder/combiner but no other restrictions. As for the massive MU-MIMO system, we would like to develop the hybrid processing scheme from another perspective that the computational complexity of the scheme should be reduced for the practical implementation where the MSs usually have quite low computation ability. Inspired by the design pattern of [8], this thesis also proposes to perform the RF processing first and then apply the traditional BD scheme to the baseband processing, which avoids multifarious iterative calculations compared to the matrix decomposition based hybrid processing.

Other than the improvement of spectral efficiency, energy harvesting wireless communications have emerged as a promising solution for enhancing the energy efficiency by powering the devices through renewable energies instead of battery or hardwire power and prolong their lifetime [29], [30]. A certain amount of work has been produced to optimize the energy harvesting system performance when different assumptions on energy arrival rate, channel conditions, communication setups, etc. are made [32]-[40]. When the energy cooperation is introduced, [45]-[51] aim to further improve the performance limit by allowing the energy to intentionally transfer among the communication nodes. Nevertheless, the power consumption of the hardware circuits (non-ideal circuits) is usually ignored by the previous work, which leads the impractical energy harvesting designs not suitable for real implementation. In this thesis, we consider the energy harvesting transmitter and receiver with non-ideal circuits. Both the practical transmitter and receiver harvest energy from the external sources, and then employ the harvested energy to support communications as well as running the power consuming circuits. Based on the save-then-transmit scheme in [53], the energy cooperation between the transmitter and receiver is also enabled to improve the communications performance by adjusting the transmission power and communication time. Such a communication setting, we believe, can guide the research of the energy harvesting in the practice systems in the future.

1.2 Overview of Thesis

This thesis focuses on the practical implementation issues of the massive MIMO and energy harvesting systems, aiming to obtain high spectral efficiency and energy efficiency performance respectively in the future 5G wireless communications systems. For the massive MIMO systems, the hybrid processing schemes based on the limited

RF chains configuration are designed, namely, the near-optimal matrix decomposition based hybrid processing (MD-HP) scheme for the P2P scenario in Chapter 2 and the hybrid block diagonalization (Hy-BD) scheme for the multiple user scenario in Chapter 3. For the energy harvesting wireless communications, energy cooperation save-then-transmit scheme (EC-ST) is developed to improve the communication performance between the practical transmitter and receiver in Chapter 4.

In Chapter 2, we investigate the processing (precoding/combining) scheme for the P2P communication between the MIMO transmitter and receiver when a large number of antenna elements are employed. In the hybrid processing, the transmitted data stream is first processed by a very low-dimensional digital baseband precoder and then up-converted to the RF domain through s small quantity of RF chains, followed by the analog RF precoder which is enable by the phase shifters. The receiver has a symmetric hybrid processing structure that consists of an RF analog combiner followed by a baseband digital combiner to demodulate the received data streams. We perform the hybrid processing by directly decomposing the pre-designed digital precoder/combiner of a large dimension. Based on the alternating optimization technique, the non-convex matrix decomposition problem can be decomposed into a series of convex sub-problems and effectively performed by restricting the phase increments of the RF precoder/combiner within a small range at each iteration. The spectral efficiency performance of the MD-HP scheme is near-optimal compared to the SVD based full-complexity processing under the large Rayleigh fading channels and millimeter wave channels.

Chapter 3 continues to implement the hybrid processing structure to the massive MU-MIMO systems. Besides the MD-HP scheme in Chapter 2, we develop a low-complexity Hy-BD scheme to approach the capacity performance of the traditional BD processing method. We aim to harvest the large array gain through the phase-only RF precoding and combining and then the BD processing is performed on the equivalent baseband channel. More specifically, the RF combiners of all the mobile stations are obtained by selecting some of the discrete Fourier transform (DFT) bases that somehow catch the strongest gains in the channel matrices, while the RF precoder of the BS is designed by extracting the phases of the conjugate transpose of the aggregate intermediate channel which incorporates the MSs' RF combiners and the original downlink channels. With the designed RF precoder and combiners, a low-dimensional BD processing can then be performed at the baseband to cancel the inter-user interference. The proposed Hy-BD schemes is also examined in both the

large Rayleigh fading channels and millimeter wave channels.

In Chapter 4, the P2P energy harvesting wireless communication between the practical transmitter and receiver is studied for the purpose of the energy efficiency enhancement in the future 5G systems. The transmitter and receiver are powered solely by the energy harvested from external sources and their hardware circuits consume non-zero power when active. An EC-ST scheme is proposed to obtain the optimal active time ratio and energy cooperation power for the maximum throughput under additive white Gaussian channels and the minimum outage probability under block Rayleigh fading channels. It is shown that one effective method for improving the communications performance between energy harvesting devices is to allow the energy flow between the devices, and then find an optimal tradeoff between the transmission power and the active time ratio.

The last chapter summarizes key points in the thesis and gives concluding remarks.

Chapter 2

Near-Optimal Hybrid Processing for Massive MIMO Systems via Matrix Decomposition

Massive multiple-input multiple-output (MIMO) is potentially one of the key technologies to achieve high capacity performance in the next generation of mobile cellular systems [1]-[4]. In the limit of an infinite number of antennas, the massive MIMO propagation channel becomes quasi-static where the effects of uncorrelated noise and fast fading vanish, and such favorable characteristics enables arbitrarily small energy per transmitted bit [2]. Prominently, in massive multiuser MIMO systems, some simple linear processing schemes, such as zero-forcing (ZF) and linear minimum mean-square error (MMSE), are able to approach the optimal capacity performance achieved by the dirty paper coding (DPC) in the downlink communication [5]. The spectral efficiency performance of the massive MIMO systems with some linear processing schemes, including ZF, MMSE and maximum-ratio combining (MRC), are analyzed with the perfect and imperfect channel state information (CSI) in [6].

For the practical implementation of the massive MIMO systems, the number of antennas required for the large antenna array gains, generally considered to be with an order of a hundred or more, is determined by examining the convergence properties over the antenna number in [7]. However, to exploit such a large antenna array in the massive MIMO systems, the amplitudes and phases of the complex transmit symbols are traditionally modified at the baseband and then upconverted to the passband around the carrier frequency after passing through radio frequency (RF) chains

(performing the analog radiowave/digital baseband conversion, signal mixing, power amplifying). All outputs of the RF chains are connected to the antenna elements, which means the number of the RF chains should exactly be equal to the antenna elements. The fabrication cost and energy consumption of such a massive MIMO system will be unacceptable due to the tremendous number of RF chains [8].

To deal with this problem, smaller number of RF chains are used in the large scale MIMO systems, where cost-effective variable phase shifters can be employed to handle the mismatch between the number of RF chains and of antennas [9]-[12]. The high-dimensional analog RF (phase only) processing is enabled by the phase shifters while the digital baseband processing can be performed in a very low dimension. Both diversity and multiplexing transmissions of MIMO communications are addressed with a limited number of RF chains in [9]. Besides, the analog RF precoding is presented to achieve full diversity order and near-optimal beamforming performance in [10], [11]. Reference [12] applies the phase-only RF precoding in the massive MIMO systems to maximize the data rate of users based on a bi-convex approximation approach. Especially, the small wavelengths of millimeter wave (mmWave) make it possible to build a large antenna array in a compact region, and the above hybrid baseband and RF processing (transmit precoding/receive combining) scheme is particularly suitable for mmWave MIMO communications by cutting down the excessive cost of RF chains [13]-[16]. Herein, hybrid processing is designed to capture the "dominant" paths in point-to-point (P2P) mmWave channels by choosing the RF control phases from the array response vectors [13], [14]. On the other hand, hybrid processing in the multiuser mmWave systems is studied in [8], [15]-[16], where analog RF processing aims to obtain the large antenna gains, while baseband processing performs on the low-dimensional equivalent channels.

Moreover, CSI is the prerequisite to perform any processing at the transmitter and the receiver, whether it is the unconstrained high-dimensional baseband processing for the traditional design that one antenna element is coupled with one dedicated RF chain or the hybrid processing. The training sequences and closed-loop sounding vectors are designed in [18] to estimate a massive multiple-input single-output (MISO) channel by making aligning the transmit beamformer with the true channel direction. Reference [19] formulates a compressive sensing (CS) based low-rank approximation problem, solved via quadratic semidefinite programming (SDP), to estimate the massive MIMO channel matrix. Considering the massive MIMO channels with limited scattering feature (especially involving the mmWave channels), the valued parameters

of paths, such as the angles of departure (AoDs), angles of arrival (AoAs) and the corresponding path loss are estimated through designing the beamforming codebook to obtain the pathloss of all paths whose AoDs/AoAs are spatially quantized among the whole angular domain [20], [21], while [21] performs the beamforming with the hybrid processing structure.

In this chapter, we propose to design the hybrid RF and baseband precoders/combiners for multi-stream transmission in the P2P massive MIMO systems, by directly decomposing the pre-designed unconstrained digital precoder/combiner of a large dimension. This is an approach that has not been attempted in the literature. The analog RF precoder/combiner are constrained by the nature of the phase shifters, namely, the amplitudes of all entries of the RF precoder/combiner matrices are constant. We begin with the optimal unconstrained precoder, which comes from the first several right singular vectors of the channel matrix. The hybrid precoders are designed by minimizing the Frobenius norm of the difference (error) between the unconstrained precoding matrix and the products of the hybird RF and baseband precoding matrices, with constraint on the RF precoder obviously non-convex. Such a matrix decomposition problem can be solved by the alternating optimization technique, however with the sub-problems that aim to updating the phases of the RF precoder still non-convex. By restricting the phase increments of all entries of the RF precoder within a small order at each iteration step, the RF precoder constraint of the non-convex problem is approximately convex and alternating optimization can be effectively performed. Once a suitable initial point that is sufficiently close to the global solution of the non-convex matrix decomposition problem is chosen, the near-optimal solution can be found with an extremely high probability.

As for the hybrid combiners design, we select the linear MMSE combiner as the unconstrained reference matrix for the matrix decomposition, and the hybrid RF and baseband combiners can be obtained in the same fashion as the hybrid precoder design. Notably, the matrix decomposition based hybrid processing design scheme, termed as MD-HP, is suitable to the hybrid processing design over any general massive MIMO channel. The only input of our proposed MD-HP scheme is the channel matrix, which is assumed to be known to the transmitter and receiver. The convergence of alternating optimization for the MD-HP scheme is examined in the simulation. The performance of the MD-HP scheme is further demonstrated to be near-optimal by comparing it to the optimal unconstrained baseband processing based on the singular value decomposition (SVD) technique.

2.1 System Model

In this section, we introduce the hybrid processing structure for the P2P massive MIMO systems and the channel models considered in this chapter.

2.1.1 System Model

We consider the communication from a transmitter with N_t antennas and M_t RF chains to a receiver equipped with N_r antennas and M_r RF chains, where N_s data streams are supported. The system model of the transceiver is shown in Fig. 2.1. To guarantee the effectiveness of the communication driven by the limited number of RF chains, the number of the communication streams is constrained by $N_s \leq M_t \leq N_t$ for the transmitter and $N_s \leq M_r \leq N_r$ for the receiver.

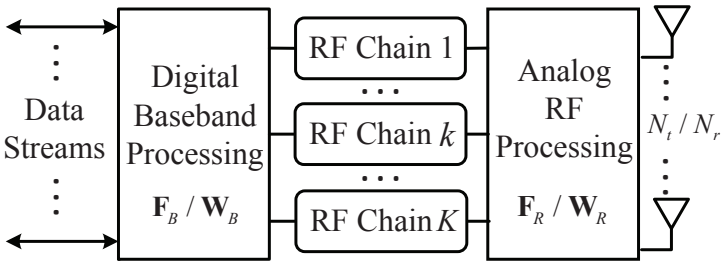

Figure 2.1: System model of the transceiver with the hybrid processing structure

At the transmitter side, the transmitted symbols are assumed to be processed by a baseband precoder $\mathbf{F}_B$ of dimension $M_t \times N_s$ and then up-converted to the RF domain through the M_t RF chains before being precoded by an RF precoder $\mathbf{F}_R$ of dimension $N_t \times M_t$. Notably, the baseband precoder $\mathbf{F}_B$ enables both amplitude and phase modification, while only phase changes can be realized by $\mathbf{F}_R$ since it is implemented by using analog phase shifters. We normalize each entry of $\mathbf{F}_R$ to satisfy $|\mathbf{F}_R^{(i,j)}| = \frac{1}{N_t}$, where $|(\cdot)^{(i,j)}|$ denotes the amplitude of the (i,j)-th element of $(\cdot)$. Furthermore, to meet the total transmit power constraint, $\mathbf{F}_B$ is normalized to satisfy $||\mathbf{F}_R\mathbf{F}_B||_F^2 = N_s$, where $||\cdot||_F$ denotes the Frobenius norm.

We assume a narrowband flat fading channel model and the received signal is given by

$$\mathbf{y} = \mathbf{H}\mathbf{F}_R\mathbf{F}_B\mathbf{s} + \mathbf{n}, \tag{2.1}$$

where $\mathbf{y} \in \mathbb{C}^{N_r \times 1}$ is the received signal vector, $\mathbf{s} \in \mathbb{C}^{N_s \times 1}$ is the signal vector such that $\mathbb{E}[\mathbf{s}\mathbf{s}^H] = \frac{P}{N_s}\mathbf{I}_{N_s}$, where $(\cdot)^H$ denotes conjugate transpose, $\mathbb{E}[\cdot]$ denotes expectation,

$\mathbf{I}_{N_s}$ is the $N_s \times N_s$ identity matrix and P is the average transmit power. $\mathbf{H} \in \mathbb{C}^{N_r \times N_t}$ is the channel matrix, normalized as $\mathbb{E}[||\mathbf{H}_F^2||] = N_t N_r$, and $\mathbf{n}$ is the vector of i.i.d. $\mathcal{CN}(0, \sigma^2)$ addictive complex Gaussian noise. Moreover, to perform the precoding and combining, we assume the perfect channel knowledge is available at both the transmitter and the receiver. Then the processed received signal at the receiver after combining is given by

$$\tilde{\mathbf{y}} = \mathbf{W}_B^H \mathbf{W}_R^H \mathbf{H} \mathbf{F}_R \mathbf{F}_B \mathbf{s} + \mathbf{W}_B^H \mathbf{W}_F^H \mathbf{n}, \tag{2.2}$$

where $\mathbf{W}_F$ is the $N_r \times M_r$ RF combining matrix and $\mathbf{W}_B$ is the $M_r \times N_s$ baseband combining matrix. Since $\mathbf{W}_F$ is also implemented by the analog phase shifters, all elements of $\mathbf{W}_F$ should have the constant amplitude such that $|\mathbf{W}_B^{(i,j)}| = \frac{1}{N_r}$. If Gaussian inputs are employed at the transmitter, the long-term average spectral efficiency achieved will be

$$R(\mathbf{F}_R, \mathbf{F}_B, \mathbf{W}_R, \mathbf{W}_B) = \log_2 \left(\left| \mathbf{I}_{N_s} + \frac{P}{N_s} \mathbf{R}_n^{-1} \tilde{\mathbf{H}} \tilde{\mathbf{H}}^H \right| \right), \tag{2.3}$$

where $\mathbf{R}_n = \sigma^2 \mathbf{W}_B^H \mathbf{W}_F^H \mathbf{W}_F \mathbf{W}_B$ is the covariance matrix of noise and $\tilde{\mathbf{H}} = \mathbf{W}_B^H \mathbf{W}_F^H \mathbf{H} \mathbf{F}_R \mathbf{F}_B$.

2.1.2 Channel Model

In this chapter, we aim to seek the optimal hybrid precoders ($\mathbf{F}_R$, $\mathbf{F}_B$) and the hybrid combiners ($\mathbf{W}_R$, $\mathbf{W}_B$) based on a general channel matrix $\mathbf{H}$. To measure the performance of our proposed MD-HP scheme, we consider two kinds of channel models in our simulations of Section 2.3:

1) Large Rayleigh fading channel $\mathbf{H}_{rl}$ with all i.i.d. $\mathcal{CN}(0, 1)$ entries;

2) Limited scattering mmWave channel $\mathbf{H}_{mmw}$.

Note that a certain number of hybrid processing schemes have been studied under the mmWave communications scenarios where a large antenna array is implemented to combat the high free-space pathloss and reflection loss [13]-[16]. Thus the mmWave channel model $\mathbf{H}_{mmw}$ is a proper instance for comparing the performance of our proposed scheme with others. Due to the limited (sparse) scattering characteristic of a mmWave channel, we would like to introduce the clustered mmWave channel model to characterize its key features [22]. The mmWave channel $\mathbf{H}_{mmw}$ is assumed to be

the sum of all propagation paths that are scattered in N_c clusters and each cluster contributes N_p paths.. Therefore, the normalized channel matrix can be expressed as

$$\mathbf{H}_{mmw} = \sqrt{\frac{N_t N_r}{N_c N_p}} \sum_{i=1}^{N_c} \sum_{l=1}^{N_p} \alpha_{il} \mathbf{a}_r(\theta_{il}) \mathbf{a}_t(\phi_{il})^H, \tag{2.4}$$

where α_{il} is the complex gain of the i-th path in the l-th cluster, which follows $\mathcal{CN}(0,1)$[1]. For the (i,l)-th path, θ_{il} and ϕ_{il} are the azimuth angles of arrival/departure (AoA/AoD), while $\mathbf{a}_r(\theta_{il})$ and $\mathbf{a}_t(\phi_{il})$ are the receive and transmit array response vectors at the azimuth angles of θ_{il} and ϕ_{il} respectively, and the elevation dimension is ignored[2]. Within the i-th cluster, θ_{il} and ϕ_{il} have the uniformly-distributed mean values of θ_i and ϕ_i respectively, while the lower and upper bounds of the uniform distribution for θ_i and ϕ_i can be defined as $[\theta_{\min}, \theta_{\max}]$ and $[\phi_{\min}, \phi_{\max}]$. The angular spreads (standard deviations) of θ_{il} and ϕ_{il} among all clusters are assumed to be constant, denoted as σ_θ and σ_ϕ. According to [14], we use the truncated Laplacian distribution to generate all the θ_{il}'s and ϕ_{il}'s base on the above parameters.

As for the array response vectors $\mathbf{a}_r(\theta_{il})$ and $\mathbf{a}_t(\phi_{il})$, we choose the uniform linear arrays (ULAs) in our simulations, while the precoding scheme in Section 2.2 can directly be applied to arbitrary antenna arrays. For an N-element ULA, the array response vector can be given by

$$\mathbf{a}_{ULA}(\theta) = \frac{1}{\sqrt{N}} \left[1, e^{j\frac{2\pi}{\lambda} d \sin(\theta)}, \cdots, e^{j(N-1)\frac{2\pi}{\lambda} d \sin(\theta)}\right]^T, \tag{2.5}$$

where λ is the wavelength of the carrier, and d is the distance between any two adjacent antenna elements. The array response vectors at both the transmitter and the receiver can be written in the form of (2.5).

2.2 Hybrid Precoding/Combining Design for A General Massive MIMO Channel

For the design of the hybrid precoders ($\mathbf{F}_R$, $\mathbf{F}_B$) and combiners ($\mathbf{W}_R$, $\mathbf{W}_B$) based on a general massive MIMO channel $\mathbf{H}$, we can directly formulate a joint transmitter-

[1]The power gain of the channel matrix is normalized such that $\mathbb{E}[||\mathbf{H}_{mmw}{}_F^2||] = N_t N_r$

[2]Only 2D beamforming is considered in this mmWave channel model.

receiver optimization problem to maximize the spectral efficiency, which is given by

$$\begin{aligned} \max \;\; & R(\mathbf{F}_R, \mathbf{F}_B, \mathbf{W}_R, \mathbf{W}_B) \\ s.t. \;\; & ||\mathbf{F}_R \mathbf{F}_B||_F^2 = N_s, \\ & \mathbf{F}_R \in \mathcal{F}_R, \;\; \mathbf{W}_R \in \mathcal{W}_R, \end{aligned} \tag{2.6}$$

where $\mathcal{F}_R(\mathcal{W}_R)$ is the set of matrices with all constant amplitude entries, which is $\frac{1}{\sqrt{N_t}}(\frac{1}{\sqrt{N_r}})$. However, this joint optimization problem with the similar constraints is often intractable [23], due to the non-convex constraints $\mathbf{F}_R \in \mathcal{F}_R$ and $\mathbf{W}_R \in \mathcal{W}_R$ that obstruct the regular progress of searching an globally optimal solution. Before gaining an insight into the solution of this joint optimization problem (2.6), we would like to introduce the optimal unconstrained precoder $\mathbf{F}^\star$ and combiner $\mathbf{W}^\star$ for achieving the maximum capacity of a general MIMO channel, based on which the near-optimal hybrid precoders/combiners are further designed. Assume that the channel matrix $\mathbf{H}$ is well-conditioned to transmit N_s data streams. Namely, rank($\mathbf{H}$) $\geq N_s$. To obtain the optimal $\mathbf{F}^\star$ and $\mathbf{W}^\star$, we perform the SVD of the channel matrix $\mathbf{H} = \mathbf{U}\mathbf{\Sigma}\mathbf{V}^H$, where $\mathbf{U}$ is an $N_r \times N_r$ unitary matrix, $\mathbf{V}$ is an $N_t \times N_t$ unitary matrix and $\mathbf{\Sigma}$ is an $N_r \times N_t$ diagonal matrix with all singular values along the diagonal in the descendant order. Respectively divide $\mathbf{V}$ and $\mathbf{U}$ into two partitions as

$$\mathbf{V} = [\mathbf{V}_1 \;\; \mathbf{V}_2], \quad \mathbf{U} = [\mathbf{U}_1 \;\; \mathbf{U}_2], \tag{2.7}$$

where $\mathbf{V}_1$ is the first N_s columns of $\mathbf{V}$, and $\mathbf{U}_1$ is the first N_s column of $\mathbf{U}$. Without incorporating the waterfilling power allocation, the optimal unconstrained precoder and combiner are given by $\mathbf{F}^\star = \mathbf{V}_1$ and $\mathbf{W}^\star = \mathbf{U}_1$. And the corresponding spectral efficiency by using such unconstrained $\mathbf{F}^\star$ and $\mathbf{W}^\star$ is given by

$$\tilde{R} = \log_2 \left(\left| \mathbf{I}_{N_s} + \frac{\gamma}{N_s} \mathbf{\Sigma}_1^2 \right| \right), \tag{2.8}$$

where $\mathbf{\Sigma}_1$ represents the first partition of dimension $N_s \times N_s$ of $\mathbf{\Sigma}$ by defining that

$$\mathbf{\Sigma} = \begin{bmatrix} \mathbf{\Sigma}_1 & \mathbf{0} \\ \mathbf{0} & \mathbf{\Sigma}_2 \end{bmatrix}, \tag{2.9}$$

where $\gamma = \frac{P}{\sigma^2}$ is the signal-to-noise ratio (SNR).

Actually, $\tilde{R}$ sets an upper bound to the spectral efficiency $R(\mathbf{F}_R, \mathbf{F}_B, \mathbf{W}_R, \mathbf{W}_B)$

in problem (2.6) where the ranges of the matrix products $\mathbf{F}_R\mathbf{F}_B$ and $\mathbf{W}_R\mathbf{W}_B$ are respectively the subsets of feasible regions of the unconstrained precoder and combiner, namely, $\mathbb{C}^{N_t\times N_s}$ and $\mathbb{C}^{N_r\times N_s}$. Considering the non-convex feature of the problem (2.6), it is impossible to guarantee a global solution to it. Therefore, one potential method is to seek the hybrid precoders and combiners such that the optimal unconstrained precoder $\mathbf{F}^\star$ and combiner $\mathbf{W}^\star$ can be sufficiently approached by $\mathbf{F}_R\mathbf{F}_B$ and $\mathbf{W}_R\mathbf{W}_B$ respectively.

2.2.1 Hybrid Precoders Design via Matrix Decomposition

With the hybrid precoding structure and the constraint on the RF precoder $\mathbf{F}_R$, there is no guarantee that we are able to find a pair of $(\mathbf{F}_R, \mathbf{F}_B)$ that perfectly makes $\mathbf{F}^\star = \mathbf{F}_R\mathbf{F}_B$. However, by relaxing the strict equality, the matrix decomposition can be realized with best-effort through reformulating the original problem as the following

$$\begin{aligned} \min_{\mathbf{F}_R,\mathbf{F}_B} \ & ||\mathbf{F}^\star - \mathbf{F}_R\mathbf{F}_B||_F \\ s.t. \ & ||\mathbf{F}_R\mathbf{F}_B||_F^2 = N_s, \\ & \mathbf{F}_R \in \mathcal{F}_R. \end{aligned} \tag{2.10}$$

Before solving the matrix decomposition problem (2.10) and examining the spectral efficiency achieved by the obtained hybrid precoders $(\mathbf{F}_R, \mathbf{F}_B)$, we still cannot validate the effectiveness of this method. In other words, it is likely that the spectral efficiency $R(\mathbf{F}_R, \mathbf{F}_B, \mathbf{W}_R, \mathbf{W}_B)$ is quite sensitive to the error between $||\mathbf{F}^\star - \mathbf{F}_R\mathbf{F}_B||_F$, and a small difference between $\mathbf{F}^\star$ and $\mathbf{F}_R\mathbf{F}_B$ could lead to a great loss of the spectral efficiency performance. For this concern, it is necessary to explain that the migration from problem (2.6) to (2.10) is reasonable.

Note that our objective is to find an estimated version of $\mathbf{F}^\star$ by using the product of the hybrid precoding matrix $\mathbf{F}_R\mathbf{F}_B$, and the error introduced by this approximation will divert the optimal unconstrained combiner away from $\mathbf{W}^\star$. Based on this fact, we first focus on the design of hybrid precoders by assuming that the N_r–dimensional minimum distance decoding can be performed at the receiver, which indicate that the achieved spectral efficiency could be equivalent to the mutual information over the MIMO channel when Gaussian inputs are used, given by

$$\mathcal{I}(\mathbf{F}_R, \mathbf{F}_B) = \log_2\left(\left|\mathbf{I}_{N_s} + \frac{\gamma}{N_s}\mathbf{H}\mathbf{F}_R\mathbf{F}_B\mathbf{F}_B^H\mathbf{F}_R^H\mathbf{H}^H\right|\right). \tag{2.11}$$

Then we can obtain the hybrid precoders by maximizing the mutual information. This mutual information maximizing problem has already been investigated in [14], where the approximation of the mutual information is performed as

$$\begin{aligned}&\mathcal{I}(\mathbf{F}_R, \mathbf{F}_B)\\ &\quad\approx \log_2\left(\left|\mathbf{I}_{N_s}+\frac{\gamma}{N_s}\mathbf{\Sigma}_1^2\right|\right)-N_s+||\mathbf{V}_1^H\mathbf{F}_R\mathbf{F}_B||_F^2.\end{aligned} \tag{2.12}$$

And $\max \mathcal{I}(\mathbf{F}_R, \mathbf{F}_B) \approx \max ||\mathbf{V}_1^H\mathbf{F}_R\mathbf{F}_B||_F^2$ is approximately equivalent to minimizing $||\mathbf{F}^\star - \mathbf{F}_R\mathbf{F}_B||_F$. Therefore, it is safe to seek $(\mathbf{F}_R, \mathbf{F}_B)$ in order to maximize the mutual information over the massive MIMO channel by solving the matrix decomposition problem (2.10). Once the hybrid precoders $(\mathbf{F}_R, \mathbf{F}_B)$ are obtained, we can then proceed the design of the hybrid combiners $(\mathbf{W}_R, \mathbf{W}_B)$ to maximally increase the system spectral efficiency.

The second constraint in (2.10) requiring that all the entries of $\mathbf{F}_R$ have the constant amplitude $\frac{1}{\sqrt{N_t}}$ is evidently non-convex, which excludes the common convex optimization techniques for solving such a problem and makes it impossible to guarantee a globally optimal solution. Hence, it is acceptable to search a near-optimal solution even though it is likely a locally optimal solution for $\min ||\mathbf{F}^\star - \mathbf{F}_R\mathbf{F}_B||_F$. The requirement for such a near-optimal solution is that the spectral efficiency achieved by the obtained hybrid precoders (also the hybrid combiners) should sufficiently approach the upper bound $\tilde{R}$. Note that the problem (2.10) has a very similar form with the rank factorization problem, which can be solved by the alternating optimization technique [24]. Our problem may potentially be proceeded by some iterative procedures: 1) solve the non-convex problem over $\mathbf{F}_R$ given $\mathbf{F}_B$ and 2) solve the convex problem over $\mathbf{F}_B$ given $\mathbf{F}_R$. If $(\mathbf{F}_R, \mathbf{F}_B)$ can converge after consistently alternating these two steps, one local solution is then found.

To perform the iteration steps of the alternating optimization, we temporarily relax the normalization constraint $||\mathbf{F}_R\mathbf{F}_B||_F^2 = N_s$ and the problem (2.10) can be simplified to

$$\begin{aligned}&\min_{\mathbf{F}_R, \mathbf{F}_B} \ ||\mathbf{F}^\star - \mathbf{F}_R\mathbf{F}_B||_F\\ &\quad s.t.\ \mathbf{F}_R \in \mathcal{F}_R.\end{aligned} \tag{2.13}$$

To begin with, we denote the obtained hybrid precoders at the k-th iteration step as $(\mathbf{F}_R^{(k)}, \mathbf{F}_B^{(k)})$, and assume the initial $\mathbf{F}_R^{(0)}$ is given. Then the update of $\mathbf{F}_B^{(k)}$ can be proceeded by solving an unconstrained convex problem $\min_{\mathbf{F}_B} ||\mathbf{F}^\star - \mathbf{F}_R^{(k)}\mathbf{F}_B||_F$ whose

closed-form solution is given by

$$\mathbf{F}_B^{(k)} = (\mathbf{F}_R^{(k)^H}\mathbf{F}_R^{(k)})^{-1}\mathbf{F}_R^{(k)^H}\mathbf{F}^\star,\ k = 0, 1, 2, \cdots . \tag{2.14}$$

In turn, we need to update the RF precoder $\mathbf{F}_R^{(k+1)}$ by solving the non-convex problem (2.15) while $\mathbf{F}_B^{(k)}$ is given as a constant matrix, which is

$$\begin{aligned} \min_{\mathbf{F}_R^{(k+1)}}\ & ||\mathbf{F}^\star - \mathbf{F}_R^{(k+1)}\mathbf{F}_B^{(k)}||_F \\ s.t.\ & \mathbf{F}_R^{(k+1)} \in \mathcal{F}_R. \end{aligned} \tag{2.15}$$

Furthermore, we keep updating the hybrid precoders $(\mathbf{F}_R^{(k)}, \mathbf{F}_B^{(k)})$ until they converge. Here, we define an error indicator as $\epsilon_k = \frac{||\mathbf{F}^\star - \mathbf{F}_R^{(k)}\mathbf{F}_B^{(k)}||_F}{||\mathbf{F}^\star||_F}$ to measure the relative distance between $\mathbf{F}^\star$ and $\mathbf{F}_R^{(k)}\mathbf{F}_B^{(k)}$. Once ϵ_k hardly changes such that $|\epsilon_k - \epsilon_{k-1}| \leq \bar{\epsilon}$, where $\bar{\epsilon}$ is a given threshold for detecting whether the change of the error indicator is small enough, the $(\mathbf{F}_R^{(k)}, \mathbf{F}_B^{(k)})$ can be considered to converge to one local minimizer for the problem (2.13), which is also the stop criterion for the alternating optimization. Finally, we revisit the constraint $||\mathbf{F}_R\mathbf{F}_B||_F^2 = N_s$ of the original matrix decomposition problem (2.10), and perform the normalization through multiplying $\mathbf{F}_B$ by $\frac{\sqrt{N_s}}{||\mathbf{F}_R\mathbf{F}_B||_F}$. This normalization step guarantees that the transmission power keeps consistent after precoding. The above procedures of the alternating optimization are summarized in Algorithm–1.

Algorithm 1 The Hybrid Precoders Design via Matrix Decomposition based on Alternating Optimization

Require: $\mathbf{F}^\star$, $\mathbf{F}_R^{(0)}$

$\mathbf{F}_B^{(0)} = (\mathbf{F}_R^{(0)^H}\mathbf{F}_R^{(0)})^{-1}\mathbf{F}_R^{(0)^H}\mathbf{F}^\star$
$\epsilon_0 = \frac{||\mathbf{F}^\star - \mathbf{F}_R^{(0)}\mathbf{F}_B^{(0)}||_F}{||\mathbf{F}^\star||_F}$, $\epsilon_{-1} = \infty$
$k = 0$
while $|\epsilon_k - \epsilon_{k-1}| \leq \bar{\epsilon}$ **do**
    $k = k + 1$
    obtain $\mathbf{F}_R^{(k)}$ by solving (2.15)
    $\mathbf{F}_B^{(k)} = (\mathbf{F}_R^{(k)^H}\mathbf{F}_R^{(k)})^{-1}\mathbf{F}_R^{(k)^H}\mathbf{F}^\star$
    $\epsilon_k = \frac{||\mathbf{F}^\star - \mathbf{F}_R^{(k)}\mathbf{F}_B^{(k)}||_F}{||\mathbf{F}^\star||_F}$
end while
$\mathbf{F}_B = \frac{\sqrt{N_s}\mathbf{F}_B}{||\mathbf{F}_R\mathbf{F}_B||_F}$
return $\mathbf{F}_R$, $\mathbf{F}_B$

In order to operate the Algorithm–1, we still need to find out how to update the RF precoder $\mathbf{F}_R^{(k+1)}$ by solving the problem (2.15) when $\mathbf{F}_R^{(k)}$ and $\mathbf{F}_B^{(k)}$ are given. Due to the non-convex constraint $\mathbf{F}_R^{(k+1)} \in \mathcal{F}_R$, we try to update $\mathbf{F}_R^{(k+1)}$ based on $\mathbf{F}_R^{(k)}$, instead of searching an optimal $\mathbf{F}_R^{(k+1)}$ in the whole feasible region $\mathcal{F}_R$. Denote the phase of the (m,n)-th entry of $\mathbf{F}_R^{(k)}$ as $\phi_{m,n}^{(k)}$, and $\mathbf{F}_R^{(k)}$ can be represented as $\frac{1}{\sqrt{N_t}}\{e^{j\phi_{m,n}^{(k)}}\},\ m = 1, \cdots, N_t,\ n = 1, \cdots, M_t$. To characterize the relation between $\mathbf{F}_R^{(k+1)}$ and $\mathbf{F}_R^{(k)}$, we rewrite $\mathbf{F}_R^{(k+1)}$ as

$$\mathbf{F}_R^{(k+1)} = \frac{1}{\sqrt{N_t}}\{e^{j\phi_{m,n}^{(k+1)}}\} = \frac{1}{\sqrt{N_t}}\{e^{j(\phi_{m,n}^{(k)}+\delta_{m,n}^{(k)})}\}, \tag{2.16}$$

where $\delta_{m,n}^{(k)}$ is the phase increment of the (m,n)-th entry of $\mathbf{F}_R^{(k)}$ at the k-th iteration step. Note that we can perform an approximation that $e^{j\delta_{m,n}^{(k)}} \approx 1 + j\delta_{m,n}^{(k)}$ when $|\delta_{m,n}^{(k)}|$ is sufficiently small, e.g. $|\delta_{m,n}^{(k)}| \leq 0.1$, based on Taylor series expansion. Therefore, we have

$$\begin{aligned}
\mathbf{F}_R^{(k+1)} &\approx \frac{1}{\sqrt{N_t}}\{(1 + j\delta_{m,n}^{(k)})e^{j\phi_{m,n}^{(k)}}\} \\
&= \mathbf{F}_R^{(k)} + \frac{j}{\sqrt{N_t}}\{\delta_{m,n}^{(k)} \cdot e^{j\phi_{m,n}^{(k)}}\} \\
&= \mathbf{F}_R^{(k)} + \{\delta_{m,n}^{(k)}\} \circ \frac{j}{\sqrt{N_t}}\{e^{j\phi_{m,n}^{(k)}}\},
\end{aligned} \tag{2.17}$$

where $\{\delta_{m,n}^{(k)}\}$ is the matrix whose (m,n)-th entry is $\delta_{m,n}^{(k)}$ and "$\circ$" indicates the Hadamard product (entrywise product) calculation, which is exactly linear. Therefore, the problem (2.15) for seeking $\mathbf{F}_R^{(k+1)}$ can be reformulated as an optimization problem over $\{\delta_{m,n}^{(k)}\}$

$$\begin{aligned}
&\min_{\{\delta_{m,n}^{(k)}\}} \ \left|\left|\mathbf{F}^\star - \left(\mathbf{F}_R^{(k)} + \{\delta_{m,n}^{(k)}\} \circ \frac{j}{\sqrt{N_t}}\{e^{j\phi_{m,n}^{(k)}}\}\right)\mathbf{F}_B^{(k)}\right|\right|_F \\
\Leftrightarrow &\min_{\{\delta_{m,n}^{(k)}\}} \ \left|\left|\mathbf{Q}^{(k)} - \left(\{\delta_{m,n}^{(k)}\} \circ \frac{j}{\sqrt{N_t}}\{e^{j\phi_{m,n}^{(k)}}\}\right)\mathbf{F}_B^{(k)}\right|\right|_F^2,
\end{aligned} \tag{2.18}$$

where $\mathbf{Q}^{(k)} = \mathbf{F}^\star - \mathbf{F}_R^{(k)}\mathbf{F}_B^{(k)}$. Besides, the constant amplitude constraint $\mathbf{F}_R^{(k+1)} \in \mathcal{F}_R$ has already been considered in (2.18), since we express $\mathbf{F}_R^{(k+1)}$ in the form of $\frac{1}{\sqrt{N_t}}\{e^{j(\phi_{m,n}^{(k+1)})}\}$. Note that all operations inside the Frobenius norm of the objective function are linear, the problem (2.18) is consequently convex. However, the above formulation is based on the approximation $e^{j\delta_{m,n}^{(k)}} \approx 1 + j\delta_{m,n}^{(k)}$ which requires that $|\delta_{m,n}^{(k)}|$ is sufficiently small. It is necessary to enable the effectiveness of this approximation

before we use (2.18) to update the RF precoder $\mathbf{F}_R^{(k+1)}$. To do this, we supplement the small $|\delta_{m,n}^{(k)}|$ constraint to the problem (2.18)

$$\begin{aligned} \min_{\{\delta_{m,n}^{(k)}\}} \quad & \left|\left|\mathbf{Q}^{(k)} - \left(\{\delta_{m,n}^{(k)}\} \circ \frac{j}{\sqrt{N_t}}\{e^{j\phi_{m,n}^{(k)}}\}\right)\mathbf{F}_B^{(k)}\right|\right|_F^2 \\ s.t. \ & |\delta_{m,n}^{(k)}| \leq \bar{\delta}^{(k)}, \forall m, n, \end{aligned} \tag{2.19}$$

where $\bar{\delta}^{(k)}$ is a small positive real number that guarantees $e^{j\delta_{m,n}^{(k)}} \approx 1 + j\delta_{m,n}^{(k)}$. Fortunately, the feasible region of $\{\delta_{m,n}^{(k)}\}$ constrained $|\delta_{m,n}^{(k)}| \leq \bar{\delta}^{(k)},\ \forall m, n$ is also convex, which means the problem (2.19) is a convex optimization problem. The global solution of such a convex problem can be easily obtained by some common convex optimization techniques. Once we obtain the solution $\{\delta_{m,n}^{(k)}\}$, the $\mathbf{F}_R^{(k+1)}$ can be updated through (2.16).

Remark 1. *The small phase increment constraints of the problem (2.19) determine that the updated* $\mathbf{F}_R^{(k+1)}$ *is within a small neighborhood of* $\mathbf{F}_R^{(k)}$*. This fact indicates that the convergence rate of the alternating optimization (Algorithm–1) could be somewhat slow. Nevertheless, it is favorable that the effective range of each entry's phase in the RF precoder matrix is* $[0, 2\pi)$*. Thus finding a locally optimal solution in an acceptable time span is still promising. Moreover, we can dynamically adjust the phase increment threshold* $\bar{\delta}^{(k)}$ *to accelerate the convergence of the iterations while guaranteeing the precision of the solution*[3]*.*

Considering that the Hadamard product calculation in (2.19) is not intuitive in terms of convex optimization, we further decouple (2.19) into N_t sub-problems where only linear combination is performed in the Frobenius norm. Denote the p-th row of $\mathbf{Q}^{(k)}$ as $\mathbf{q}_p^{(k)}$, and the objective function of problem (2.19) is equivalent to

$$\begin{aligned} &\sum_{p=1}^{N_t} \left|\left|\mathbf{q}_p^{(k)} - \left[\frac{j\delta_{p,1}^{(k)}}{\sqrt{N_t}}e^{j\phi_{p,1}^{(k)}}, \cdots, \frac{j\delta_{p,N_t}^{(k)}}{\sqrt{N_t}}e^{j\phi_{p,N_t}^{(k)}}\right]\mathbf{F}_B^{(k)}\right|\right|_2^2 \\ =&\sum_{p=1}^{N_t} \left|\left|\mathbf{q}_p^{(k)} - \mathbf{\Delta}_p^{(k)}\mathbf{G}_p^{(k)}\right|\right|_2^2, \end{aligned} \tag{2.20}$$

where $\mathbf{\Delta}_p^{(k)} = [\delta_{p,1}^{(k)}, \delta_{p,2}^{(k)}, \cdots, \delta_{p,N_t}^{(k)}]$ and $\mathbf{G}_p^{(k)} = \frac{j}{\sqrt{N_t}}\mathbf{diag}\left(e^{j\phi_{p,1}^{(k)}}, \cdots, e^{j\phi_{p,N_t}^{(k)}}\right)\mathbf{F}_B^{(k)}$. Note

[3]The dynamic $\bar{\delta}^{(k)}$ will be explained in Section 2.2.1.

that

$$\begin{aligned}&\min_{\{\delta_{m,n}^{(k)}\}} \sum_{p=1}^{N_t} \left|\left|\mathbf{q}_p^{(k)} - \boldsymbol{\Delta}_p^{(k)}\mathbf{G}_p^{(k)}\right|\right|_2^2 \\ =&\sum_{p=1}^{N_t} \min_{\boldsymbol{\Delta}_p^{(k)}} \left|\left|\mathbf{q}_p^{(k)} - \boldsymbol{\Delta}_p^{(k)}\mathbf{G}_p^{(k)}\right|\right|_2^2,\end{aligned} \tag{2.21}$$

and there is no cross-term of $\boldsymbol{\Delta}_p^{(k)}, p = 1, \cdots, N_t$ among all the constraints of (2.19). Hence, we can obtain the solution of the problem (2.19) by equivalently solving N_t sub-problems corresponding to $p = 1, 2, \cdots, N_t$

$$\begin{aligned}&\min_{\boldsymbol{\Delta}_p^{(k)}} \quad \left|\left|\mathbf{q}_p^{(k)} - \boldsymbol{\Delta}_p^{(k)}\mathbf{G}_p^{(k)}\right|\right|_2^2 \\ &s.t.\ |\delta_{p,n}^{(k)}| \leq \bar{\delta}^{(k)}, \forall n,\end{aligned} \tag{2.22}$$

which is exactly a general quadratic programming problem with linear constraints, and can be directly solved, e.g., by interior point method [25]. Finally, all $\boldsymbol{\Delta}_p^{(k)}$'s obtained through (2.22) can be grouped into the phase increment matrix $\{\delta_{m,n}\}$ for updating the RF precoder according to (2.16).

Choosing the Initial Point

Until now, we have converted a non-convex problem into an approximated convex one, which can be solved by the alternating iterations in Algorithm–1. On the other hand, the original optimizatin problem (2.10) may have multiple local minimizers so that one arbitrary initial point may lead to a local minimizer (one of the closest local minimizers to the initial point) with unacceptable performance. Hence, we need to select one initial point which is potentially close to the global solution (the minimizer that makes the $||\mathbf{F}^\star - \mathbf{F}_R\mathbf{F}_B||_F$ smallest), by which the global solution will be located with relatively high probability.

When the constant amplitude constraint of $\mathbf{F}_R$ is not considered, the perfect decomposition of $\mathbf{F}^\star$ can be performed through SVD decomposition $\mathbf{F}^\star = \mathbf{U}_F\boldsymbol{\Sigma}_F\mathbf{V}_F^H$. We want to generate the initial point of the matrix decomposition based on the SVD of $\mathbf{F}^*$. As the optimal unconstrained RF precoder $\mathbf{F}^\star$ comes from the first M_t right singular vectors of the channel matrix $\mathbf{H}$, $\mathbf{F}^\star$ has the full column rank, which means all N_s entries along the diagonal of $\boldsymbol{\Sigma}_F$ are non-zero. Note that $\mathbf{U}_F\boldsymbol{\Sigma}_F$ is an $N_t \times N_s$ matrix with full column rank, $\mathbf{V}_F^H$ is an $N_s \times N_s$ matrix and $\mathbf{F}_R$ consists of N_t^{RF} columns. To deal with the dimension issue of the matrix decomposition problem, we

generate an $N_t \times (M_t - N_S)$ matrix $\hat{\mathbf{F}}_R$ where the amplitude of each entry is equal to $\frac{1}{\sqrt{N_t}}$ and the phase of each entry follows a uniform distribution over $[0, 2\pi)$. Then one decomposition of $\mathbf{F}^\star$ can be presented as

$$\mathbf{F}^\star = [\mathbf{U}_F\mathbf{\Sigma}_F \quad \hat{\mathbf{F}}_R] \begin{bmatrix} \mathbf{V}_F^H \\ \mathbf{0} \end{bmatrix}. \tag{2.23}$$

Therefore, ($\mathbf{F}_R = [\mathbf{U}_F\mathbf{\Sigma}_F \quad \hat{\mathbf{F}}_R]$, $\mathbf{F}_B = [\mathbf{V}_F \quad \mathbf{0}]^H$) is exactly one global solution for $\min ||\mathbf{F}^\star - \mathbf{F}_R\mathbf{F}_B||$ without any constraint. It should be pointed out that $\mathbf{F}_R = [\mathbf{U}_F\mathbf{\Sigma}_F \quad \hat{\mathbf{F}}_R]$ is infeasible when the constant amplitude constraint of $\mathbf{F}_R$ is reconsidered. Nevertheless, we can select one feasible initial point $\mathbf{F}_R^{(0)}$ that is close to the above $[\mathbf{U}_F\mathbf{\Sigma}_F \quad \hat{\mathbf{F}}_R]$ by applying some modifications on the first partition $\mathbf{U}_F\mathbf{\Sigma}_F$ as follows,

1) keeping the phases of all entries in $\mathbf{U}_F\mathbf{\Sigma}_F$;

2) enforcing the amplitudes of all the entries in $\mathbf{U}_F\mathbf{\Sigma}_F$ into $\frac{1}{\sqrt{N_t}}$ to make $\mathbf{F}_R^{(0)}$ feasible.

Since the modified $\mathbf{U}_F\mathbf{\Sigma}_F$ still incorporates the information of the phases in the perfect decomposition (2.23), we believe that the generated $\mathbf{F}_R^{(0)}$ is probably near the global solution for the constrained decomposition problem (2.13) and choose it as the initial point for Algorithm–1.

Dynamic Threshold for the Phase Increment

As we mentioned, the phase increment $\delta_{m,n}^{(k)}$ for each entry in $\mathbf{F}_R^{(k)}$, upper bounded by the threshold $\bar{\delta}^{(k)}$, should be sufficiently small so that the approximation $e^{j\delta_{m,n}^{(k)}} \approx 1 + j\delta_{m,n}^{(k)}$ holds. However, this requirement will make Algorithm–1 converge very slowly since it only allows slight change in $\mathbf{F}_R^{(k)}$. To accelerate the convergence rate, we dynamically change the upper bound of the phase increment $\bar{\delta}^{(k)}$ so that the iterations can converge quickly while the precision of the solution is guaranteed. The dynamic $\bar{\delta}^{(k)}$ can be realized through

1) setting a $\bar{\delta}^{(k+1)}$ slightly larger than $\bar{\delta}^{(k)}$ when the error indicator ϵ_k is still far greater than $\bar{\epsilon}$, and $\epsilon_k < \epsilon_{k-1}$ holds;

2) setting a smaller $\bar{\delta}^{(k+1)}$ than $\bar{\delta}^{(k)}$ when the error indicator ϵ_k is close to $\bar{\epsilon}$, or $\epsilon_k \geq \epsilon_{k-1}$ holds.

The above 1) allows the larger phase increment while Algorithm–1 converges in the right direction (ϵ_k is deceasing), and 2) diminishes the $\bar{\delta}^{(k)}$ to a smaller $\bar{\delta}^{(k+1)}$ when ϵ_k increases due to that the previous large phase increment destroys the approximation $e^{j\delta_{m,n}^{(k)}} \approx 1 + j\delta_{m,n}^{(k)}$, or when ϵ_k is close to the required $\bar{\epsilon}$ which means higher precision is required. The specific adjustment on $\bar{\delta}^{(k)}$ will be shown in Section 2.3.

2.2.2 Hybrid Combiners Design

The hybrid precoders are designed by assuming that the N_r–dimensional minimum distance decoding can be performed at the receiver. However, such a decoding scheme is hard to be implemented in the practical system due to its high complexity. In this chapter, we employ the linear combining at the receiver side. As we know, if the hybrid precoders can be equivalent to the unconstrained optimal precoder $\mathbf{F}^\star = \mathbf{V}_1$, the optimal unconstrained combiner $\mathbf{W}^\star$ should be $\mathbf{U}_1$, to which the hybrid combiners $(\mathbf{W}_R, \mathbf{W}_B)$ aim to approach. Note that the error $||\mathbf{F}^\star - \mathbf{F}_R\mathbf{F}_B||_F$ could not be absolutely zero, and $\mathbf{U}_1$, hence, may deviate from the optimal unconstrained combiner $\mathbf{W}^\star$ corresponding to the obtained hybrid precoders $(\mathbf{F}_R, \mathbf{F}_B)$. In this situation, the linear MMSE combiner $\mathbf{W}_{MMSE}$ will achieve the maximum spectral efficiency when only linear combination is performed before detection and only 1-dimensional detection is allowed for each data stream. The unconstrained linear MMSE combiner is given in [26] as

$$\begin{aligned}
\mathbf{W}^\star &= \mathbf{W}_{MMSE} \\
&= \arg\min_{\mathbf{W}} \ \mathbb{E}\left[||\mathbf{s} - \mathbf{W}\mathbf{y}||_2\right] \\
&= \frac{\sqrt{P}}{N_s}\left(\frac{P}{N_s}\mathbf{H}\mathbf{F}_R\mathbf{F}_B\mathbf{F}_B^H\mathbf{F}_R^H\mathbf{H}^H + \sigma^2\mathbf{I}_{N_r}\right)^{-1}\mathbf{H}\mathbf{F}_R\mathbf{F}_B.
\end{aligned} \tag{2.24}$$

Once $\mathbf{W}^\star$ is obtained, the alternating optimization method presented in Section 2.2.1 can be directly applied in its decomposition, which is characterized as the problem

$$\begin{aligned}
\min_{\mathbf{W}_R, \mathbf{W}_B} \ & ||\mathbf{W}^\star - \mathbf{W}_R\mathbf{W}_B||_F \\
s.t. \ & \mathbf{W}_R \in \mathcal{W}_R.
\end{aligned} \tag{2.25}$$

By far, given any massive MIMO channel $\mathbf{H}$, the design of hybrid precoders and combiners $(\mathbf{F}_R, \mathbf{F}_B, \mathbf{W}_R, \mathbf{W}_B)$ can be fulfilled through the above matrix decomposition based on the alternating optimization method. We will further evaluate the

performance of our proposed hybrid precoding scheme through simulation in Section 2.3.

2.2.3 Approach To Waterfilling Spectral Efficiency

For an capacity-achieving processing scheme, the waterfilling power allocation should also be applied to the precoder. In this case, the optimal unconstrained precoder and combiner in Section 2.2 can be updated to $\mathbf{F}^\star = \mathbf{V}_1\mathbf{\Gamma}$ and $\mathbf{W}^\star = \mathbf{U}_1$, where $\mathbf{\Gamma}$ is a diagonal matrix that performs the waterfilling power allocation. Then, such a precoder can directly be decomposed through Algorithm-1. However, there may be cases where no power is allocated to some data streams corresponding to the lowest singular values of $\mathbf{H}$, especially when the SNR is small. In other words, $\mathbf{F}^* = [\mathbf{F}', \mathbf{0}]$, where $\mathbf{F}'$ is the non-zero columns of $\mathbf{F}^\star = \mathbf{V}_1\mathbf{\Gamma}$ after waterfilling power allocation. In this case, we can applied the MD-HP scheme to the $\mathbf{F}'$ part first, $\mathbf{F}' = \mathbf{F}_R\mathbf{F}'_B$. And then the whole decomposition for $\mathbf{F}^*$ is given by $\mathbf{F}^* = [\mathbf{F}', \mathbf{0}] = [\mathbf{F}_R\mathbf{F}'_B, \mathbf{0}] = \mathbf{F}_R[\mathbf{F}'_B, \mathbf{0}] = \mathbf{F}_R\mathbf{F}_B$, which means the zero-power allocation part is realized through the baseband precoding rather than the phase shift in the RF domain.

2.2.4 Quantized RF Phase Control

Consider that the phase of each entry in the RF precoder $\mathbf{F}_R$ or combiner $\mathbf{W}_R$ is difficult to be set to be an arbitrary value due to the limited precision in the practical implementation. Therefore, we also introduce the quantized phase implementation of $\mathbf{F}_R$ and $\mathbf{W}_R$. Assume the phase of each entry in $\mathbf{F}_R$ and $\mathbf{W}_R$ can be quantized up to L bits of precision through choosing the closet neighbor based on the shortest Euclidean distance, given by

$$\phi = \frac{2\pi\bar{n}}{2^L}, \tag{2.26}$$

where $\bar{n} = \arg\min_{n\in\{0,\cdots,2^L-1\}} \left|\phi - \frac{2\pi n}{2^L}\right|$.

2.3 Simulation Results

In this section, we evaluate the convergence of our matrix decomposition method based on alternating optmization as well as the performance of the proposed MD-HP scheme through simulation.

2.3.1 Convergence Properties of Algorithm–1

Before we apply Algorithm–1 to design the hybrid precoders and combiners, it is necessary to examine whether it can converge to a level where the error ϵ_k is acceptably small, since the original optimization problem (2.10) to be solved is non-convex and there is no guarantee that Algorithm–1 will certainly result in a well-performed matrix decomposition.

We take a 256×64 MIMO system as example,, and set $N_s = 4$, $M_t = 6$. An i.i.d Rayleigh fading channel matrix $\mathbf{H}_{rl}$ where each entry follows $\mathcal{CN}(0,1)$ is randomly generated. According to Section 2.2.1, the optimal unconstrained precoder $\mathbf{F}^\star$ is obtained by selecting the first N_s right singular vectors based on the SVD decomposition on $\mathbf{H}_{rl}$. And the choice of initial RF precoder $\mathbf{F}_R^{(0)}$ is given in Section 2.2.1. Furthermore, the error detecting threshold $\bar{\epsilon} = 10^{-5}$ and the first phase increment threshold $\bar{\delta}^{(1)} = 0.1$. We examine two kinds of options for $\bar{\delta}^{(k)}$ in the simulation:

1) $\bar{\delta}^{(k)} = 0.1, \ \forall k$;

2) $\bar{\delta}^{(k)} = \begin{cases} 1.25 \cdot \bar{\delta}^{(k-1)}, \ \text{when } |\epsilon_{k-1} - \epsilon_{k-2}| > 100 \cdot \bar{\epsilon} \\ 0.8 \cdot \bar{\delta}^{(k-1)}, \ \text{when } |\epsilon_{k-1} - \epsilon_{k-2}| \leq 100 \cdot \bar{\epsilon} \end{cases}$.

For option 2) with the dynamic phase increment threshold, the adjustment of $\bar{\delta}^{(k)}$ depends on how close the previous two error indicators are. When the difference of the previous error indicators is smaller than $100 \cdot \bar{\epsilon}$, which means Algorithm–1 is going to converge, $\bar{\delta}^{(k)}$ should be reduced to enhance the precision of the solution by guaranteeing the effectiveness of the approximation $e^{j\delta_{m,n}^{(k)}} \approx 1 + j\delta_{m,n}^{(k)}$. Otherwise, $\bar{\delta}^{(k)}$ can be augmented to accelerate the algorithm by enlarging the feasible region of (2.19). Moreover, we need to decrease $\bar{\delta}^{(k)}$ whenever $\epsilon_{k-1} > \epsilon_{k-2}$ which means the previous $\bar{\delta}^{(k-1)}$ is too large to guarantee $e^{j\delta_{m,n}^{(k)}} \approx 1 + j\delta_{m,n}^{(k)}$. Finally, we restrict $\bar{\delta}^{(k)} \in [0.1, 0.5]$ by clamping $\bar{\delta}^{(k)}$ to 0.1 (0.5) when it is smaller (larger) than 0.1 (0.5) in case that the feasible region for (2.19) is too small or too large[4].

To examine the effectiveness of the approximation $e^{j\phi_{m,n}^{(k+1)}} = e^{j(\phi_{m,n}^{(k)} + \delta_{m,n}^{(k)})} \approx (1 + j\delta_{m,n}^{(k)})e^{j\phi_{m,n}^{(k)}}$, we compare two traces of $e^{j(\phi_{m,n}^{(k)} + \delta_{m,n}^{(k)})}$ and $(1 + j\delta_{m,n}^{(k)})e^{j\phi_{m,n}^{(k)}}$ within 100 iterations in Fig. 2.2, where the red dash line indicates the unit circle on the complex plane. It is shown that the points of the two traces ($m = 1, n = 5$) update simultaneously and the corresponding two points are close enough, which means the iteration $e^{j\phi_{m,n}^{(k+1)}} = e^{j(\phi_{m,n}^{(k)} + \delta_{m,n}^{(k)})}$ can be safely considered as a linear operation over $\delta_{m,n}^{(k)}$. By

[4]All parameters given in this section can be revised for other specific cases

applying the dynamic $\bar{\delta}^{(k)}$, $e^{j\phi_{m,n}^{(k)}}$ updates by relatively large step size at the beginning when it is far from the solution $e^{-j1.0026} \approx 0.5381 - j0.8429$, and then slowly converges to it. In Fig. 2.3, we show how the error indicator ϵ_k converges to about 0.2 as the number of iterations increases when the dynamic and static $\bar{\delta}^{(k)}$ are applied respectively. It can be observed that the dynamic threshold $\bar{\delta}^{(k)}$ helps the algorithm converge more quickly since the solution for (2.19) is searched in a larger feasible region when the error ϵ_k is relative small. The above parameters for Algorithm–1 will continue to be used in the following simulations.

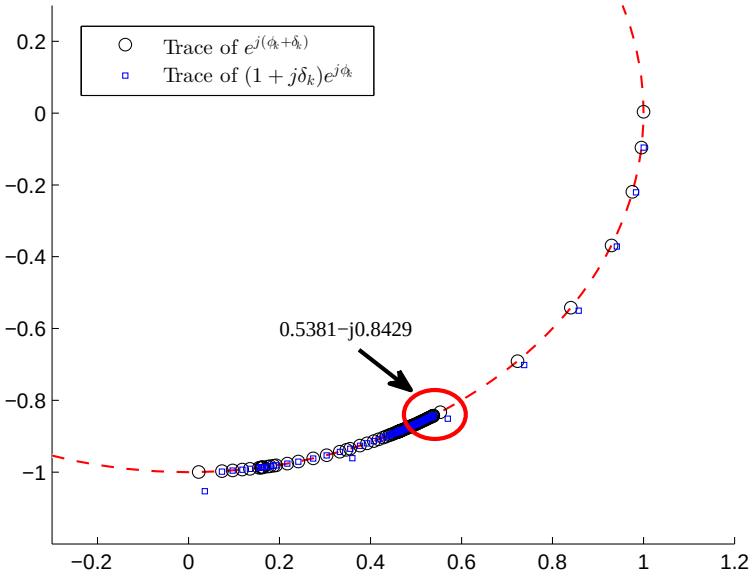

Figure 2.2: The traces of $e^{j(\phi_{m,n}^{(k)}+\delta_{m,n}^{(k)})}$ and $(1+j\delta_{m,n}^{(k)})e^{j\phi_{m,n}^{(k)}}$ on the complex plane.

2.3.2 Spectral Efficiency Evaluation

In the simulations of this section, we illustrate the spectral efficiency performance of our proposed MD-HP scheme by comparing it with others under the large i.i.d. Rayleigh channel and mmWave channel settings respectively. The SNR $\gamma = \frac{P}{\sigma^2}$ range is set to be from -40 dB to 0 dB in all simulations.

Large i.i.d Rayleigh Fading Channels

The MD-HP scheme is compared in Fig. 2.4 against the optimal unconstrained SVD based processing scheme when $N_s = 8$ data streams are transmitted in the 256×64 massive MIMO system. For the MD-HP scheme, the situations of using 8 and 12

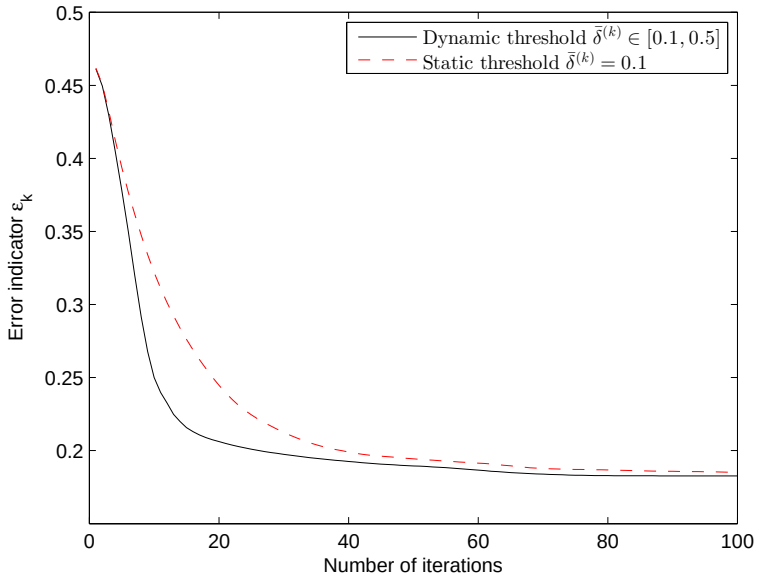

Figure 2.3: The convergence performance of Algorithm–1 when applying the dynamic and static $\bar{\delta}^{(k)}$ respectively

RF chains (along with their quantized versions) are examined. When 12 RF chains are implemented at both the transmitter and receiver, the performance of the MD-HP scheme is near-optimal compared with the optimal unconstrained SVD based scheme. Even though we reduce the number of the RF chains to the number of the data streams, namely, 8 RF chains are employed, the spectral efficiency achieved by the MD-HP scheme slightly decreases by around 3 bps/Hz. As for the heavily quantized versions ($L = 2$ bits with the phase candidates $\{0, \pm\frac{\pi}{2}, \pi\}$) corresponding to the 8 and 12 RF chains settting, the spectral efficiency only suffers less than 1 dB loss, which is basically acceptable in the practical implementation. Fig. 2.5 further demonstrates the spectral efficiency performance by also setting the number of transmit data streams to 4 while 8 RF chains are used. Compared with the case of 4 transmit data streams, the performance of the 8 data stream case is evidently improved thanks to the multiplexing gain. Notably, there is a small gap between the MD-HP scheme and the SVD based scheme which can be eliminated by properly increasing the number of RF chains, e.g. double the number of the data streams in the case of $N_s = 4$. In addition, the quantized versions ($L = 2$) also results in less than 1 dB loss in the performance.

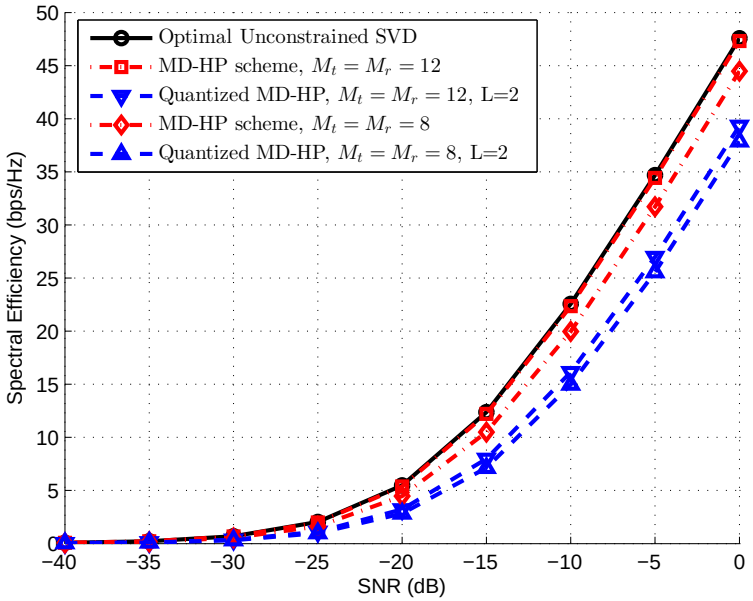

Figure 2.4: Spectral efficiency achieved by different processing schemes of a 256×64 massive MIMO system in i.i.d. Rayleigh fading channels where $N_s = 8$ data streams are transmitted through 8 and 12 RF chains respectively.

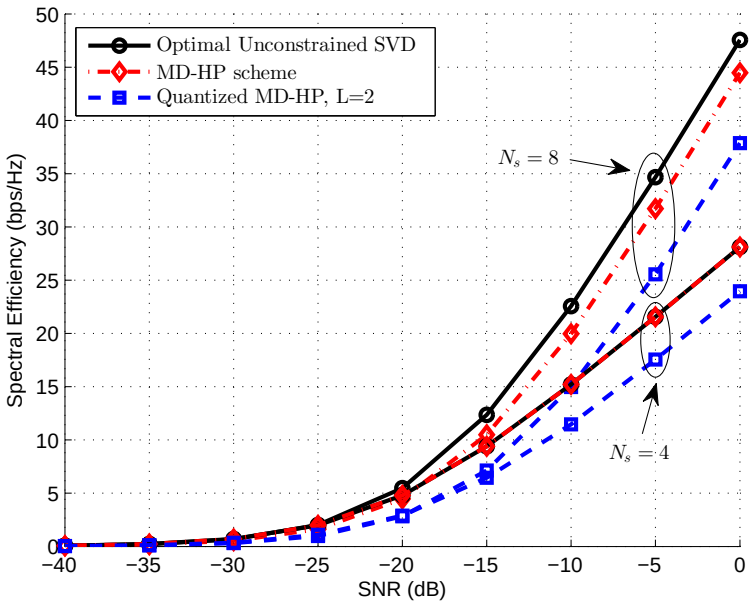

Figure 2.5: Spectral efficiency achieved by different processing schemes of a 256×64 massive MIMO system in i.i.d. Rayleigh fading channels where $N_s = 4$ and 8 data streams are transmitted through 8 RF chains respectively.

Large mmWave Channels

Our proposed MD-HP scheme can also be applied to the large mmWave channels where a certain number of hybrid processing schemes have been studied in the lit-

erature. In the simulation, the clustered mmWave channel model (2.4) is adopted to characterize its limited scattering feature. Apart from the unconstrained SVD based processing and our MD-HP schemes, we introduce the spatially sparse processing which designed the hybrid precoders/combiners by capturing the characteristics of the dominant paths. The propagation model mainly follows the settings in [14]: 1) the mmWave channel incorporates $N_c = 8$ clusters, each of which has $N_p = 10$ paths; 2) the transmitter angle sector is assumed to be 60°-wide in the azimuth while the receiver with a smaller omni-directional antenna array; 3) the angle spreads of the transmitter and receiver σ_θ and σ_ϕ are all set to be 7.5°; 4) the antenna spacing d is equal to half-wavelength. In Fig. 2.6, the spectral efficiency performance is demonstrated in the 256×64 mmWave MIMO system, where $N_s = 8$ data streams are transmitted through 8 or 12 RF chains. Our proposed MD-HP scheme apparently outperforms the spatially sparse processing scheme when the same number of RF chains are implemented. Moreover, the MD-HP scheme can even achieve higher spectral efficiency with only 8 RF chains than the spatially sparse processing scheme with 12 RF chains. Particularly, the SVD based processing is sufficiently approached by the MD-HP scheme given 12 RF chains. It is shown that our proposed MD-HP scheme can better capture the characteristics of the mmWave channel than the spatially sparse processing scheme.

2.4 Summary

In this chapter, we design the hybrid RF and baseband precoders/combiners for multi-stream transmission in P2P massive MIMO systems via solving a non-convex matrix decomposition problem. Based on the alternating optimization technique, we transfer the non-convex matrix decomposition into a series of convex sub-problems and effectively solve by restricting the phase increments of the RF precoder within a small range at each iteration. The near-optimal hybrid precoders/combiners are located by choosing an appropriate initial point using SVD technique. The MD-HP scheme can be applied in any general massive MIMO channels. By providing enough number of RF chains (double the number of the transmit data streams), the pre-designed unconstrained digital precoder/combiner of a large dimension can be sufficiently approached and thus the near-optimal performance is achieved. We aim to incorporate channel estimation issue and reduce the time complexity of the MD-HP scheme in the future.

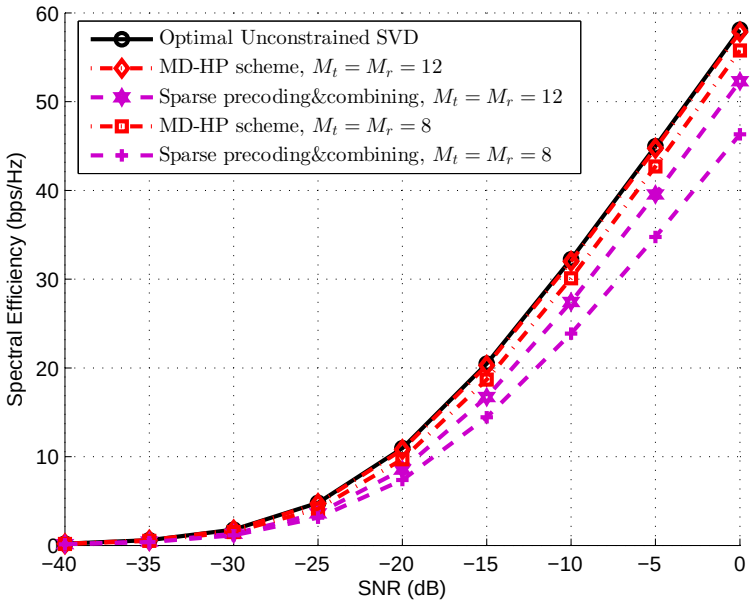

Figure 2.6: Spectral efficiency achieved by different processing schemes of a 256×64 massive MIMO system in mmWave channels where $N_s = 8$ data streams are transmitted through 8 and 12 RF chains respectively.

Chapter 3

Hybrid Block Diagonalization for Massive Multiuser MIMO Systems

To realize the tremendous capacity target of the next generation mobile cellular systems, one promising option is scaling up to massive multiple-input multiple-output (MIMO) systems [1]-[2]. Chapter 2 has developed the near-optimal hybrid processing scheme in massive P2P MIMO systems, and we further investigated the processing scheme in the massive multiuser MIMO (MU-MIMO) scenario in this chapter. As the previous chapter mentioned, in the massive MU-MIMO systems, some simple linear pre/post-processing (transmit precoding/receive combining) schemes, such as zero-forcing (ZF) and linear minimum mean-square error (MMSE), are able to approach the optimal capacity performance achieved by the dirty paper coding (DPC) as the number of antennas goes to infinity [5]. Moreover, the ZF processing that cancels the inter-user interference through channel inversion can be generalized as block diagonalization (BD) when the base stations (BSs) and mobile stations (MSs) are both equipped with multiple antennas [28]. For the downlink spatial multiplexing in MU-MIMO systems, the BD method achieves sub-optimal capacity performance; however, it reduces the complexity of the transmitter and receiver structures by providing closed-form precoder and combiner solutions.

In massive MIMO systems, the large array gain is rendered by a massive number of antennas at the order of a hundred or more [3]. Conventionally pre-processing is performed through modifying the amplitudes and phases of the complex transmit symbols at the baseband and then upconverted to the passband after passing through radio frequency (RF) chains (including the digital-to-analog conversion, signal mixing

and power amplifying), which requires that the number of the RF chains is in the range of hundreds, equal to the number of the antenna elements. Post-processing is similar involving a large number of analog receive RF chains and digital baseband operations. This leads to unacceptably high implementation cost and energy consumption.

Here, we re-enter the literature review on the massive MIMO system designs with a limited number of RF chains that are enabled by the cost-effective variable phase shifters [10]-[17]. The analog RF processing provides the high-dimensional phase-only control while the digital baseband processing can be performed in a very low dimension, termed as hybrid processing. Under the limited RF chains constraint, references [9] and [10] investigate the hybrid processing schemes in the point-to-point (P2P) MIMO systems. A single-stream communication under the Rayleigh fading MIMO channels achieves the full diversity order through the equal gain transmission/combining (EGT/EGC) in [10], while the multiple-stream transmission under MIMO channels is proposed in [9]. In addition, [8] and [12] implement the hybrid processing to the downlink of the massive MU-MIMO systems with single-antenna users. In [8], the near-optimal capacity performance, compared to the full-complexity systems, is achieved through the ZF baseband precoding combined with the ECT processing in the RF domain. Note that this technique also works for the millimeter wave (mmWave) channel. In [12], the phase-only RF precoding are employed to maximize the minimum average data rate of users via a bi-convex approximation approach. In mmWave communications systems, it is likely to build a large antenna array in a compact region and apply hybrid processing technique [13]-[17]. The "dominant" paths in P2P mmWave channels are captured through the hybrid processing in [13] and [14], where the former considers the single-stream transmission while the latter enables the multiple-stream communication. [14] presents a hybrid processing by decomposing the optimal precoding/combining matrix via orthogonal matching pursuit with the transmit/receive array response vectors as the basis vectors. Reference [13] can be regarded as a special one-RF-chain case of reference [14]. On the other hand, in the mmWave MU-MIMO systems, reference [16] considers the single-antenna users and designs the analog RF precoding based on the transmit beam directions, while the digital processing (matched filter, zero-forcing or Wiener filter) performs on the baseband equivalent channels. With the multiple-antenna users, some baseband processing schemes such MMSE and BD are examined in [17], which, however, neglects the design of the analog RF processing.

In this chapter, we consider the downlink communication of a massive MU-MIMO

system where the BS and all MSs have multiple antennas. With a limited number of RF chains, the hybrid processing is applied to both BS and MSs as an alternative to the traditional high-cost full dimensional RF and baseband processing. We propose to utilize the RF precoding and combining to harvest the large array gain provided by the large number of antennas in the massive MU-MIMO channels, which shares the similar objective with the above references that study the hybrid processing in the MU-MIMO systems. However, the analog RF processing design for the MU-MIMO systems with multiple-antenna MSs accommodating multiple data streams per MS is not available in the literature and the novel BS RF precoder design is based on a newly defined "aggregate intermediate channel". More specifically, the RF combiners of all the MSs are obtained by selecting some of the discrete Fourier transform (DFT) bases, while the RF precoder of the BS is designed by extracting the phases of the conjugate transpose of the aggregate intermediate channel which incorporates the MS RF combiners and the original downlink channels. With the designed RF precoder and combiners, a low-dimensional BD processing can be performed at the baseband to cancel the inter-user interference, and the whole operation is named the hybrid BD (Hy-BD) scheme. Simulation results demonstrate that the proposed Hy-BD scheme achieves a capacity performance that is quite close to, sometimes even higher than, that of the full-complexity BD scheme in [28] with a lower implementation and computational cost. The Hy-BD scheme is also examined in the mmWave MU-MIMO communication channels and compared to the spatially sparse precoding/combining method [14] initially proposed for SU-MIMO but extended to MU-MIMO in this chapter.

3.1 System Model

3.1.1 System Model

We consider the downlink communication of a massive multiuser MIMO system shown in Fig. 3.1, where a base station with N_{BS} antennas and M_{BS} RF chains is assumed to schedule K mobile stations. Each MS is equipped with N_{MS} antennas and M_{MS} RF chains to support N_S data streams, which means total KN_S data streams are handled by the BS. To guarantee the effectiveness of the communication carried by the limited number of RF chains, the number of the transmitted steams is constrained by $KN_S \leq M_{BS} \leq N_{BS}$ for the BS and $N_S \leq M_{MS} \leq N_{MS}$ for each MS.

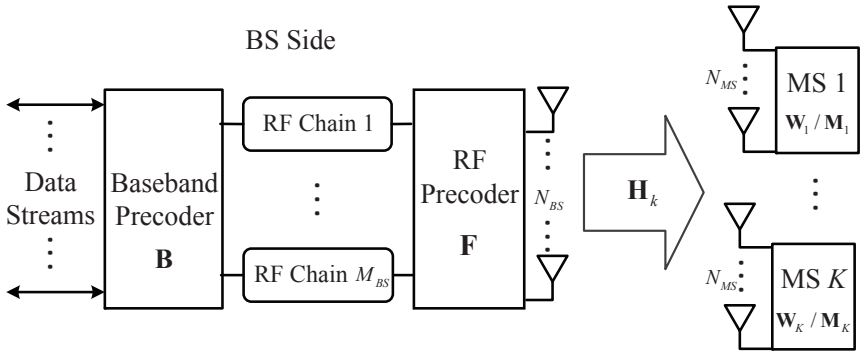

Figure 3.1: System diagram of a massive MU-MIMO system with hyrbid processing structure.

At the BS, the transmitted symbols are assumed to be processed by a baseband precoder $\mathbf{B}$ of dimension $M_{BS} \times KN_S$ and then by an RF precoder $\mathbf{F}$ of dimension $N_{BS} \times M_{BS}$. Notably, the baseband precoder $\mathbf{B}$ enables both amplitude and phase modification, while only phase changes (phase-only control) can be realized by $\mathbf{F}$ since it is implemented by using analog phase shifters. Each entry of $\mathbf{F}$ is normalized to satisfy $|\mathbf{F}^{(i,j)}| = \frac{1}{\sqrt{N_{BS}}}$, where $|\mathbf{F}^{(i,j)}|$ denotes the amplitude of the (i,j)-th element of $\mathbf{F}$. Furthermore, to meet the total transmit power constraint, $\mathbf{B}$ is normalized to satisfy $||\mathbf{FB}||_F^2 = KN_S$, where $||\cdot||_F$ the Frobenius norm.

We assume a narrowband flat fading channel model and obtain the received signal of the k-th MS

$$\mathbf{y}_k = \mathbf{H}_k\mathbf{FBs} + \mathbf{n}_k,\ k = 1, 2, \cdots, K, \tag{3.1}$$

where $\mathbf{s} \in \mathbb{C}^{KN_S \times 1}$ is the signal vector for a total of K MSs, each of which processes a $N_S \times 1$ signal vector $\mathbf{s}_k$. Namely, $\mathbf{s} = [\mathbf{s}_1^T, \mathbf{s}_2^T, \cdots, \mathbf{s}_K^T]^T$, where $(\cdot)^T$ denotes transpose. And the signal vector satisfies $\mathbb{E}[\mathbf{ss}^H] = \frac{P}{KN_S}\mathbf{I}_{KN_S}$, where $(\cdot)^H$ denotes conjugate transpose, $\mathbb{E}[\cdot]$ denotes expectation, P is the average transmit power and $\mathbf{I}_{KN_S}$ is the $KN_S \times KN_S$ identity matrix. $\mathbf{H}_k \in \mathbb{C}^{N_{MS} \times N_{BS}}$ is the channel matrix for the k-th MS with $\mathbb{E}[||\mathbf{H}_k||_F^2] = N_{BS}N_{MS}$, and $\mathbf{n}_k$ is the $N_{MS} \times 1$ vector of i.i.d. $\mathcal{CN}(0, \sigma^2)$ additive complex Gaussian noise. And the processed received signal at the k-th MS after combining is given by

$$\tilde{\mathbf{y}}_k = \mathbf{M}_k^H\mathbf{W}_k^H\mathbf{H}_k\mathbf{FBs} + \mathbf{M}_k^H\mathbf{W}_k^H\mathbf{n}_k,\ k = 1, 2, \cdots, K, \tag{3.2}$$

where $\mathbf{W}_k$ is the $N_{MS} \times M_{MS}$ RF combining matrix and $\mathbf{M}_k$ is the $M_{MS} \times N_S$ baseband combining matrix for the k-th MS. Since $\mathbf{W}_k$ is also implemented by the

analog phase shifters, all elements of $\mathbf{W}_k$ should have the constant amplitude such that $|\mathbf{W}_k^{(i,j)}| = \frac{1}{\sqrt{N_{MS}}}$. We define an equivalent baseband channel for each MS as

$$\tilde{\mathbf{H}}_k = \mathbf{W}_k^H \mathbf{H}_k \mathbf{F},\ k = 1, 2, \cdots, K, \tag{3.3}$$

and the entire equivalent multiuser baseband channel can be denoted as

$$\mathbf{H}_{eq} = \begin{bmatrix} \tilde{\mathbf{H}}_1 \\ \tilde{\mathbf{H}}_2 \\ \vdots \\ \tilde{\mathbf{H}}_K \end{bmatrix} = \begin{bmatrix} \mathbf{W}_1^H & \mathbf{0} & \cdots & \mathbf{0} \\ \mathbf{0} & \mathbf{W}_2^H & \cdots & \mathbf{0} \\ \vdots & \vdots & \ddots & \vdots \\ \mathbf{0} & \mathbf{0} & \cdots & \mathbf{W}_K^H \end{bmatrix} \begin{bmatrix} \mathbf{H}_1 \\ \mathbf{H}_2 \\ \vdots \\ \mathbf{H}_K \end{bmatrix} \mathbf{F}. \tag{3.4}$$

Then the processed received signal at the k-th MS can also be represented as

$$\begin{aligned} \tilde{\mathbf{y}}_k = \mathbf{M}_k^H \tilde{\mathbf{H}}_k \mathbf{B}_k \mathbf{s}_k + \underbrace{\sum_{i=1, i\neq k}^{K} \mathbf{M}_k^H \tilde{\mathbf{H}}_k \mathbf{B}_i \mathbf{s}_i}_{\text{interference}} \\ + \underbrace{\mathbf{M}_k^H \mathbf{W}_k^H \mathbf{n}_k}_{\text{noise}},\ k = 1, 2, \cdots, K, \end{aligned} \tag{3.5}$$

where $\mathbf{B}_k$ is the $((k-1)N_S + 1)$-th to the (kN_S)-th columns of $\mathbf{B}$, corresponding to the baseband precoding for $\mathbf{s}_k$. When the Gaussian symbols are used by the BS, the long-term average spectral efficiency achieved will be

$$R = \sum_{k=1}^{K} \log_2 \left(\left| \mathbf{I}_{N_S} + \frac{P}{KN_S} \mathbf{R}_i^{-1} \mathbf{M}_k^H \tilde{\mathbf{H}}_k \mathbf{B}_k \mathbf{B}_k^H \tilde{\mathbf{H}}_k^H \mathbf{M}_k \right| \right), \tag{3.6}$$

where $\mathbf{R}_i = \frac{P}{KN_S} \sum_{i=1, i\neq k}^{K} \mathbf{M}_k^H \tilde{\mathbf{H}}_k \mathbf{B}_i \mathbf{B}_i^H \tilde{\mathbf{H}}_k^H \mathbf{M}_k + \sigma^2 \mathbf{M}_k^H \mathbf{W}_k^H \mathbf{W}_k \mathbf{M}_k$ is the covariance matrix of both interference and noise.

3.1.2 Channel Model

In this chapter, based on a general channel matrix set $\mathbf{H} = [\mathbf{H}_1^T, \mathbf{H}_2^T, \cdots, \mathbf{H}_K^T]^T$, we aim to seek the BS hybrid precoders ($\mathbf{F}$, $\mathbf{B}$) and the hybrid combiners ($\mathbf{W}_k$, $\mathbf{M}_k$)'s for all K MSs through the Hy-BD scheme, which achieves a sub-optimal spectral efficiency for massive MU-MIMO systems by perfectly canceling the inter-user interference. Two kinds of channel models are considered in this chapter:

1) large i.i.d. Rayleigh fading channel $\mathbf{H}_{rl}$;

2) limited scattering mmWave channel $\mathbf{H}_{mmw}$.

In the large Rayleigh fading channel, which is commonly considered in massive MU-MIMO systems, all entries of the channel matrix $\mathbf{H}_k$ for the k-th MS follow i.i.d. $\mathcal{CN}(0,1)$. On the other hand, a large antenna array is often implemented in mmWave communications to combat the high free-space pathloss [13]-[16]. We adopt the clustered mmWave channel model to characterize the limited scattering feature of the mmWave channel. The mmWave downlink channel for the k-th MS $\mathbf{H}_k$ is assumed to be the sum of all propagation paths that are scattered in N_c clusters and each cluster contributes N_p paths, which can be expressed as

$$\mathbf{H}_k = \sqrt{\frac{N_{BS}N_{MS}}{N_c N_p}} \sum_{i=1}^{N_c} \sum_{l=1}^{N_p} \alpha_{il}^k \mathbf{a}_{MS}^k(\theta_{il}^k)\mathbf{a}_{BS}^k(\phi_{il}^k)^H, \tag{3.7}$$

where α_{il}^k is the complex gain of the i-th path in the l-th cluster, which follows $\mathcal{CN}(0,1)$. To reflect the sparsity of the mmWave channel, both of N_c and N_p should not be too large. For the (i,l)-th path, θ_{il}^k and ϕ_{il}^k are the azimuth angles of arrival/departure (AoA/AoD), while $\mathbf{a}_{MS}^k(\theta_{il}^k)$ and $\mathbf{a}_{BS}^k(\phi_{il}^k)$ are the receive and transmit array response vectors at the azimuth angles of θ_{il}^k and ϕ_{il}^k respectively, and the elevation dimension is ignored. Within the cluster i, θ_{il}^k and ϕ_{il}^k have the uniformly-distributed mean values of θ_i^k and ϕ_i^k respectively, while the lower and upper bounds of the uniform distribution for θ_i^k and ϕ_i^k can be defined as $[\theta_{\min}^k, \theta_{\max}^k]$ and $[\phi_{\min}^k, \phi_{\max}^k]$. The angle spreads (standard deviations) of θ_{il}^k and ϕ_{il}^k among all clusters are assumed to be constant, denoted as σ_θ^k and σ_ϕ^k. Finally, the truncated Laplacian distribution is employed to generate all the AoDs/AoAs for this mmWave propagation channel matrix, base on the above parameters.

The uniform linear array (ULA) is employed by the BS and MSs in our study, while the Hy-BD scheme in Section-3.2 can directly be applied to arbitrary antenna arrays. For an N-element ULA, the array response vector can be given by

$$\mathbf{a}_{ULA}(\theta) = \frac{1}{\sqrt{N}} \left[1, e^{j\frac{2\pi}{\lambda}d\sin(\theta)}, \cdots, e^{j(N-1)\frac{2\pi}{\lambda}d\sin(\theta)}\right]^T, \tag{3.8}$$

where λ is the wavelength of the carrier, and d is the distance between neighboring antenna elements. The array response vectors of the BS and MSs can be written in the form of (3.8).

3.2 Hybrid Block Diagonalization

In the MU-MIMO systems, the generalized zero-forcing method (i.e., the traditional BD scheme) is infeasible to be practically implemented due to the high cost brought by the large number of RF chains as many as the antennas. By reducing the number of RF chains $M_{BS}(M_{MS})$ to far less than the antenna elements $N_{BS}(N_{MS})$ at both the BS and MSs, we propose to utilize the RF precoding matrix $\mathbf{F}$ at the BS and the RF combining matrix $\mathbf{W}_k$ at each MS to harvest the large array gain provided by the large number of antennas in the massive MU-MIMO channel. With the found $\mathbf{F}$ and all $\mathbf{W}_k$'s, the entire multiuser equivalent baseband channel $\mathbf{H}_{eq}$ can be determined based on (3.4), which consists of all the equivalent channels for the MSs, namely $\tilde{\mathbf{H}}_k,\ k = 1, 2, \cdots, K$. Finally, a low-dimensional BD processing, involving the design of $\mathbf{B}$ and all $\mathbf{M}_k$'s, can be performed at the baseband.

3.2.1 Array Gain Harvesting

Owing to the large number of antennas in the massive MU-MIMO systems, the channel gains of the equivalent channel $\mathbf{H}_{eq}$ can be scaled up through the appropriate phase-only control at the RF domain, which is called the large array gain. To be noted, each element in $\mathbf{H}_{eq}$ represents the equivalent channel gain from one RF chain at the BS to one RF chain at one MS. To achieve the high capacity with such a hybrid processing structure, the equivalent channel matrix $\mathbf{H}_{eq}$ are desired to have the following properties:

1) Rank sufficiency: $\mathbf{H}_{eq}$ should be well-conditioned to support the multi-stream transmission, which means the rank of $\mathbf{H}_{eq}$ should be at least KN_S;

2) Large array gain: $\mathbf{H}_{eq}$ should sufficiently harvest the array gain so that it can provide as large gain for each stream transmission as possible. We propose to pursue the large array gain by enlarging the sum of the squares of the diagonal entries in $\mathbf{H}_{eq}$.

By definition, $\mathbf{H}_{eq}$ consists of the equivalent channels of all the MSs, namely $\tilde{\mathbf{H}}_k = \mathbf{W}_k^H \mathbf{H}_k \mathbf{F},\ k = 1, 2, \cdots, K$. We design the RF domain processing matrices $\mathbf{W}_k$'s and $\mathbf{F}$ and construct the equivalent channel $\mathbf{H}_{eq}$ by approximately satisfying the above two requirements, which will lead to a suboptimal performance under the hybrid precoding structure, but with significantly low complexity.

Assume that all the RF combiners $\mathbf{W}_k$'s are given (the actual design of $\mathbf{W}_k$'s will be presented shortly). Define an aggregate intermediate channel given by

$$\mathbf{H}_{int} = \begin{bmatrix} \mathbf{W}_1^H \mathbf{H}_1 \\ \vdots \\ \mathbf{W}_K^H \mathbf{H}_K \end{bmatrix}_{KM_{MS} \times N_{BS}}, \tag{3.9}$$

and then the baseband equivalent channel is $\mathbf{H}_{eq} = \mathbf{H}_{int}\mathbf{F}$. To harvest the array gain with the RF precoder $\mathbf{F}$, similar to the equal gain transmission (EGT) method proposed in [8], we perform the phase-only RF precoding by setting

$$\mathbf{F}^{(i,j)} = \frac{1}{\sqrt{N_{BS}}} e^{j\psi_{i,j}}, \tag{3.10}$$

where $\psi_{i,j}$ is the phase of the (i,j)-th element of the conjugate transpose of $\mathbf{H}_{int}$. This EGT precoding method requires $M_{BS} = KM_{MS}$ RF chains at the BS, which means $\mathbf{F}$ is an $N_{BS} \times KM_{MS}$ matrix and $\mathbf{H}_{eq}$ should be a square matrix. The entries along the diagonal of the baseband equivalent channel $\mathbf{H}_{eq}$ denote the equivalent channel gains in terms of the RF chains, while the remaining entries indicate the inter-chain interference. We focus on the large array gain design through the RF precoding/combining and leave the interference canceling to the baseband processing in the Hy-BD scheme.

Now let us return to the design of the RF combiners $\mathbf{W}_k$'s. Denote the m-th column of $\mathbf{W}_k$ as $\mathbf{w}_k^{(m)}$. As the result of the EGT precoding method, the $((k-1)M_{MS}+m)$-th diagonal entry of $\mathbf{H}_{eq}$ is then given by $||(\mathbf{w}_k^{(m)})^H \mathbf{H}_k||_1$, where $||\cdot||_1$ denotes the 1-norm of a vector, corresponding to the m-th RF chain of the k-th MS. we aim to maximize the sum of the squares of diagonal entries of the baseband equivalent channel $\mathbf{H}_{eq}$, given by $\sum_{k=1}^{K}\sum_{m=1}^{M_{MS}} ||(\mathbf{w}_k^{(m)})^H \mathbf{H}_k||_1^2$, to pursue the large array gain. Due the independence of $\mathbf{W}_k$'s for all the MSs, maximizing $\sum_{k=1}^{K}\sum_{m=1}^{M_{MS}} ||(\mathbf{w}_k^{(m)})^H \mathbf{H}_k||_1^2$ is equivalent to maximizing $\sum_{m=1}^{M_{MS}} ||(\mathbf{w}_k^{(m)})^H \mathbf{H}_k||_1^2$ for all $k = 1, \cdots, K$ respectively. Hence, the design of the RF combiners can be obtained by solving

$$\begin{aligned} \max_{\mathbf{W}_k} \quad & \sum_{m=1}^{M_{MS}} ||(\mathbf{w}_k^{(m)})^H \mathbf{H}_k||_1^2 \\ s.t. \quad & |\mathbf{W}_k^{(i,j)}| = \frac{1}{\sqrt{N_{MS}}}, \ \forall i,j. \end{aligned} \tag{3.11}$$

In this chapter, instead of solving the non-convex problem (3.11) directly, we modify the constraints to choose from a set of DFT basis, as explained in details next. Note that $||(\mathbf{w}_k^{(m)})^H\mathbf{H}_k||_1^2 = (\sum_{n=1}^{N_{BS}} |(\mathbf{w}_k^{(m)})^H\mathbf{h}_k^{(n)}|)^2$, where $\mathbf{h}_k^{(n)}$ denotes the n-th column of $\mathbf{H}_k$. Moreover, the geometric MIMO channel models, including the Rayleigh fading[1] and mmWave channels, can be represented in the form of (3.7), which means $\mathbf{h}_k^{(n)}$ is the linear combination of all the array response vectors of the AoAs. This fact implies that $||(\mathbf{w}_k^{(m)})^H\mathbf{H}_k||_1$ is the sum of the projections of those array response vectors on $\mathbf{w}_k^{(m)}$. From this perspective, we first propose to set $\mathbf{w}_k^{(m)}$ in the form of array response vector (3.8) to extract the gain from these projections, namely,

$$\mathbf{d}(\omega) = \frac{1}{\sqrt{N_{MS}}}\left[1, e^{j\omega}, e^{j2\omega}, \cdots, e^{j(N_{MS}-1)\omega}\right]^T, \tag{3.12}$$

where $\omega = \frac{2\pi}{\lambda} d \sin\theta$ denotes the corresponding spatial frequency [20].

Furthermore, to meet the rank sufficiency requirement of $\mathbf{H}_{eq}$, it is desirable that the rank of $\mathbf{H}_k$ is not reduced after it being multiplied by $\mathbf{W}_k$. For this purpose, we require the columns of $\mathbf{W}_k$ to be pairwise orthogonal so that the rank of $\mathbf{W}_k^H\mathbf{H}_k$ is lower bounded by $M_{MS} > N_S$ (the rank of the high-dimensional $\mathbf{H}_k$ is assumed to be larger than M_{MS}), which means the equivalent channel $\mathbf{H}_{eq}$ is potentially capable of supporting the transmission of $KM_{MS} > KN_S$ streams. Considering the form of $\mathbf{w}_k^{(m)}$, we discretize the ω into N_{MS} levels over $[0, 2\pi)$ and construct N_{MS} bases, given by $\mathbf{D} = \{\mathbf{d}(0), \mathbf{d}(\frac{2\pi}{N_{MS}}), \cdots, \mathbf{d}(\frac{2\pi(N_{MS}-1)}{N_{MS}})\}$ as the candidates from which the $\mathbf{w}_k^{(m)}$ is choosen. As we can see, these bases in $\mathbf{D}$ exactly form an N_{MS}-dimensional DFT basis set, which simultaneously conforms to the rank sufficiency and large arrary gain requirements of $\mathbf{H}_{eq}$. Therefore, we finally design the RF combiners by solving

$$\begin{aligned} \max_{\mathbf{W}_k} \ & \sum_{m=1}^{M_{MS}} ||(\mathbf{w}_k^{(m)})^H\mathbf{H}_k||_1^2 \\ s.t. \ & \mathbf{w}_k^{(m)} \in \mathbf{D}, \ m = 1, \cdots, M_{MS}. \end{aligned} \tag{3.13}$$

To solve the problem (3.13), we just need to sort all N_{MS} $||\mathbf{d}(\omega)^H\mathbf{H}_k||_1$'s in the descendant order and then choose the first M_{MS} $\mathbf{d}(\omega)$'s as the columns of $\mathbf{W}_k$.

Remark 2. *Omitting the cross-terms of* $||(\mathbf{w}_k^{(m)})^H\mathbf{H}_k||_1^2$*, we construct another crite-*

[1]In the Rayleigh fading channel, all AoDs/AoAs of the paths (non-LOS) are uniformly distributed among $[0, 2\pi)$ and the number of paths approaches to infinity.

rion to achieve the large array gain, given by

$$\begin{aligned} ||(\mathbf{w}_k^{(m)})^H \mathbf{H}_k||_1^2 &= (\sum_{n=1}^{N_{BS}} |(\mathbf{w}_k^{(m)})^H \mathbf{h}_k^{(n)}|)^2 \\ \Rightarrow \sum_{n=1}^{N_{BS}} (|(\mathbf{w}_k^{(m)})^H \mathbf{h}_k^{(n)}|)^2 &= ||(\mathbf{w}_k^{(m)})^H \mathbf{H}_k||_F^2. \end{aligned} \tag{3.14}$$

The large array gain can also be attained by solving

$$\begin{aligned} \max_{\mathbf{W}_k} \ ||\mathbf{W}_k^H \mathbf{H}_k||_F^2 &= \sum_{m=1}^{M_{MS}} ||(\mathbf{w}_k^{(m)})^H \mathbf{H}_k||_F^2 \\ s.t. \ \mathbf{w}_k^{(m)} &\in \mathbf{D}, \ m = 1, \cdots, M_{MS}. \end{aligned} \tag{3.15}$$

The solution to this maximizing problem (3.15) can be obtained through the sorting operation similar to that of (3.13). Notably, the simulation results in Section 3.3 demonstrate that such a Frobenius norm based problem achieves a similar spectral efficiency performance in the massive MU-MIMO systems with the 1-norm based solution.

3.2.2 Baseband Block Diagonalization

In this section, based on the obtained baseband equivalent channel $\mathbf{H}_{eq}$, given the found RF processing matrices $\mathbf{W}_k$ and $\mathbf{F}$, we perform the low-dimensional BD processing with the baseband precoder $\mathbf{B}$ and combiners $\mathbf{M}_k$'s to cancel the inter-user interference, which forces the interference terms $\tilde{\mathbf{H}}_k \mathbf{B}_i = \mathbf{0}$ for $i \neq k$ in (3.5). The spectral efficiency of the MU-MIMO system can be further simplified to

$$\begin{aligned} R = \sum_{k=1}^{K} \log_2 \Bigg(\Bigg| \mathbf{I}_{N_S} + \frac{P}{\sigma^2 K N_S} (\mathbf{M}_k^H \mathbf{W}_k^H \mathbf{W}_k \mathbf{M}_k)^{-1} \\ \mathbf{M}_k^H \tilde{\mathbf{H}}_k \mathbf{B}_k \mathbf{B}_k^H \tilde{\mathbf{H}}_k^H \mathbf{M}_k \Bigg| \Bigg). \end{aligned} \tag{3.16}$$

To obtain the baseband precoder $\mathbf{B} = [\mathbf{B}_1, \mathbf{B}_2, \cdots, \mathbf{B}_K]$, where $\mathbf{B}_k$ incorporates the precoding vectors for the data streams of the k-th MS, we first define $\overline{\mathbf{H}}_k$ as

$$\overline{\mathbf{H}}_k = [\tilde{\mathbf{H}}_1^T, \cdots, \tilde{\mathbf{H}}_{k-1}^T, \tilde{\mathbf{H}}_{k+1}^T, \cdots, \tilde{\mathbf{H}}_K^T]^T. \tag{3.17}$$

The $\mathbf{B}_k$ is supposed to lie in the null space of $\overline{\mathbf{H}}_k$. Denote the rank of $\overline{\mathbf{H}}_k$ as $r_k \leq (K-1)M_{MS}$. Then the singular value decomposition (SVD) of $\overline{\mathbf{H}}_k$ is given by

$$\overline{\mathbf{H}}_k = \overline{\mathbf{U}}_k \overline{\mathbf{\Sigma}}_k [\overline{\mathbf{V}}_k^{((K-1)M_{MS})} \quad \overline{\mathbf{V}}_k^{(M_{MS})}]^H, \tag{3.18}$$

where $\overline{\mathbf{V}}_k^{((K-1)M_{MS})}$ consists of the first $(K-1)M_{MS}$ right singular vectors of $\overline{\mathbf{H}}_k$, and $\overline{\mathbf{V}}_k^{(M_{MS})}$ holds the rest M_{MS} ones which are exactly the orthogonal bases of the null space of $\overline{\mathbf{H}}_k$. Then we know

$$\tilde{\mathbf{H}}_i \overline{\mathbf{V}}_k^{(M_{MS})} = \begin{cases} \mathbf{0}, \ i \neq k \\ \tilde{\mathbf{H}}_k \overline{\mathbf{V}}_k^{(M_{MS})}, \ i = k \end{cases} \tag{3.19}$$

Given the above results, block diagonalization of the baseband equivalent channel matrix to remove inter-user interference is written as

$$\begin{aligned} \mathbf{H}_{BD} &= \mathbf{H}_{eq} [\overline{\mathbf{V}}_1^{(M_{MS})}, \cdots, \overline{\mathbf{V}}_K^{(M_{MS})}] \\ &= \begin{bmatrix} \tilde{\mathbf{H}}_1 \overline{\mathbf{V}}_1^{(M_{MS})} & \cdots & \mathbf{0} \\ \vdots & \ddots & \vdots \\ \mathbf{0} & \cdots & \tilde{\mathbf{H}}_K \overline{\mathbf{V}}_K^{(M_{MS})} \end{bmatrix}. \end{aligned} \tag{3.20}$$

Until now, all the MSs can perform interuser-interference-free multi-stream transmission through their own sub-channels (the non-zero block in $\mathbf{H}_{BD}$). Further precoding/combining will be performed to achieve each MS's optimal spectral efficiency based on SVD, given by

$$\tilde{\mathbf{H}}_k \overline{\mathbf{V}}_k^{(M_{MS})} = \mathbf{U}_k \mathbf{\Sigma}_k \mathbf{V}_k^H. \tag{3.21}$$

With the above rank sufficiency requirement, $\tilde{\mathbf{H}}_k \overline{\mathbf{V}}_k^{(M_{MS})}$ is a M_{MS}-by-M_{MS} full-rank sub-channel matrix which enables $M_{MS} \geq N_S$ data streams transmission for the k-th MS. Therefore, the optimal precoder and combiner on the k-th effective sub-channel $\tilde{\mathbf{H}}_k \overline{\mathbf{V}}_k^{(M_{MS})}$ should be $\mathbf{V}_k^{(N_S)}$ and $\mathbf{U}_k^{(N_S)}$, where $\mathbf{V}_k^{(N_S)}$ and $\mathbf{U}_k^{(N_S)}$ are the first N_S columns of the $\mathbf{V}_k$ and $\mathbf{U}_k$ respectively. Finally, the overall baseband precoder is given by

$$\begin{aligned} \mathbf{B} &= [\overline{\mathbf{V}}_1^{(M_{MS})}, \cdots, \overline{\mathbf{V}}_K^{(M_{MS})}] \begin{bmatrix} \mathbf{V}_1^{(N_S)} & \cdots & \mathbf{0} \\ \vdots & \ddots & \vdots \\ \mathbf{0} & \cdots & \mathbf{V}_K^{(N_S)} \end{bmatrix} \\ &= [\overline{\mathbf{V}}_1^{(M_{MS})} \mathbf{V}_1^{(N_S)}, \cdots, \overline{\mathbf{V}}_K^{(M_{MS})} \mathbf{V}_K^{(N_S)}]_{KM_{MS} \times KN_S}. \end{aligned} \tag{3.22}$$

And the baseband combiner for the k-th MS is given by $\mathbf{M}_k = \mathbf{U}_k^{(N_S)},\ k = 1, 2, \cdots, K$.

The spectral efficiency achieved by the Hy-BD scheme finally becomes

$$R = \sum_{k=1}^{K} \log_2 \left(\left| \mathbf{I}_{N_S} + \frac{P\mathbf{\Lambda}(\mathbf{M}_k^H \mathbf{W}_k^H \mathbf{W}_k \mathbf{M}_k)^{-1} (\mathbf{\Sigma}_k^{(N_S)})^2}{\sigma^2 K N_S} \right| \right), \tag{3.23}$$

where $\mathbf{\Lambda}$ is a diagonal matrix that performs water-filling power allocation, and $\mathbf{\Sigma}_k^{(N_S)}$ represents the first $N_S \times N_S$ block partition of $\mathbf{\Sigma}_k$.

3.3 Simulation Results

In this section, we evaluate the spectral efficiency achieved by the Hy-BD scheme in the massive MU-MIMO systems by comparing it with the traditional high-dimensional baseband BD scheme in large i.i.d Rayleigh fading and mmWave multiuser channels and also with the previously proposed spatially sparse precoding/combining scheme [14] in mmWave channels. The range of the signal-to-noise ratio SNR $= \frac{P}{\sigma^2}$ is from -40 dB to 0 dB in all processing solutions.

Fig. 3.2 illustrates the sum spectral efficiency achieved by the traditional BD scheme and our proposed Hy-BD scheme (through solving the 1-norm and Frobenius norm based optimization problems in Section 3.2.1) in the large i.i.d. Rayleigh fading channel. The BS with $M_{BS} = 16$ RF chains is employed to schedule $K = 8$ MSs, each of which processes $N_S = 2$ data streams with $M_{MS} = 2$ RF chains. Furthermore, the BS and MSs are equipped with 256 (16) and 64 (4) antennas respectively. In both 256×16 and 64×4 antenna settings, the sum spectral efficiency of the Hy-BD scheme consistently approaches the performance achieved by the traditional BD scheme, however, with lower implementation and computational complexity. In addition, the Hy-BD designs based on solving the 1-norm problem (3.13) and the Frobenius norm problem (3.15) respectively lead to the nearly identical sum spectral efficiency, supporting the statement in **Remark 2**. Notably, the results of the 64×4 antenna setting indicate that the Hy-BD scheme is still effective in a small scale antenna system.

Furthermore, the maximally supported number of data streams of a massive MU-MIMO system is examined in the large i.i.d. Rayleigh fading channel in Figs. 3.3 and 3.4. The BS is set to have $N_{BS} = 64$ antennas, theoretically supporting up to 64 data streams transmission, while the MSs are assumed to only have 1 or 2 antennas

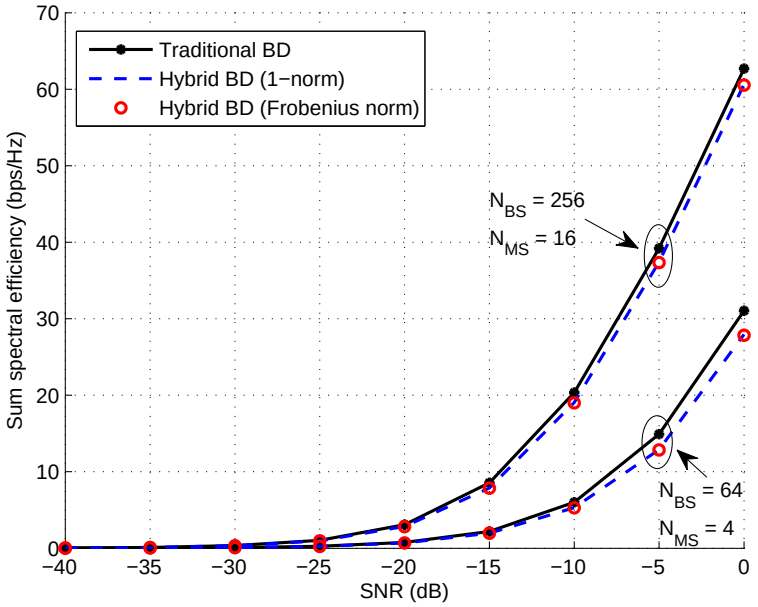

Figure 3.2: Sum spectral efficiency achieved by different processing schemes in an 8-user MU-MIMO system in i.i.d. Rayleigh fading channels where $N_S = 2, M_{MS} = 2, M_{BS} = 16$.

(scheduling 1 or 2 data streams respectively). In this scenario, the SNR is chosen as 5 dB. In Fig. 3.3, the spectral efficiency performance gap between the traditional BD and the Hy-BD scheme remains acceptably small when the number of MSs K increases to 24. As for Fig. 3.4, the suitable number of MSs K should be less than about 12 (corresponding to 24 data streams) to obtain acceptable performance. The above results indicate that the Hy-BD scheme is able to catch up with the traditional BD scheme when the number of total scheduled data streams $K * N_S$ does not exceed $\frac{N_{BS}}{4}$ (a quarter of the number of BS antennas).

On the other hand, the spectral efficiency performance of the Hy-BD scheme under imperfect channel state information (CSI), compared to that of the traditional BD scheme, is also shown in Fig. 3.5. We use 64-antenna BS and single-antenna MSs in this scenario. Assume that the estimated channel for the k-th MS is $\hat{\mathbf{H}}_k = \mathbf{H}_k + \mathbf{E}_k$, where $\mathbf{E}_k$ is the channel estimation error. All entries in $\mathbf{E}_k$ follow the identical complex Gaussian distribution with zero means. We define the normalized channel estimation error power as $\frac{\sum_{k=1}^{K} ||\mathbf{E}_k||_F^2}{\sum_{k=1}^{K} ||\mathbf{H}_k||_F^2}$. In Fig. 3.5, the channel estimation error power is set from -40 dB to -6 dB and the SNR for transmit signal is 10 dB. The solid lines represent the performance with no channel estimation while the dash lines indicate the performance for the two scheme with the given channel estimation error. As Fig. 3.5 shows, the

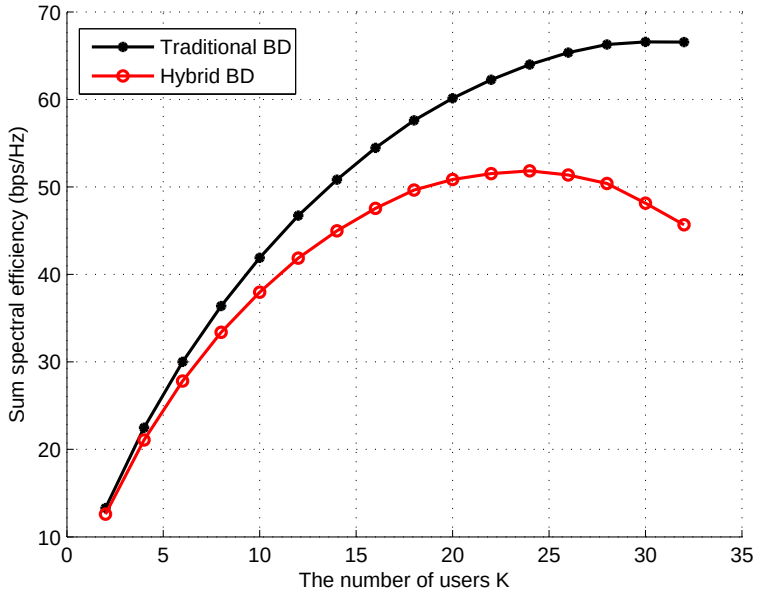

Figure 3.3: Sum spectral efficiency by different processing schemes in an MU-MIMO system in i.i.d. Rayleigh fading channels where $N_t = 64$, $N_r = 1$.

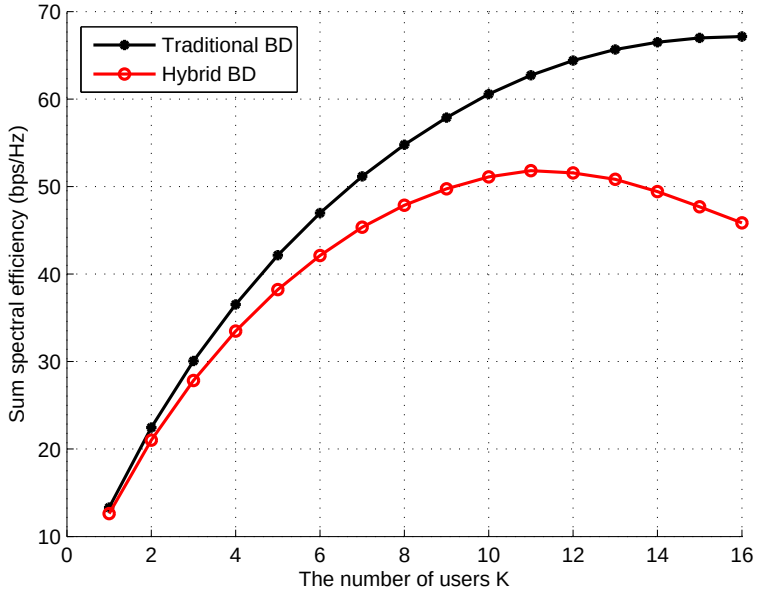

Figure 3.4: Sum spectral efficiency by different processing schemes in an MU-MIMO system in i.i.d. Rayleigh fading channels where $N_t = 64, N_r = 2$.

thresholds for the channel estimation error power for both the schemes are about -10 dB. Once the channel estimation error power reaches this value, the performance will drop drastically.

In the mmWave MU-MIMO channels, the traditional full-complexity BD and Hy-

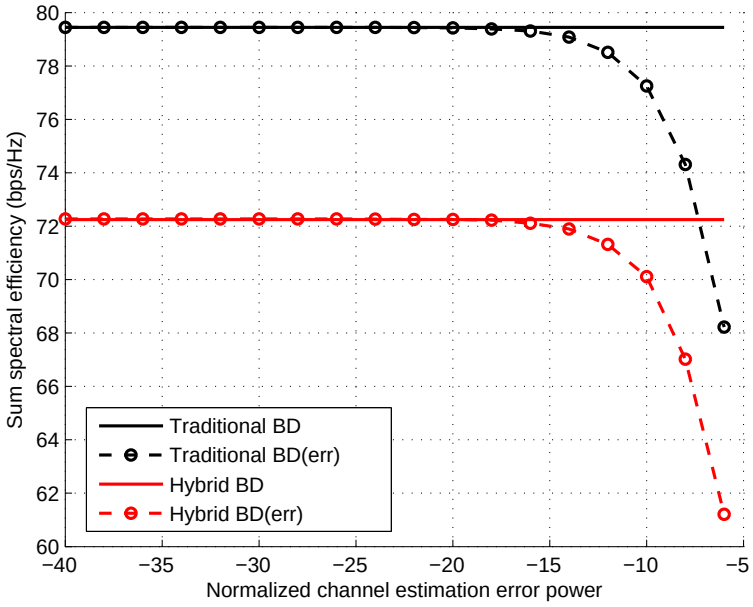

Figure 3.5: Sum spectral efficiency by different processing schemes in an MU-MIMO system in i.i.d. Rayleigh fading channels with channel estimation error.

BD schemes perform in a similar fashion as in the Rayleigh fading channels. Based on the limited number of paths scattered in the mmWave channels, the spatially sparse precoding/combining scheme in [14] can be extended to the hybrid processing in MU-MIMO systems through decomposing the solution to the traditional BD scheme (the precoder $\mathbf{M}_S$ and the MMSE combiners in [28]) via orthogonal matching pursuit where the BS and MSs choose the array response vectors of the corresponding AoDs and AoAs as the basis vectors respectively. Fig. 3.6 shows the sum spectral efficiency of the above processing schemes. We set the mmWave propagation channel with $N_c = 8$ and $N_p = 10$. The range of the mean azimuth angles of AoDs at the BS $|\theta^k_{\max} - \theta^k_{\min}|$ is 120° while the MSs are assumed to be omni-directional due to the relatively smaller antenna array elements. The angle spreads σ^k_θ's and σ^k_ϕ's are all equal to 7.5°. Moreover, the BS is set to have $N_{BS} = 256$ antennas and $M_{BS} = 16$ RF chains, while $K = 8$ MSs, with $N_{MS} = 16$ antennas and $M_{MS} = 2$ RF chains, all dealing with $N_S = 2$ data streams. In this scenario, the proposed Hy-BD scheme even achieves slightly higher spectral efficiency than the traditional BD scheme. Note that the traditional BD scheme is a sub-optimal solution for the processing of MU-MIMO systems, and it is possible that the Hy-BD outperforms the traditional BD in some situations. As for the spatially sparse precoding/combining scheme, it lags behind the

traditional BD and Hy-BD schemes because the columns of the traditional BD precoding and combining matrices do not directly come from the linear combination of the array response vectors of AoDs/AoAs, although the spatially sparse precoding/-combining scheme does effectively decompose the SVD based precoder and combiner in P2P scenario, whose columns can be written as the linear combinations of the array response vectors of AoDs/AoAs respectively, according to the observation 3) in [14]. Even though the number of RF chains is enlarged to $M_{MS} = 4$ and $M_{BS} = 32$, the performance of the spatially sparse precoding/combining scheme is still inferior to the full-complexity BD and Hy-BD schemes.

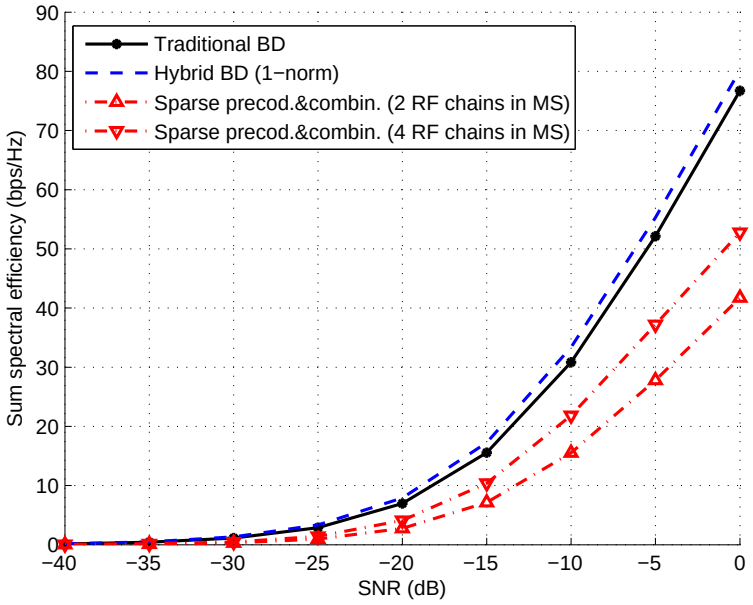

Figure 3.6: Sum spectral efficiency achieved by different processing schemes in an 256×16 8-user MU-MIMO system in mmWave channels where $N_S = 2, M_{MS} = 2(4), M_{BS} = 16(32)$.

3.4 Summary

In this chapter, a low-complexity hybrid block diagonalization processing scheme has been proposed for the downlink communication of a massive multiuser MIMO system with the limited number of RF chains. We harvest the large array gain through the phase-only RF precoding and combining and then the BD technique is performed at the equivalent baseband channel. It has been demonstrated that the Hy-BD scheme, with a lower implementation and computational complexity, achieves a

capacity performance approaching that of the traditional high-dimensional baseband BD processing. Such a low-complexity, low cost Hy-BD scheme can be a promising option for the practical implementation of a massive MU-MIMO system.

Chapter 4

Energy Harvesting Wireless Communications with Energy Cooperation

Energy harvesting for communication devices has emerged as a prominent research area due to its benefit of powering the devices through alternative energies instead of battery or hardwire power [29], [30]. By employing the piezoelectric, electromagnetic, photo-voltaic or other energy harvesting technologies, external sources, such as kinetic, solar energy and ambient radio waves, can be harvested to power the devices. Thus, energy harvesting becomes an attractive and effective solution for powering the energy-constrained devices and prolonging their lifetime, which makes it possible that the energy efficiency can be improved by utilizing the renewable energy sources in 5G wireless communications.

In an energy harvesting wireless communications system, the cumulatively consumed energy by the system is not allowed to exceed the cumulatively harvested energy at any time instant [31], based on which a significant amount of works have investigated energy harvesting communications. Beginning with an energy harvesting transmitter design, [31] analyzes the communication channel capacity with random energy arrival from the information-theoretic view. An offline power allocation algorithm is put forward to minimize the outage probability over a finite horizon considering an infinite battery storage [32]. Considering time-varying channels and energy sources, as well as finite battery storage, [33] uses dynamic programming to maximize the system throughput over a finite horizon. For the energy harvesting

receiver, Varshney introduced the concept of scavenging information and energy simultaneously [34]. This idea leads to the simultaneous wireless information and power transfer (SWIPT) proposed in [35] and [36], where the transmitter sends one signal and the receiver divides the received signal into two parts by either power splitting or time switching: one for information decoding and one for energy harvesting. [37] and [38] extend the works of [34]-[36] to MIMO and cognitive radio scenarios. Moreover, [39] applies the power splitting and time switching schemes at an energy harvesting relay in wireless cooperative networks, termed as cooperative SWIPT. Reference [40] investigates different power allocation strategies in a wireless network with multiple source-destination pairs communicating through an energy harvesting relay where the cooperative SWIPT technique is applied. So far, some prototypes of wirelessly-powered platforms can work solely by absorbing the ambient RF energy from the air [41]–[43].

Rather than purely harvesting energy from the unintentional sources, energy cooperation allows the devices to intentionally transfer some energy to others to assist communications, which is inspired by the work of Brown on power transfer by radio waves [44]. Note that both SWIPT and energy cooperation involve the wireless information transmission and energy transfer. However, compared to the SWIPT technology that embeds the transferred energy into the information signal, an independent energy transfer channel is used in this chapter for energy cooperation. Such approach provides more freedom to optimize the energy transfer design for higher efficiency and the direction of energy transfer can be different from that of the information flow at any time instant. Reference [45] proposes a one-way energy cooperation scheme under two-way and multiple-access communications system respectively, using a bidirectional water-filling algorithm to control the energy flows. The papers [46] and [47] investigate the uni-directional energy cooperation between the source node and relay node, while in [48] the downlink wirelss energy transfer is employed to assist the uplink information transmissions in a wireless powered communication network. The analysis of the bi-directional energy cooperation is given in [49], where two communications nodes are assumed to wirelessly exchange their energy. In addition, the energy cooperation between base stations in wireless cellular systems have been considered in [50] and [51].

The above-mentioned work all assume the power consumption of the hardware circuits can be ignored (ideal circuits). In fact, the power consumption of the hardware circuits (non-ideal circuits) is a significant factor that influences the system's

behaviors, like sleeping or keeping active. The papers [52] and [53] investigate the designs of such practical transmitters with non-ideal circuits: the former proposes both offline and online energy/power allocation algorithms for optimizing average throughput under a deterministic energy arrival profile, while the latter introduces a save-then-transmit (ST) protocol that the energy harvesting transmitter sleeps for a period of time to save energy and then wakes up to communicate. The optimal save-ratio of the ST protocol is derived in [54].

In this chapter, we consider both the energy harvesting transmitter and receiver with non-ideal circuits, based upon [52]-[54] which did not consider the design of the energy harvesting receiver. We assume that both the practical transmitter and receiver harvest energy from the external sources, and then employ the harvested energy to support communications as well as running the non-ideal circuits. We choose the ST scheme to handle the harvested energy and enable energy cooperation between the transmitter and receiver, which is termed energy cooperation ST (EC-ST) scheme. The EC-ST scheme allows the active transmitter and receiver to transfer some of their stored energy to each other to improve the communications performance by adjusting the transmission power and communication time, while the common ST scheme is merely applied to a transmitter without energy cooperation.

It is noted that the transmitter and receiver employ two pairs of antennas to realize information transmission and energy transfer. The energy and information channels are assumed to be orthogonal to each other [46], by using two different frequency bands that are respectively accessed by two pairs of narrow-band antennas. The energy channel may be assigned to a relatively lower frequency band in order to obtain a higher energy transfer efficiency by avoiding the large path loss resulting from a higher frequency. Fig. 4.1 shows the circuit model for a practical energy harvesting device (applied to both the transmitter and receiver). The energy harvester contains several energy harvesting units for different energy sources, like photo-voltaic and electromagnetic energy harvesting units. The rate (joules/second) of energy harvesting is called energy arrival rate. Functional circuits manage communications and energy cooperation through the control unit. Two antennas, Ac, Ae, are integrated into two RF modules respectively, where Ac is used to communicate while Ae transfers energy between the transmitter and receiver to realize energy cooperation. Moreover, Ae needs to feed the received energy transferred by another device to the electromagnetic energy harvesting unit for harvesting and storage.

For modeling convenience, we divide the time horizon into infinite identical-length

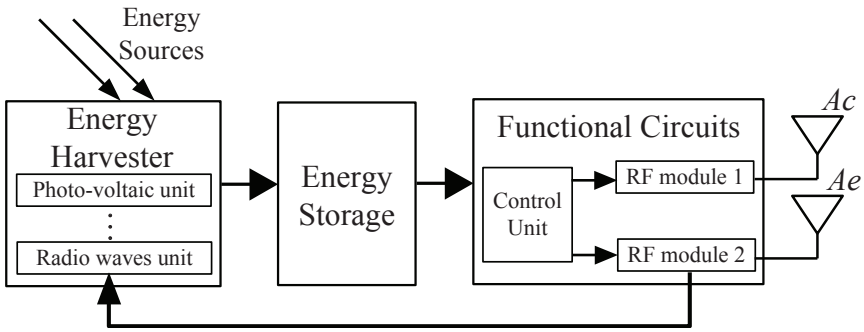

Figure 4.1: Practical Circuit Model for Energy Harvesting Device

time blocks, each of which has the length of T seconds. This study concentrates on the optimal performance of the P2P wireless communications within T seconds. To begin with, we apply the EC-ST scheme to additive white Gaussian noise (AWGN) one-way channels with two-way energy transfer under a deterministic energy arrival rate. In this case, the active ratios of the transmitter and the receiver and the energy cooperation strategies between the transmitter and the receiver are derived to maximize the communication throughput. The second part of the study considers a more general situation where the harvested energy arrives with a stochastic rate and the communication channel is modeled as Rayleigh block fading. In this case, the active ratios and the energy cooperation strategies are designed to minimize the outage probability, which characterizes the occurrence of events where there is not sufficient energy to maintain the transmitter or the receiver active or the communication data rate falls below a certain threshold.

The rest of this chapter is organized as follows. Section 4.1 introduces the system model and related assumptions. Section 4.2 applies the EC-ST scheme to the AWGN channel with a deterministic energy arrival rate and derives a closed-form solution of the scheme parameters for maximizing the throughput. Section 4.3 analyzes the outage probability minimization problem in the Rayleigh block fading channel with a stochastic energy arrival rate. Section 4.4 presents the numerical results of optimized throughput and the simulation results of outage probability. Finally, Section 4.5 concludes this chapter.

4.1 System Model

This section describes the definitions and assumptions of the energy source, and explains how the system deals with communications as well as energy cooperation. The system model is illustrated in Fig. 4.2. The energy source can be the sun, a TV signal tower, or a vibration source, etc.. We assume that the distance between the transmitter and receiver is far less than the distance between the system and the energy source. This means the energy arrival rates of the transmitter and receiver are identical at any time instant, since the amount of harvested energy in a period mainly depends on the distance from the source. Note that the charging rate of the energy storage is usually less than the energy arrival rate, because of the limited energy conversion efficiency of the circuits. Denote the charging rate and energy arrival rate as X and $\hat{X}$ respectively. We have $X = \eta\hat{X} \geq 0$, where $0 < \eta \leq 1$ is the imperfect conversion efficiency. In the rest of the chapter, the energy arrival rate refers to the effective energy arrival rate that is assimilated by the system, i.e., the charging rate of the storage X. Due to the fact that the output power of an energy harvester is usually at a relatively low level, we also assume that the energy storage capacity of the transmitter and receiver are finite but large enough to store all the harvested energy within one time block (i.e., the overflow of the energy can be ignored). We set the time block length T much smaller than the time constant of the arrival energy rate, and hence, X should remain constant over a time block [53, 54]. The harvested energy is used by the transmitter and the receiver for communications and for bi-directional wireless energy transfer between them to support maximum information rate.

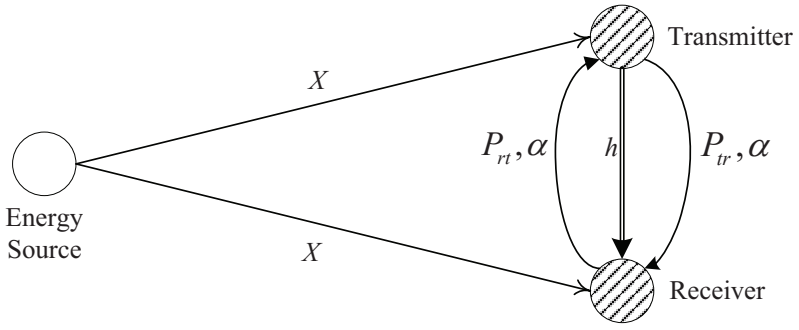

Figure 4.2: System model of energy harvesting transmitter and receiver

We apply the EC-ST scheme: both the transmitter and receiver sleep during the first proportion of T (*sleep* mode), and then communicate with each other during the

rest of the time in T (*active* mode) [52, 53]. In the *active* mode, the transmitter is modulating and transmitting signal or the receiver is receiving and demodulating data through the antenna pair Ac (See Fig. 4.1). In the *sleep* mode all the circuits in the transmitter or receiver turn off except the energy harvester which consistently charges the energy storage of the transmitter and receiver with rate of X. The ratio of time during which the device is active to the whole time block length T is denoted as the active-ratio ρ_t and ρ_r for both the transmitter and receiver respectively. Additionally, we assume the energy storage of the transmitter and receiver have multiple cells thus can be charged and discharged simultaneously, which makes the charging operation at any time instant in T feasible. The amount of the harvested energy of the transmitter and receiver is therefore XT.

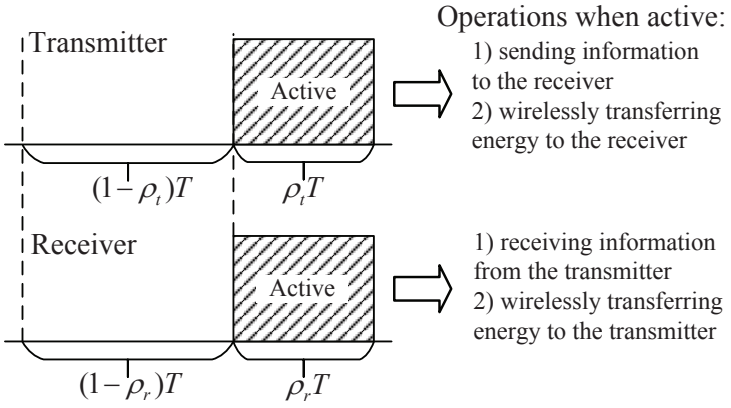

Figure 4.3: Sleep/Active mode of the transmitter and receiver

For the transmitter using the EC-ST scheme, it turns into the sleep mode in the time interval $[0, (1-\rho_t)T)$, while it is active in the interval $[(1-\rho_t)T, T]$, where the active-ratio of the transmitter $0 \leq \rho_t \leq 1$ is shown in Fig. 4.3. When the transmitter is active, the power consumption of the hardware circuits, such as the control units and the baseband processing units, excluding the RF modules, is $P_{tc} > 0$; and the power consumption of the RF modules is equal to the signal transmission power P_s, assuming the perfect efficiency of the RF chain. Furthermore, the transmitter simultaneously transfers energy with a constant power[1] of P_{tr} and efficiency of α $(0 < \alpha \leq 1)$ to the receiver in $[(1-\rho_t)T, T]$, through the antenna pair Ae (See Fig. 4.1). That means the receiver can be charged with additional power of αP_{tr}.

[1]Since the active radio ρ_t is unknown, maybe nearly zero, it is more reasonable to assume the transmitter or receiver do energy transfer with a finite power instead of directly characterizing the amount of transferred energy, due to the limitation on the antenna radiated power.

Therefore, the total power consumption of the transmitter is given by

$$P_t = \begin{cases} P_{tc} + P_s + P_{tr}, & \textit{active} \text{ mode}, \\ 0, & \textit{sleep} \text{ mode}, \end{cases} \tag{4.1}$$

where $P_{tr} \geq 0, P_s \geq 0$. Similarly, the receiver is in the sleep mode during $[0, (1-\rho_r)T)$ and in the active mode during $[(1-\rho_r)T, T]$, where the active-ratio of the receiver $\rho_r \in (0, 1]$. When the receiver is active, the power consumption of the circuits is $P_{rc} > 0$. It is reasonable to assume that $P_{rc} > P_{tc}$, because the receiver usually needs more power to do the baseband detection than the transmitter which usually has relatively simple baseband processing [55]. In addition, the receiver transfers energy to the transmitter with power P_{rt} and efficiency α in $[(1-\rho_r)T, T]$ (symmetric energy transfer channel). The total power consumption of the receiver is

$$P_r = \begin{cases} P_{rc} + P_{rt}, & \textit{active} \text{ mode}, \\ 0, & \textit{sleep} \text{ mode}, \end{cases} \tag{4.2}$$

where $P_{rc} \geq 0$.

In this chapter, we consider two kinds of channel models: AWGN channels and Rayleigh block fading channels. The baseband equivalent channel output is given by

$$y = h \cdot x + n, \tag{4.3}$$

where y is the received signal, x is the transmitted signal, h is the channel gain, and n is the additive Gaussian noise with zero mean and variance σ^2. We define the channel power gain factor as $H = \frac{|h|^2}{\sigma^2}$. In AWGN channels, H is a positive constant, while in Rayleigh block fading channels, the length of T is chosen to be far less than the coherence time of the information transmission channel so that H remains constant in one time block but randomly changes over different time blocks (following exponential distribution with mean of λ_H). The energy transfer efficiency α is dependent on the channel power gain of the energy transfer channel. For the AWGN channel scenario, α is also assumed to be constant similar to H. On the other hand, in the Rayleigh block fading channel scenario, the coherence time of the energy transfer channel is also larger than the time block length T. Therefore, we assume the energy transfer efficiency α remains constant within one time block but may change over different time blocks.

4.2 Throughput Maximization under AWGN Channels

4.2.1 Normalized Throughput Maximization Problem

In a certain number of applications, especially in WSNs, where most devices in the network stay in fixed locations and their surrounding environment is stationary, the AWGN channel is a suitable model to evaluate the P2P wireless communications performance. Furthermore, due to the static locations of the transmitter and receiver, the energy arrival rate X should be consistent during a considerable time period, far longer than T. Consequently, both transmitter and receiver are capable to estimate X. In other words, X is assumed to be deterministic, and known by the transmitter and receiver.

In AWGN channels, the normalized throughput in one time block is given by $R_A = \log_2(1 + HP_s)$. However, the communications link can only be established if both the transmitter and receiver are active, and hence the normalized throughput should be multiplied by $\min\{\rho_r, \rho_t\}$:

$$R_A(\rho_t, \rho_r, P_{tr}, P_{rt}) = \min\{\rho_r, \rho_t\} \cdot \log_2(1 + HP_s). \tag{4.4}$$

In each time block, the transmitter and receiver use up all available energy by signal transmission and energy cooperation over time T, which is made possible given that X is deterministic and known[2]. To obtain an expression for the transmission power P_s in (4.4), we formulate the total power of the transmitter and receiver in the active mode as

$$\begin{aligned} P_t &= P_{tc} + P_s + P_{tr} = \frac{XT + \alpha P_{rt} \cdot \rho_r T}{\rho_t T} = \frac{X + \alpha P_{rt} \cdot \rho_r}{\rho_t}, \\ P_r &= P_{rc} + P_{rt} = \frac{XT + \alpha P_{tr} \cdot \rho_t T}{\rho_r T} = \frac{X + \alpha P_{tr} \cdot \rho_t}{\rho_r}. \end{aligned} \tag{4.5}$$

Here, $(XT + \alpha P_{rt} \cdot \rho_r T)$ is all the available energy for the transmitter in a time block, where XT comes from energy harvesting and $(\alpha P_{rt} \cdot \rho_r T)$ is the amount of energy transferred from the receiver. Moreover, $\rho_t T$ is the active time of the transmitter, during which the transmitter operates with power P_t. The total power of the receiver is given by the second formula in (4.5). The transmission power P_s in (4.4) can then

[2]Instead of using up all energy in one time block, coordinating and managing energy usage over multiple blocks has the potential to improve performance, but is out of the scope of this thesis and a topic for future studies.

be expressed as $P_s = (X + \alpha P_{rt} \cdot \rho_r)/\rho_t - P_{tc} - P_{tr}$. In the rest of this section, we aim to find an optimal energy cooperation scheme $(\rho_t^*, \rho_r^*, P_{tr}^*, P_{rt}^*)$ to maximize the normalized throughput (4.4) subject to the following three practical constraints:

1) Active-ratio length: $0 \leq \rho_t \leq 1$, $0 \leq \rho_r \leq 1$,

2) Energy causality: the energy for cooperation can not exceed the amount of the harvested energy at the transmitter (receiver): $0 \leq \rho_t P_{tr} \leq X$, $0 \leq \rho_r P_{rt} \leq X$,

3) Effective Transmission: the signal transmission power must be non-negative, $P_s = (X + \alpha P_{rt} \cdot \rho_r)/\rho_t - P_{tc} - P_{tr} \geq 0$.

That is, the throughput optimization problem is given by

$$\begin{aligned} \max_{\rho_t, \rho_r, P_{tr}, P_{rt}} \; & R_A(\rho_t, \rho_r, P_{tr}, P_{rt}) \\ s.t. \; & 0 \leq \rho_t \leq 1, 0 \leq \rho_r \leq 1, \\ & 0 \leq \rho_t P_{tr} \leq X, 0 \leq \rho_r P_{rt} \leq X, \\ & P_s = (X + \alpha P_{rt} \cdot \rho_r)/\rho_t - P_{tc} - P_{tr} \geq 0. \end{aligned} \tag{4.6}$$

Next, we present in **Lemma 1** that the independent active ratios $\rho_r = \rho_t$ is necessary for maximizing $R_A(\rho_t, \rho_r, P_{tr}, P_{rt})$. This reduces the optimization variables by one dimension and coincides with the intuition that the transmitter and receiver should operate at the same time to guarantee the effective communications.

Lemma 1. *For an optimal solution that maximizes R_A in (4.6), the transmitter and receiver must keep active in the identical time interval: $\rho_r = \rho_t$, due to the invalidity of single-sided communication.*

Proof. In a time block, the energy arrival rate X and normalized channel power gain H keep constant. When $\rho_r \neq \rho_t$, we can enhance R_A by adjusting the energy cooperation power P_{tr} and P_{rt} until $\rho_r = \rho_t$. Here, we have two situations to discuss:

- If $\rho_r > \rho_t$, $R_A = \min\{\rho_r, \rho_t\} \cdot \log_2(1 + HP_s) = \rho_t \log_2(1 + HP_s)$. For any fixed ρ_t and P_{tr}, the R_A will only depend on ρ_r and P_{rt}. According to the second formula in (4.5), if we increase P_{rt}, $\rho_r = (X + \alpha P_{tr}\rho_t)/(P_{rt} + P_{rc})$ will reduce. Similarly, according to the first formula in (4.5), the value of P_s, which uniquely depends on the value of $P_{rt}\rho_r = (X + \alpha P_{tr}\rho_t) \cdot \frac{P_{rt}}{P_{rt}+P_{rc}}$, will be enhanced with the increasing P_{rt}. Finally, as long as $\rho_r \geq \rho_t$, R_A will consistently grow by increasing the energy cooperation power P_{rt} until $\rho_r = \rho_t$.

- If $\rho_r < \rho_t$, $R_A = \min\{\rho_r, \rho_t\} \cdot \log_2(1 + HP_s) = \rho_r \log_2(1 + HP_s)$. Beginning with the fixed ρ_r and P_{rt}, we can find that $P_{tr}\rho_t$ is also a constant, according the second formula of (4.5). Then we can increase P_{tr}, which makes ρ_t reduced. Eventually, $P_s = (X + \alpha P_{rt}\rho_r - P_{tr}\rho_t)/\rho_t - P_{tc}$ will increase since the value of $(X + \alpha P_{rt}\rho_r - P_{tr}\rho_t)$ keeps fixed. Obviously, as long as $\rho_r \leq \rho_t$, increasing P_{tr} leads to higher R_A until $\rho_r = \rho_t$.

Therefore, the maximum normalized throughput is achieved when $\rho_r = \rho_t$. □

Define $\rho = \rho_t = \rho_r$ and $R_A(\rho, P_{tr}, P_{rt}) = R_A(\rho, \rho, P_{tr}, P_{rt})$. By substituting $\rho = \rho_r = \rho_t$ into $\rho_r = (X + \alpha P_{tr}\rho_t)/(P_{rt} + P_{rc})$, we obtain

$$\rho = \frac{X}{P_{rt} + P_{rc} - \alpha P_{tr}}. \tag{4.7}$$

Then the normalized throughput is reformulated as

$$\begin{aligned} R_A(P_{tr}, P_{rt}) &= R_A(\rho, P_{tr}, P_{rt})|_{\rho=\frac{X}{P_{rt}+P_{rc}-\alpha P_{tr}}} \\ &= \frac{X \log_2\left[1 + H((\alpha+1)(P_{rt} - P_{tr}) + \Delta P_c)\right]}{P_{rt} - \alpha P_{tr} + P_{rc}}, \end{aligned} \tag{4.8}$$

where $\Delta P_c = P_{rc} - P_{tc} > 0$. Until now, we have transformed the 4-variable maximization problem (4.6) into a 2-variable one:

$$\begin{aligned} &\max_{P_{tr}, P_{rt} \geq 0} R_A(P_{tr}, P_{rt}) \\ &\quad s.t.\ 0 \leq \rho \leq 1, \rho = X/(P_{rt} + P_{rc} - \alpha P_{tr}), \\ &\qquad 0 \leq \rho P_{tr} \leq X, 0 \leq \rho P_{rt} \leq X, \\ &\qquad P_s = (\alpha+1)(P_{rt} - P_{tr}) + (P_{rc} - P_{tc}) \geq 0. \end{aligned} \tag{4.9}$$

Before directly tackling (4.9), we introduce **Lemma 2** that effectively gives a constraint to shrink the feasible region without changing the optimal solution.

Lemma 2. *(Necessary condition of optimal energy cooperation) Due to the imperfect efficiency of energy transfer, $0 \leq \alpha \leq 1$, only one-way energy transfer is active for maximizing $R_A(P_{tr}, P_{rt})$ over a time block T, which means $P_{rt} \cdot P_{tr} = 0$.*

Proof. Suppose there is always a solution $(P_{rt}^{\Delta}, P_{tr}^{\Delta})$ for $\max_{\{P_{rt}, P_{tr}\}} R_A$. If $P_{rt}^{\Delta} - \alpha P_{tr}^{\Delta} \geq 0$, we can get another pair $(P_{rt}^{*} = P_{rt}^{\Delta} - \alpha P_{tr}^{\Delta}, P_{tr}^{*} = 0)$, and $R_A(P_{rt}^{*}, P_{tr}^{*}) \geq R_A(P_{rt}^{\Delta}, P_{tr}^{\Delta})$ with the same ρ and a larger P_s due to $0 \leq \alpha \leq 1$. On the other hand, if $P_{rt}^{\Delta} - \alpha P_{tr}^{\Delta} <$

0, we can also obtain another pair $(P_{rt}^* = 0, P_{tr}^* = P_{tr}^{\Delta} - \frac{P_{rt}^{\Delta}}{\alpha})$, which leads to a larger $R_A(P_{rt}^*, P_{tr}^*)$. Therefore, $P_{rt}^* \cdot P_{tr}^* = 0$, which means only one way energy transfer is needed to maximize the throughput R_A over a time block. □

Based on **Lemma 2**, the maximum throughput of (4.9) can be found in two sub-regions: $\{P_{tr} = 0, P_{rt} \geq 0\}$ and $\{P_{tr} \geq 0, P_{rt} = 0\}$. By substituting the constraints of these two sub-regions into (4.9), we finally decompose (4.9) into two corresponding sub-problems

$P_{tr} = 0, P_{rt} \geq 0$:

$$\begin{aligned} \max_{P_{rt}} \ & \frac{X}{P_{rt} + P_{rc}} \log_2 \left[1 + H((\alpha+1)P_{rt} + (P_{rc} - P_{tc}))\right] \\ s.t. \ & P_{rt} \geq \max\{X - P_{rc}, 0\}. \end{aligned} \tag{4.10}$$

$P_{tr} \geq 0, P_{rt} = 0$:

$$\begin{aligned} \max_{P_{tr}} \ & \frac{X}{P_{rc} - \alpha P_{tr}} \log_2 \left[1 + H(-(\alpha+1)P_{tr} + (P_{rc} - P_{tc}))\right] \\ s.t. \ & 0 \leq P_{tr} \leq \min\{\frac{P_{rc} - X}{\alpha}, \frac{P_{rc} - P_{tc}}{\alpha + 1}\}. \end{aligned} \tag{4.11}$$

The final solution (P_{tr}^*, P_{rt}^*) is obtained by comparing the solved R_A values of the two sub-problems (4.10) and (4.11), and choosing the solution that leads to a larger R_A.

4.2.2 Energy Cooperation for Maximizing Throughput

Observing the constraints of (4.10) and (4.11), we can easily find that $X = P_{rc}$ is a threshold of the maximization problem. Here, we solve (4.9) through discussing the value of X.

$\underline{X \geq P_{rc}}$:

When $X \geq P_{rc}$, the feasible region of the sub-problem (4.11) becomes the empty set or just $\{P_{tr} = 0\}$, because $\min\{\frac{P_{rc}-X}{\alpha}, \frac{P_{rc}-P_{tc}}{\alpha+1}\} = \frac{P_{rc}-X}{\alpha} \leq 0$. We set $P_{tr}^* = 0$ in this case. This result agrees with the intuition that if the harvested energy at the receiver overflows (can not be used up by circuits), it should at least transfer the extra energy to transmitter to assist communications, thus getting better performance. In this case, the optimal solution for (4.9) is identical to that of (4.10). Moreover, the constraint of (4.10) becomes $P_{rt} \geq X - P_{rc}$:

$$\begin{aligned} \max_{P_{rt}} \ & R_A(P_{rt}) = \frac{X \log_2 \left[1 + H((\alpha+1)P_{rt} + (P_{rc} - P_{tc}))\right]}{P_{rt} + P_{rc}} \\ s.t. \ & P_{rt} \geq X - P_{rc}. \end{aligned} \tag{4.12}$$

Lemma 3. *The optimal solution to (4.12) is given by*

$$P_{rt}^* = \left\{ \frac{1}{H(\alpha+1)} \left[\frac{-A}{W_0(\frac{-A}{e})} - [1 + H(P_{rc} - P_{tc})] \right] \right\}^+, \tag{4.13}$$

where $A = 1 - H(P_{tc} + \alpha P_{rc})$, $\{\cdot\}^+ = \max\{\cdot, X - P_{rc}\}$ *and* $W_0(\cdot)$ *is the principle branch of LambertW function [56].*

Proof. The derivative of $R_A(P_{rt})$ is given by

$$\frac{\mathrm{d}R_A(P_{rt})}{\mathrm{d}P_{rt}} = \frac{X \cdot D_{rt}(P_{rt})}{(P_{rt} + P_{rc})^2 (1 + HP_s) \ln(2)}, \tag{4.14}$$

where $D_{rt}(P_{rt}) = H(\alpha+1)(P_{rt} + P_{rc}) - (1 + HP_s)\ln(1 + HP_s)$, $P_s = (\alpha+1)P_{rt} + (P_{rc} - P_{tc}) \geq 0$. Hence, the sign of derivative of $R_A(P_{rt})$ depends on $D_{rt}(P_{rt})$.

We continue to take the derivative of $D_{rt}(P_{rt})$

$$\frac{\mathrm{d}D_{rt}(P_{rt})}{\mathrm{d}P_{rt}} = -H(\alpha+1)\ln(1 + HP_s) \leq 0. \tag{4.15}$$

Moreover, we have $D_{rt}(-\frac{P_{rc}-P_{tc}}{\alpha+1}) = H(\alpha P_{rt} + P_{rc}) > 0$, and $\lim_{P_{rt}\to+\infty} D_{rt}(P_{rt}) < 0$ [3], which means $D_{rt}(P_{rt})$ only has a unique zero point (global maximizer of $R_A(P_{rt})$) in $(-\frac{P_{rc}-P_{tc}}{\alpha+1}, +\infty)$ due to $P_s \geq 0$. When P_{rt} is less than this zero point, $D_{rt}(P_{rt}) \geq 0$; otherwise, $D_{rt}(P_{rt}) \leq 0$. Denoting $1 - H(P_{tc} + \alpha P_{rc})$ as A, and $(1 + HP_s)$ as t, we obtain from $D_{rt}(P_{rt}) = 0$ that $-\frac{A}{t}\exp(-\frac{A}{t}) = -\frac{A}{e}$. With $-\frac{A}{e} > -\frac{1}{e}$, the zero point of t is given by $t = \frac{-A}{W_0(\frac{-A}{e})}$ [56]. Finally, the global maximizer of $R_A(P_{rt})$ is given by

$$P_{rt}^{ep} = \frac{1}{H(\alpha+1)} \left[\frac{-A}{W_0(\frac{-A}{e})} - [1 + H(P_{rc} - P_{tc})] \right]. \tag{4.16}$$

Owing to the non-negativity of P_{rt}, $R_A(P_{rt})$ will decrease monotonically for $P_{rt} \geq 0$ if $P_{rt}^{ep} \leq 0$, and the optimal $P_{rt}^* = 0$. Thus, $P_{rt}^* = \{P_{rt}^{ep}\}^+ = \max\{0, P_{rt}^{ep}\}$. □

[3] It is easy to prove by applying L'Hopital's rule to the ratio of the derivatives of two subtracting parts.

$\underline{0 \le X \le P_{rc}}$:

We first examine the subproblem (4.11), where $P_{rt} = 0$. Defining $\bar{P}_{tr} = -P_{tr}$, (4.11) is reformulated as

$$\begin{aligned} \max_{P_{tr}} \ & \frac{X}{P_{rc} + \alpha \bar{P}_{tr}} \log_2 \left[1 + H((\alpha+1)\bar{P}_{tr} + (P_{rc} - P_{tc}))\right] \\ s.t. \ & -\min\{\frac{P_{rc} - X}{\alpha}, \frac{P_{rc} - P_{tc}}{\alpha + 1}\} \le \bar{P}_{rt} \le 0. \end{aligned} \tag{4.17}$$

Based on the similarities of (4.17) and (4.10), we summarize a general form of the objective function:

$$f_\beta(x) = \frac{X}{P_{rc} + \beta x} \log_2[1 + HP_s(x)], \tag{4.18}$$

where $P_s(x) = (\alpha+1)x + (P_{rc} - P_{tc}) \ge 0$, and $\beta = \alpha$ or 1. Then the original problem (4.9) is equivalent to

$$\max_x \ g(x) = \begin{cases} f_\alpha(x), \ -m_\beta < x < 0, \ (x = -P_{tr}, \ P_{rt} = 0), \\ f_\alpha(x) = f_1(x), \ x = 0, \ (P_{tr} = P_{rt} = 0), \\ f_1(x), \ x > 0, \ (x = P_{rt}, \ P_{tr} = 0), \end{cases} \tag{4.19}$$

where $m_\beta = \min\{\frac{P_{rc}-X}{\alpha}, \frac{P_{rc}-P_{tc}}{\alpha+1}\}$. We first investigate the maximizer of $f_\beta(x)$, and then applied it to (4.19) to obtain the optimal solution (P^*_{tr}, P^*_{rt}) for the original maximization problem (4.9).

The derivative of $f_\beta(x)$ is given by

$$\frac{\mathrm{d}f_\beta(x)}{\mathrm{d}x} = \frac{X \cdot D_\beta(x)}{(P_{rc} + \beta x)^2 (1 + HP_s) \ln(2)}, \tag{4.20}$$

where $D_\beta(x) = H(\alpha+1)(P_{rc} + \beta x) - \beta[1 + HP_s(x)] \ln[1 + HP_s(x)]$, which determines the sign of $\frac{\mathrm{d}f_\beta(x)}{\mathrm{d}x}$. Similar to (4.15), we have

$$\frac{\mathrm{d}D_\beta(x)}{\mathrm{d}x} = -H\beta(\alpha+1) \ln[1 + HP_s(x)] \le 0. \tag{4.21}$$

According to the proof of **Lemma 3**, we still have $D_\beta(-\frac{P_{rc}-P_{tc}}{\alpha+1}) = H[(1-\beta)P_{rc} + P_{tc}] > 0$ and $\lim_{x \to +\infty} D_\beta(x) < 0$. Thus there exists a global maximizer $x^*_\beta \in (-\frac{P_{rc}-P_{tc}}{\alpha+1}, +\infty)$ for a fixed β. When $x < x^*_\beta$, $f_\beta(x)$ is monotonically increasing, and then decreasing once x exceeds x^*_β. The global maximizers x^*_β of $f_\beta(x)$ with $\beta = \alpha$ or

1 are denoted as x_1^*, x_α^*. By transforming $f_\beta(x)$, where $\beta = \alpha$ or 1, into the form of $-\frac{A_c}{t}\exp(-\frac{A_c}{t}) = -\frac{A}{e}$ (A_c is a constant), these two maximizers are given by

- $x_\alpha^* = -\frac{1}{H(\alpha+1)}\left[\frac{-A_\alpha}{W_0(\frac{-A_\alpha}{e})} - [1 + H(P_{rc} - P_{tc})]\right]$,
- $x_1^* = \frac{1}{H(\alpha+1)}\left[\frac{-A_1}{W_0(\frac{-A_1}{e})} - [1 + H(P_{rc} - P_{tc})]\right]$,

where $A_\alpha = 1 - H(P_{tc} + P_{rc}/\alpha)$, $A_1 = 1 - H(P_{tc} + \alpha P_{rc})$. The next question is whether the global maximizers x_α^* for $f_\alpha(x)$ and x_1^* for $f_1(x)$ fall in the functions' corresponding feasible regions. The first to examine is whether they are greater or smaller than 0, the answer to which highly depends on H. **Lemma 4** describes the relationship of the locations of x_α^* and x_1^* and the values of H.

Lemma 4. *There exist two special points for H: H_α and H_1, which are the positive solutions of $D_\beta(0) = 0$ with respect to H when $\beta = \alpha$ or 1. The two points must satisfy $H_\alpha \geq H_1$. And it holds that:*

- *$H < H_1$: $0 < x_1^*, x_\alpha^*$;*
- *$H_1 \leq H \leq H_\alpha$: $x_1^* \leq 0 \leq x_\alpha^*$;*
- *$H_\alpha < H$: $x_1^*, x_\alpha^* < 0$.*

Proof. In this proof, we show the relationship of the values of H and the signs of x_α^* and x_1^*. It is known in Section 4.2.2 that $f_\beta(x)$, $\beta = \alpha$ or 1, has a global maximizer $x_\beta^* \in (-\frac{P_{rc}-P_{tc}}{\alpha+1}, +\infty)$, and $\frac{\mathrm{d}f_\beta(x)}{\mathrm{d}x} = M \cdot D_\beta(x)$, where $M \geq 0$. When $x < x_\beta^*$, $D_\beta(x) \geq 0$ and $f_\beta(x)$ is monotonically increasing; when $x > x_\beta^*$, $D_\beta(x) \leq 0$ and $f_\beta(x)$ is monotonically decreasing. It is obvious that $x_\beta^* \cdot D_\beta(0) \geq 0$. Therefore, to determine the sign of x_β^*, we can first examine the sign of $D_\beta(0)$, which depends on the value of H. Denote $D_\beta(0)$ as $Z_\beta(H)$ with respect to H:

$$Z_\beta(H) = H(\alpha+1)P_{rc} - \beta[1 + H\Delta P_c]\ln[1 + H\Delta P_c], \tag{4.22}$$

where $\Delta P_c = P_{rc} - P_{tc} > 0$. Taking the derivatives of $Z_\beta(H)$ with respect to H, we obtain

$$\begin{aligned} \frac{\mathrm{d}Z_\beta(H)}{\mathrm{d}H} &= [(\alpha + 1 - \beta)P_{rc} + \beta P_{tc}] - \beta\Delta P_c \ln[1 + H\Delta P_c], \\ \frac{\mathrm{d}^2 Z_\beta(H)}{\mathrm{d}H^2} &= -\frac{\beta\Delta P_c^2}{1 + H\Delta P_c} \leq 0 \end{aligned} \tag{4.23}$$

which indicates that (4.22) is a concave function with respect to $H \in [0, +\infty)$ and the global maximizer of $Z_\beta(H)$ is located in $H \in (0, +\infty)$ due to $\frac{\mathrm{d}Z_\beta(H)}{\mathrm{d}H}|_{H=0} > 0$. It is easy to see that $Z_\beta(0) = 0, \lim_{H\to+\infty} Z_\beta(H) < 0$. Therefore, there must be a zero point $H_\beta > 0$ that makes $Z_\beta(H_\beta) = 0$. In sum, we have $D_\beta(0) = Z_\beta(H) > 0$ for any $0 < H < H_\beta$, and $D_\beta(0) = Z_\beta(H) < 0$ for any $H > H_\beta$. Some common root search algorithms such as bisection, Newton methods, etc., can be used to find H_β.

As for the cases of $\beta = \alpha$ and 1, it always holds that $Z_\alpha(H) - Z_1(H) = (1-\alpha)[1 + H\Delta P_c]\ln[1 + H\Delta P_c] \geq 0$, which implies that $H_\alpha \geq H_1$. Due to the fact that $D_\beta(0)$ has the same sign as x^*_β, we conclude that:

- $H < H_1$: $0 < x^*_1, x^*_\alpha$;
- $H_1 \leq H \leq H_\alpha$: $x^*_1 \leq 0 \leq x^*_\alpha$;
- $H_\alpha < H$: $x^*_1, x^*_\alpha < 0$.

Lemma 4 is thus proved. □

Finally, we can summarize the optimal solution for (4.9):

- $H < H_1$ $(0 < x^*_1, x^*_\alpha)$: it holds that $\max_{x\leq 0}\{g(x)\} = \max_{x\leq 0}\{f_\alpha(x)\} = g(0) = f_1(0) \leq \max_{x\geq 0}\{g(x)\} = \max_{x\geq 0}\{f_1(x)\} = f_1(x^*_1)$. The solution is $(P^*_{tr} = 0, P^*_{rt} = x^*_1)$;
- $H_1 \leq H \leq H_\alpha$ $(x^*_1 \leq 0 \leq x^*_\alpha)$: $\max_{x\leq 0}\{g(x)\} = \max_{x\geq 0}\{g(x)\} = g(0)$. The solution is $(P^*_{tr} = P^*_{rt} = 0)$;
- $H_\alpha < H$ $(x^*_1, x^*_\alpha < 0)$: we have $\max_{x\leq 0}\{g(x)\} = \max_{x\leq 0}\{f_\alpha(x)\} = f_\alpha(x^*_\alpha) \geq \max_{x\geq 0}\{g(x)\} = \max_{x\geq 0}\{f_1(x)\} = g(0)$. The solution is $(P^*_{tr} = -x^*_\alpha, P^*_{rt} = 0)$. However, P_{tr} has an upper bound of $\min\{\frac{P_{rc}-X}{\alpha}, \frac{P_{rc}-P_{tc}}{\alpha+1}\}$, and hence the optimal solution should be revised as $P^*_{tr} = \min\{\frac{P_{rc}-X}{\alpha}, \frac{P_{rc}-P_{tc}}{\alpha+1}, -x^*_\alpha\}$.

Furthermore, the optimal $\rho^*_t = \rho^*_r = \rho^*$ is given by (4.7).

In summary, the optimal energy cooperation scheme (P^*_{tr}, P^*_{rt}) under the EC-ST scheme for maximizing the normalized throughput of P2P wireless communications can be intuitively explained. When the energy arrival rate X overflows at the receiver $(X > P_{rc})$, only one-way energy transfer from the receiver to the transmitter is necessary to improve the throughput by making use of extra energy. When the receiver harvests insufficient energy for running circuits $(X \leq P_{rc})$, the direction of

energy transfer depends on the channel condition H. Energy is transferred from the receiver to transmitter to support the transmission by reducing the active-ratio ρ^* if the channel power gain is too low ($H < H_1$), or from the transmitter to receiver to extend the active-ratio if the channel condition is good ($H > H_\alpha$). Otherwise, no energy cooperation is allowed.

4.3 Outage Probability Minimization under Fading Channels

In this section, we consider a more general and practical scenario, where the communications environment is changing, with a mobile transmitter and receiver, and thus, the channel condition varies randomly. Assume a Rayleigh block fading channel. The normalized channel power gain $H = \frac{|h|^2}{\sigma^2}$ follows exponential distribution with mean of λ_H. We further assume the energy arrival rate X follows the Gamma distribution $\Gamma(k, \theta)$ with a shape parameter $k \geq 1$ and a scale parameter $\theta > 0$ [53]-[54]. The mean value of X is given by $\lambda_X = k\theta$. Thus, the probability density functions (PDF) of H and X are respectively given by

$$p_H(H) = \frac{1}{\lambda_H} \exp(-\frac{H}{\lambda_H}),\ p_X(X) = \frac{X^{k-1} \exp(-\frac{X}{\theta})}{\theta^k \Gamma(k)}, \tag{4.24}$$

where $\Gamma(k)$ is the gamma function evaluated at k. In addition, the Gamma distribution is reduced to the exponential distribution when $k = 1$.

In block fading channels, H remains constant during the time within one block but varies randomly from block to block [27]. In such scenarios, it is more essential to investigate the system outage performance than the ergodic throughput. Suppose the transmitter encodes and transmits data at a required rate $\bar{R}$ and the channel capacity gives a maximum rate R_S of reliable communications supported by this channel. A channel outage event happens when $R_S < \bar{R}$. Furthermore, we also introduce the circuit outage event due to the insufficient power to sustain circuit operations similar to [53]. However, [53] only considers the circuit power consumption in the transmitter and assumes an ideal receiver that has a constant power supply. The circuit outage event thus only happens at the transmitter side. In our model, a practical receiver needs to harvest energy from the external environment for running circuits, and the EC-ST scheme allows the transmitter and receiver to share their

energy in one time block. Under such assumptions, the circuit outage event can occur at both the transmitter and receiver after energy cooperation.

4.3.1 Outage Probability Minimization Problem

The EC-ST scheme is applied at the transmitter and receiver, and they share the identical active-ratio ρ. In the following analysis, we only focus on the parameter optimization of the energy cooperation scheme: (ρ, P_{tr} and P_{tr}). During the active time, the total power of transmitter and receiver with energy transfer can be formulated as

$$P_t = \frac{X}{\rho} + \alpha P_{rt} - P_{tr}, \quad P_r = \frac{X}{\rho} + \alpha P_{tr} - P_{rt}, \tag{4.25}$$

where P_t and P_r are the total available power of the transmitter and receiver respectively, resulting from energy harvesting and cooperation. In order to make the system work, P_t and P_r must, at least, be larger than the power consumption on hardware circuits P_{tc} and P_{rc} respectively: $P_t \geq P_{tc}$, $P_r \geq P_{rc}$, so that the rest of the energy could be used for communications after energy cooperation. In terms of X, we rewrite these two conditions into one:

$$X \geq \Theta(\rho, P_{tr}, P_{rt}) = \max\{\Theta_1(\rho, P_{tr}, P_{rt}), \Theta_2(\rho, P_{tr}, P_{rt})\}, \tag{4.26}$$

where $\Theta_1(\rho, P_{tr}, P_{rt}) = \rho(P_{tc} + P_{tr} - \alpha P_{rt})$, $\Theta_2(\rho, P_{tr}, P_{rt}) = \rho(P_{rc} + P_{rt} - \alpha P_{tr})$. The circuit outage event happens at either the transmitter or receiver when $X < \Theta(\rho, P_{tr}, P_{rt})$.

Once both the transmitter and receiver work normally, they need to communicate with the required rate $\bar{R}$ bps/Hz over a time block. The available transmission power is given by $P_s = P_t - P_{tc}$, and the achievable rate, when $P_s \geq 0$, is

$$R_S = \rho \log_2(1 + HP_s) = \rho \log_2[1 + H(P_t - P_{tc})]. \tag{4.27}$$

The channel outage event happens due to insufficient data rate $R_S < \bar{R}$. Finally, the combination of the circuit outage and the channel outage (mutually exclusive) is the ultimate outage event for such a system [53], and given by

$$\begin{aligned} P_{out}^{circuit} &= \Pr\{X < \Theta(\rho, P_{tr}, P_{rt})\} \\ &= \int_0^{\Theta(\cdot)} p_X(X) \mathrm{d}X. \end{aligned} \tag{4.28}$$

$$\begin{aligned} P_{out}^{channel} &= \Pr\{R_S < \bar{R}, X \geq \Theta(\rho, P_{tr}, P_{rt})\} \\ &= \Pr\{H < \frac{2^{(\bar{R}/\rho)} - 1}{P_t - P_{tc}}, X \geq \Theta(\rho, P_{tr}, P_{rt})\} \\ &= \int_{\Theta(\cdot)}^{\infty} F_H \left(\frac{2^{(\bar{R}/\rho)} - 1}{P_t - P_{tc}} \right) p_X(X) \mathrm{d}X, \end{aligned} \tag{4.29}$$

where $\Theta(\cdot)$ means $\Theta(\rho, P_{tr}, P_{rt})$, and $F_H(a) = \int_0^a p_H(H)\mathrm{d}H$, which is the cumulative distribution function of random variable H.

The outage probability of the communications system is finally

$$\begin{aligned} P_{out} &= \int_0^{\Theta(\cdot)} p_X(X)\mathrm{d}X + \int_{\Theta(\cdot)}^{\infty} F_H \left(\frac{2^{\frac{\bar{R}}{\rho}} - 1}{P_t - P_{tc}} \right) p_X(X)\mathrm{d}X \\ &= \int_0^{\Theta(\cdot)} p_X(X)\mathrm{d}X + \int_{\Theta(\cdot)}^{\infty} \left[1 - \exp\left(-\frac{T(\rho, \bar{R})}{\lambda_H[X - \Theta_1(\cdot)]} \right) \right] p_X(X)\mathrm{d}X \\ &= 1 - \int_{\Theta(\cdot)}^{\infty} \exp\left(-\frac{T(\rho, \bar{R})}{\lambda_H[X - \Theta_1(\cdot)]} \right) p_X(X)\mathrm{d}X, \end{aligned} \tag{4.30}$$

where $T(\rho, \bar{R}) = \rho(2^{\frac{\bar{R}}{\rho}} - 1)$.

By observing (4.30), one can find that P_{out} depends on both the channel and energy harvesting condition. Under the EC-ST scheme, we can adjust the energy cooperation power P_{tr}, P_{rt} or active-ratio ρ to obtain better communications performance. Since we extend the feasible region from $\{\rho \in (0, 1], P_{tr} = P_{rt} = 0\}$ (no energy cooperation) to $\{\rho \in (0, 1], P_{tr}, P_{rt} \geq 0\}$, we may obtain smaller outage probability by applying the EC-ST scheme than without energy cooperation. The outage probability minimization problem can finally be expressed as

$$\begin{aligned} \min_{\rho, P_{tr}, P_{rt}} \quad & \left\{ 1 - \int_{\Theta(\cdot)}^{\infty} \exp\left(-\frac{T(\rho, \bar{R})}{\lambda_H[X - \Theta_1(\cdot)]} \right) p_X(X)\mathrm{d}X \right\} \\ s.t. \quad & \rho \in (0, 1], P_{tr}, P_{rt} \geq 0. \end{aligned} \tag{4.31}$$

4.3.2 Energy Cooperation for Minimizing Outage Probability

Remark 3. *To solve the problem (4.31), first we discretize the continuous ρ into a finite number of discrete values, like {1%, 2%, ..., 100%}, and then optimize the parameters P_{tr}, P_{rt} for a given ρ value, and finally choose an optimal ρ among all*

the discrete values that minimizes the outage probability. In most applications, the required resolution of duty cycle (active-ratio in this chapter) of a device is relatively low (integer percent is enough), and therefore, it is reasonable to find optimal ρ by discretization.

For a given ρ, the outage probability minimization problem (4.31) is reformulated as

$$\max_{P_{tr},P_{rt}\geq 0} \; I(P_{tr},P_{rt}) = \int_{\Theta(\cdot)}^{\infty} \exp\left(-\frac{T(\rho,\bar{R})}{\lambda_H[X-\Theta_1(\cdot)]}\right) p_X(X)\mathrm{d}X, \tag{4.32}$$

where ρ is a constant in $(0,1]$.

To solve (4.32), we first expand the integral:

$$\begin{aligned} I(P_{tr},P_{rt}) =& \int_{\Theta(\cdot)}^{\infty} \exp\left(-\frac{T(\rho,\bar{R})}{\lambda_H[X-\Theta_1(\cdot)]}\right)\cdot\left[\frac{X^{k-1}\exp(-\frac{X}{\theta})}{\theta^k\Gamma(k)}\right]\mathrm{d}X \\ =& \frac{\exp\left(-\frac{\Theta_1(\cdot)}{\theta}\right)}{\theta^k\Gamma(k)}\int_{\Theta(\cdot)-\Theta_1(\cdot)}^{\infty} E(X)\mathrm{d}X, \end{aligned} \tag{4.33}$$

where $E(X)=\exp\left(-\frac{T(\rho,\bar{R})}{\lambda_H X}-\frac{X}{\theta}\right)[X+\Theta_1(\cdot)]^{(k-1)}$. Due to $I(P_{tr},P_{rt})\in[0,1]$ and $\exp\left(-\frac{\Theta_1(\cdot)}{\theta}\right)/[\theta^k\Gamma(k)]\geq 0$, it always holds that $\int_{\Theta(\cdot)-\Theta_1(\cdot)}^{\infty}E(X)\mathrm{d}X\geq 0$.

Although the integral in (4.33) does not have a closed form, note that the energy cooperation related variables (P_{tr},P_{rt}) only appear in the lower limit of the integral and in the exponential function outside the integral. Considering that $\Theta(\cdot)=\max\{\Theta_1(\cdot),\Theta_2(\cdot)\}$, we divide the feasible region constrained by $\{(P_{tr},P_{rt}):P_{tr}\geq 0,P_{rt}\geq 0\}$ into two sub-region: $R_1=\{(P_{tr},P_{rt}):P_{tr}\geq 0,P_{rt}\geq 0,\Theta_1(\cdot)\geq\Theta_2(\cdot)\}$ and $R_2=\{(P_{tr},P_{rt}):P_{tr}\geq 0,P_{rt}\geq 0,\Theta_1(\cdot)<\Theta_2(\cdot)\}$. Once we find the optimal solutions in both sub-regions and choose a better one, the optimization of (4.33) is completed.

$\underline{\Theta_1(\cdot)\geq\Theta_2(\cdot)}$:

In this case, $\Theta_1(\cdot)\geq\Theta_2(\cdot)$ is equivalent to $P_{rt}-P_{tr}\leq-\frac{P_{rc}-P_{tc}}{\alpha+1}$. Moreover, due to $\Theta(\cdot)=\Theta_1(\cdot)$, the integral in (4.33) becomes a constant since the lower limit of the integral becomes zero. The only part that still contains (P_{tr},P_{rt}) is $\exp\left(-\frac{\Theta_1(\cdot)}{\theta}\right)$, and

hence the outage probability minimization problem in R_1 is reduced into

$$\begin{aligned} &\max_{(P_{tr},P_{rt})\in R_1} \exp\left(-\frac{\Theta_1(\cdot)}{\theta}\right) \\ \Rightarrow &\min_{(P_{tr},P_{rt})\in R_1} \frac{\Theta_1(\cdot)}{\rho} = (P_{tc}+P_{tr}-\alpha P_{rt}). \end{aligned} \tag{4.34}$$

It is easy to get the optimal solution (P_{tr}^*, P_{rt}^*) in the sub-region R_1 by using linear programming, which is

$$P_{tr}^* = \frac{P_{rc}-P_{tc}}{\alpha+1},\ P_{rt}^* = 0. \tag{4.35}$$

The corresponding outage probability is given by

$$P_{out} = 1 - \frac{1}{\theta^k\Gamma(k)} \exp\left[-\frac{\rho(P_{rc}+\alpha P_{tc})}{\theta(\alpha+1)}\right] \int_0^{+\infty} E(X)\mathrm{d}X. \tag{4.36}$$

$\underline{\Theta_1(\cdot) < \Theta_2(\cdot)}$:

We still express $\Theta_1(\cdot) < \Theta_2(\cdot)$ as $P_{rt} - P_{tr} > -\frac{P_{rc}-P_{tc}}{\alpha+1}$. In this case $\Theta(\cdot) = \Theta_2(\cdot)$, and (4.33) can be represented as

$$I(P_{tr}, P_{rt}) = \frac{\exp\left(-\frac{\Theta_1(\cdot)}{\theta}\right)}{\theta^k\Gamma(k)} \int_{\Theta_2(\cdot)-\Theta_1(\cdot)}^{\infty} E(X)\mathrm{d}X. \tag{4.37}$$

Furthermore, sub-region R_2 is composed of all half-lines defined as $\{(P_{tr}, P_{rt}) : P_{tr} \geq 0, P_{rt} \geq 0, \Theta_2(\cdot) - \Theta_1(\cdot) = C\}$, where C is a positive constant. In addition, $\Theta_2(\cdot) - \Theta_1(\cdot) = C$ is equivalent to $P_{rt} - P_{tr} = C_p$, where the constant $C_p = \frac{C}{\rho} - \frac{P_{rc}-P_{tc}}{\alpha+1} > -\frac{P_{rc}-P_{tc}}{\alpha+1}$. It is feasible to find the optimal point on each half-line as C increases from zero to positive infinity, and then combine all found optimal points to search the optimal solution in R_2. For a fixed C, the integral part of (4.37) remains constant, and we just need to minimize $\Theta_1(\cdot)/\rho = P_{tc}+P_{tr}-\alpha P_{rt}$ (ρ is given). Then we have $\min\{P_{tc}+P_{tr}-\alpha P_{rt}\} = \min\{P_{tc}+(1-\alpha)P_{tr}+\alpha C_p\} = \min\{(1-\alpha)P_{tr}\}$. Therefore, the optimal point in a half-line with parameter C and C_p is $(P_{tr} = -C_p, P_{rt} = 0)$ if $C_p < 0$, or $(P_{tr} = 0, P_{rt} = C_p)$ if $C_p \geq 0$. In summary, the optimal point for minimizing the outage probability in R_2 must satisfy $P_{tr}^* \cdot P_{rt}^* = 0$. It is exactly identical to the necessary condition for optimal energy cooperation in the AWGN channel scenario in **Lemma 2**. This confirms the intuition that the performance will degrade once we transfer energy forward and backward simultaneously, because some

energy can be wasted due to the imperfect transfer efficiency α.

Finally, synthesizing the analysis about R_1 and R_2, the feasible region for the whole outage probability minimization can be reduced to

$$R = \{(P_{tr}, P_{rt}) : \frac{P_{rc} - P_{tc}}{\alpha + 1} \geq P_{tr} \geq 0, P_{rt} \geq 0, P_{tr}P_{rt} = 0\}. \tag{4.38}$$

Here, we define a variable $P_d = P_{rt} - P_{tr} \geq -\frac{P_{rc}-P_{tc}}{\alpha+1}$. For all the feasible points in R, it holds

$$P_d = \begin{cases} P_{rt}, & P_d \geq 0, P_{tr} = 0 \\ -P_{tr}, & P_d \leq 0, P_{rt} = 0. \end{cases} \tag{4.39}$$

And (4.37) can be rewritten in terms of P_d as

$$I_\beta(P_d) = \frac{\exp\left(L_1(P_d)\right)}{\theta^k \Gamma(k)} \int_{L_2(P_d)}^{\infty} E(X) \mathrm{d}X, \tag{4.40}$$

where $L_1(P_d) = -\frac{\rho}{\theta}(P_{tc} - \beta P_d)$, $L_2(P_d) = \rho[(P_{rc} - P_{tc}) + (\alpha + 1)P_d]$, $\beta = \alpha$ when $P_d \geq 0$, and $\beta = 1$ when $P_d \leq 0$. And $I(P_{tr}, P_{rt})$ which is feasible in R is reformulated as

$$I(P_{tr}, P_{rt}) = \begin{cases} I_1(P_d), & P_d = -P_{tr} \leq 0, P_{rt} = 0, \\ I_\alpha(P_d), & P_d = P_{rt} \geq 0, P_{tr} = 0, \end{cases} \tag{4.41}$$

which is continuous in $[-\frac{P_{rc}-P_{tc}}{\alpha+1}, +\infty)$.

Lemma 5. *For any $\beta \in \{\alpha, 1\}$, $I_\beta(P_d)$ is a quasi-concave function in $[-\frac{P_{rc}-P_{tc}}{\alpha+1}, +\infty)$ (P_{out} is thus quasi-convex with respect to P_d). There is a global maximizer $-\frac{P_{rc}-P_{tc}}{\alpha+1} < P_d^* < +\infty$. When $P_d < P_d^*$, $I_\beta(P_d)$ is non-decreasing; when $P_d \geq P_d^*$, $I_\beta(P_d)$ is non-increasing. Besides, using P_α^*, P_1^* to present P_d^* when $\beta = \alpha, 1$ respectively, we have $P_\alpha^* \leq P_1^*$.*

Proof. To prove that $I_\beta(P_d)$ is quasi-concave, we first see the properties of its derivative. It is known that $E(X) = \exp\left(-\frac{T(\rho,\bar{R})}{\lambda_H X} - \frac{X}{\theta}\right)[X + \Theta_1(\cdot)]^{(k-1)}$ and we have

$$\frac{\mathrm{d}I_\beta(P_d)}{\mathrm{d}P_d} = \frac{\rho(\alpha+1)}{\theta^k \Gamma(k)} \exp\left[L_1(P_d)\right] \cdot V_\beta(P_d), \tag{4.42}$$

where $V_\beta(P_d) = \frac{\beta}{\theta(\alpha+1)} \int_{L_2(P_d)}^{\infty} E(X)\mathrm{d}X - E[L_2(P_d)]$ with $\beta \in \{\alpha, 1\}$, $L_1(P_d) = -\frac{\rho}{\theta}(P_{tc} - \beta P_d)$, and $L_2(P_d) = \rho[(P_{rc} - P_{tc}) + (\alpha + 1)P_d]$. Here, we use the numerical integration method to approach the value of $V_\beta(P_d)$. It is obvious that $\frac{\rho(\alpha+1)}{\theta^k\Gamma(k)} \exp\left[L_1(P_d)\right] \geq 0$,

so the sign of (4.42) only depends on $V_\beta(P_d)$. Taking the derivative of $V_\beta(P_d)$ yields

$$\frac{\mathrm{d}V_\beta(P_d)}{\mathrm{d}P_d} = \rho(\alpha+1)E[L_2(P_d)]\left\{\frac{\alpha+1-\beta}{\theta(\alpha+1)} - \frac{T(\rho,\bar{R})}{\lambda_H L_2(P_d)^2} - \frac{(k-1)(\alpha+1-\beta)}{\rho(\alpha+1)[P_{rc}+(\alpha+1-\beta)P_d]}\right\}. \tag{4.43}$$

Here, we first check the sign of $\rho(\alpha+1)E[L_2(P_d)]$. It is obvious that $\rho(\alpha+1)\exp\left(-\frac{T(\rho,\bar{R})}{\lambda_H L_2(P_d)} - \frac{L_2(P_d)}{\theta}\right) \geq 0$. As for $[L_2(P_d)+\Theta_1(\cdot)]^{(k-1)}$, we have

$$\begin{aligned} L_2(P_d)+\Theta_1(\cdot) &= \rho[P_{rc}-P_{tc}+(\alpha+1)P_d]+\rho(P_{tc}-\beta P_d) \\ &= \rho[P_{rc}+(\alpha+1-\beta)P_d] \\ &\geq \rho[P_{rc}-(\alpha+1-\beta)\frac{P_{rc}-P_{tc}}{\alpha+1}] \\ &= \rho\left[\frac{\beta}{\alpha+1}P_{rc}+\frac{\alpha+1-\beta}{\alpha+1}P_{tc}\right] \geq 0. \end{aligned} \tag{4.44}$$

Therefore, the first part of (4.43) $\rho(\alpha+1)E[L_2(P_d)] \geq 0$. Furthermore, Taking the derivative of the second part $S(P_d) = \left[\frac{\alpha+1-\beta}{\theta(\alpha+1)} - \frac{T(\rho,\bar{R})}{\lambda_H L_2(P_d)^2} - \frac{(k-1)(\alpha+1-\beta)}{\rho(\alpha+1)[P_{rc}+(\alpha+1-\beta)P_d]}\right]$ with respect to P_d, we see that the derivative $\frac{2\rho(\alpha+1)T(\rho,\bar{R})}{\lambda_H L_2(P_d)^3} + \frac{(k-1)(\alpha+1-\beta)^2}{\rho(\alpha+1)[P_{rc}+(\alpha+1-\beta)P_d]^2} \geq 0$. Therefore, $V_\beta(P_d)$ is quasi-convex [25] when $P_d \in [-\frac{P_{rc}-P_{tc}}{\alpha+1}, +\infty)$, and the minimizer of $V_\beta(P_d)$, denoted as P_d^{ep}, should make the monotonically increasing function $S(P_d) = 0$. Note that $\frac{(k-1)(\alpha+1-\beta)}{\rho(\alpha+1)[P_{rc}+(\alpha+1-\beta)P_d]} \geq 0$ according to (4.44). P_d^{eq} should not be less than the zero point of $\left[\frac{\alpha+1-\beta}{\theta(\alpha+1)} - \frac{T(\rho,\bar{R})}{\lambda_H L_2(P_d)^2}\right]$, which means

$$P_d^{ep} \geq -\frac{P_{rc}-P_{tc}}{\alpha+1} + \sqrt{\frac{(\alpha+1)\theta T(\rho,\bar{R})}{\rho^2(\alpha+1-\beta)\lambda_H}} > -\frac{P_{rc}-P_{tc}}{\alpha+1}, \tag{4.45}$$

and $\frac{\mathrm{d}V_\beta(P_d)}{\mathrm{d}P_d}|_{P_d=P_d^{ep}} = 0$. For $P_d \leq P_d^{ep}$, $\frac{\mathrm{d}V_\beta(P_d)}{\mathrm{d}P_d} \leq 0$ and $V_\beta(P_d)$ is non-increasing, while for $P_d \geq P_d^{ep}$, $\frac{\mathrm{d}V_\beta(P_d)}{\mathrm{d}P_d} \geq 0$ and $V_\beta(P_d)$ is non-decreasing. Furthermore, due to $E(0) = [\Theta_1(\cdot)]^{(k-1)}\exp(-\infty) = 0$, $E(+\infty) = \lim_{X\to+\infty}\exp(-\frac{X}{\theta})[X+\Theta_1(\cdot)]^{(k-1)} = 0$ and $\int_{\Theta_2(\cdot)-\Theta_1(\cdot)}^{\infty} E(X)\mathrm{d}X \geq 0$ for all feasible P_d, it holds that

$$\begin{aligned} V_\beta(-\frac{P_{rc}-P_{tc}}{\alpha+1}) &= \frac{\beta}{\theta(\alpha+1)}\int_0^\infty E(X)\mathrm{d}X > 0, \\ \lim_{P_d\to+\infty} V_\beta(P_d) &= \frac{\beta}{\theta(\alpha+1)}\int_{+\infty}^{+\infty} E(X) - E(+\infty) = 0. \end{aligned} \tag{4.46}$$

According to the quasi-convexity of $V_\beta(P_d)$ and (4.46), $V_\beta(P_d)$ has a unique zero

point $P_d^* \in (-\frac{P_{rc}-P_{tc}}{\alpha+1}, P_d^{ep})$: $V_\beta(P_d) \geq 0$ for all $P_d \leq P_d^*$, and $V_\beta(P_d) \leq V_\beta(+\infty) = 0$ for all $P_d \geq P_d^*$. Finally, we return to the monotonicity of $I_\beta(P_d)$ predicated on the sign of $V_\beta(P_d)$:

- $I_\beta(P_d)$ is non-decreasing for $P_d \in [-\frac{P_{rc}-P_{tc}}{\alpha+1}, P_d^*)$;
- $I_\beta(P_d)$ is non-increasing for $P_d \in [P_d^*, +\infty)$.

With such properties, $I_\beta(P_d)$ is quasi-concave with a global maximizer $P_d = P_d^*$ for $P_d \in [-\frac{P_{rc}-P_{tc}}{\alpha+1}, +\infty)$ [25]. Moreover, we use P_α^*, P_1^* to present P_d^* when $\beta = \alpha, 1$ respectively. Since $V_\beta(P_d^*) = 0$, and $L_2(P_d)$ is irrelevant to β, we have

$$\begin{aligned} &V_\alpha(P_\alpha^*) = 0;\ V_1(P_1^*) = 0; \\ &V_1(P_\alpha^*) = \frac{1-\alpha+\alpha}{\theta(\alpha+1)} \int_{L_2(P_\alpha^*)}^{\infty} E(X)\mathrm{d}X - E[L_2(P_\alpha^*)] \\ &\qquad = V_\alpha(P_\alpha^*) + \frac{1-\alpha}{\theta(\alpha+1)} \int_{L_2(P_\alpha^*)}^{\infty} E(X)\mathrm{d}X \geq 0. \end{aligned} \tag{4.47}$$

Considering the monotonicity of $V_\beta(P_d)$, no matter $\beta = \alpha$ or 1, the inequality $P_\alpha^* \leq P_1^*$ is tenable. The proof of **Lemma 5** is completed. □

Since (4.41) includes all the cases of $I(P_{tr}, P_{rt})$: $I_1(P_d)$ with $P_{rt} = 0$ and $I_\alpha(P_d)$ with $P_{tr} = 0$, the larger one of $\max_{-\frac{P_{rc}-P_{tc}}{\alpha+1} \leq P_d \leq 0}\{I_1(P_d)\}$ and $\max_{P_d \geq 0}\{I_\alpha(P_d)\}$ will be the maximum of $I(P_{tr}, P_{rt})$, corresponding to the minimum outage probability. Here is the summary of steps to find the optimal (P_{tr}^*, P_{rt}^*):

1) Apply bisection search to find the unique zero point of $V_\beta(P_d)$ (defined in the proof of **Lemma 5**): P_α^*, P_1^* for $\beta = \alpha$ and 1;
2) Check the value of P_α^* and P_1^*:
   a) $P_1^* < 0$: $\max\{I(P_{tr}, P_{rt})\} = \max_{P_d \leq 0}\{I_1(P_d)\} = I_1(P_1^*) \geq I_\alpha(0) = \max_{P_d \geq 0}\{I_\alpha(P_d)\}$, and the optimal solution is $P_d^* = P_1^*$;
   b) $P_\alpha^* \leq 0 \leq P_1^*$: we have $\max\{I(P_{tr}, P_{rt})\} = \max_{P_d \leq 0}\{I_1(P_d)\} = \max_{P_d \geq 0}\{I_\alpha(P_d)\} = I_1(0) = I_\alpha(0)$, and the optimal solution is $P_d^* = 0$;
   c) $P_\alpha^* > 0$: $\max\{I(P_{tr}, P_{rt})\} = \max_{P_d \geq 0}\{I_\alpha(P_d)\} = I_\alpha(P_\alpha^*) \geq I_1(0) = \max_{P_d \leq 0}\{I_1(P_d)\}$, and the optimal solution is $P_d^* = P_\alpha^*$.
3) Use the relation between P_d and (P_{tr}, P_{rt}) to obtain the final energy cooperation scheme (P_{tr}^*, P_{rt}^*).

This result parallels that of the AWGN channel in Section 4.2.2, depending on the energy arrival rate from the external source and channel condition.

4.4 Numerical & Simulation Results

The optimization results of the EC-ST scheme are obtained by numerical computation of the theoretical analysis. The throughput performance in AWGN is calculated by numerical methods, and the outage probability results in Rayleigh channels are obtained by simulation. The simulation setups are based on the communications between the energy harvesting transmitter and receiver with practical circuits that consume non-zero power when they are active. We introduce two other schemes based on ST for comparison: the practical transmitter (Tx) ST scheme and idealistic transmitter (Tx) ST scheme:

- The practical Tx ST scheme makes the best use of the harvested energy at the transmitter side where a certain part of the harvested energy is consumed by active circuits, to reach an optimal tradeoff between the transmission power and active ratio for the transmitter [52], [53]. However, it treats the receiver as an ideal one that can work continuously without any energy constraints.

- Idealistic Tx ST scheme performs like the practical Tx ST scheme, but assumes that the power consumption of active transmitter's circuits is also zero.

None of the practical and idealistic Tx ST schemes allow energy cooperation between the transmitter and receiver. For all examples, we assume that the power consumption of active circuits on transmitter and receiver are $P_{tc} = 50$ mW and $P_{rc} = 200$ mW respectively.

4.4.1 Numerical Examples for the AWGN Channel Case

In the AWGN channel scenario, numerical results using the closed form optimization solutions that were derived in Section 4.2 are presented. Fig. 4.4 shows the direction of energy transfer to realize optimal energy cooperation under different energy transfer efficiency α's and normalized channel power gain H's, illustrated by **Lemma 4**. When the energy arrival rate $X < P_{rc}$ ($X = 100$ mW), the energy can be transferred from the transmitter to receiver or in the inverse direction. The whole plane of (α, H) is divided into three regions:

- When $H < H_1$, energy should be transferred from the receiver to the transmitter to fight the poor channel condition;
- When $H_1 \leq H \leq H_\alpha$, no energy cooperation is needed;
- When $H > H_\alpha$, energy should be transferred from the transmitter to the receiver to extend the active ratio, with the well-conditioned channel.

The values of H_1 and H_α are determined by α. When α gets closer to 0, the difference of H_α and H_1 will become larger and finally approach infinity, which means no energy cooperation is allowed. Intuitively and theoretically, α determines how much energy will disappear after energy transfer. Under a low α, energy cooperation may be prohibited to prevent wasting energy, while energy cooperation can improve the communications performance with a high α. To give an idea of the energy cooperation power, we sample 4 points in Fig. 4.4 when $\alpha = 0.75$ and show the corresponding energy cooperation power in TABLE 4.1. It is shown that when $H = 16$ or 21 dB which correspond to the points close to the borders of the no energy cooperation region, the energy cooperation power can be negligible ($P_{rt} = 2.9$ mW or $P_{tr} = 1.1$ mW). On the other hand, when $H = 10$ or 30 dB, corresponding to the points located far away from the no energy cooperation region, the energy cooperation power is $P_{rt} = 62.3$ mW or $P_{tr} = 34.8$ mW, comparable to the energy harvesting rate $X = 100$ mW, which means the energy cooperation is necessary under these conditions.

Table 4.1:

H	10 dB	16 dB	21 dB	30 dB
P_{tr}	0	0	1.1 mW	34.8 mW
P_{rt}	62.3 mW	2.9 mW	0	0

Fig. 4.5 compares the throughput performances under the EC-ST, practical Tx ST, and idealistic Tx ST schemes with $\alpha = 0.75, H = 60$ dB, by increasing the energy arrival rate X. Note that the energy transfer efficiency $\alpha = 0.75$ can be possibly achieved by the magnetic resonant coupling technique [57]. Obviously, the EC-ST scheme outperforms the others. Failing to consider the power consumption of circuits, the performance of the idealistic Tx ST scheme is slightly degraded compared to the practical Tx ST scheme when $100 < X < 150$ mW because the former cannot arrive at the proper transmission power P_s when ignoring the power consumption of circuits. When $X \geq 150$ mW, the idealistic Tx ST scheme falls significantly behind

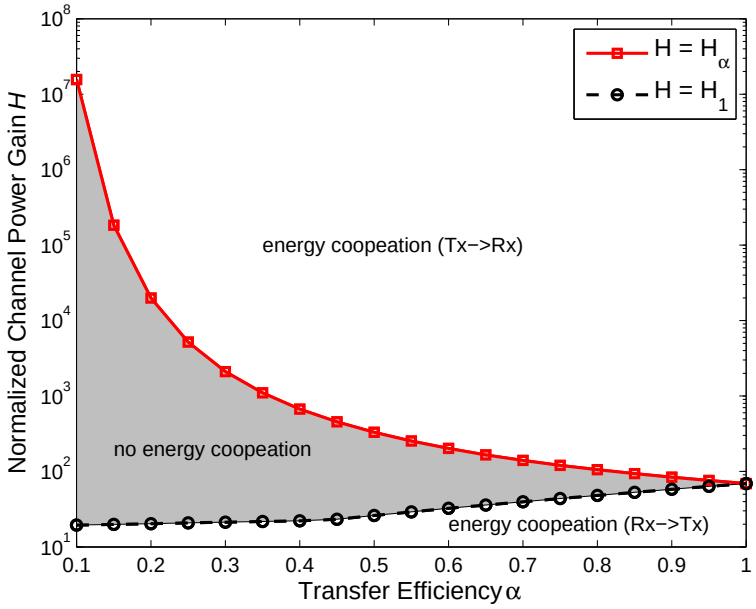

Figure 4.4: The regions with/without energy cooperation in AWGN channels (Transmitter: Tx, Receiver: Rx).

the practical Tx ST scheme because its ρ_t starts to be less than ρ_r, which means the receiver keeps active for a period of $(\rho_r - \rho_t)T$ but cannot receive any information from the non-active transmitter, wasting the harvested energy. The EC-ST scheme outperforms the practical Tx ST scheme because the latter does not perform any energy cooperation. When $X < 200$ mW, the transmitter in the EC-ST scheme transfers energy to the receiver to extend the active ratio ρ, through appropriately reducing transmission power for communications, and finally improves the throughput. When $X = 200$ mW, no energy cooperation is necessary and hence the EC-ST scheme is equivalent to the practical Tx ST at this point. When $X > 200$ mW, the energy that overflows at the receiver will be transferred to the transmitter in the EC-ST scheme and thus enhance transmission power. In this case, the performance is still improved slightly.

In Fig. 4.6, X is fixed to 100 mW with $\alpha = 0.75$, and we compare the throughput performances under these three schemes. The EC-ST scheme still achieves the optimal performance. It is noted that the performance of the EC-ST scheme coincides with that of the practical Tx ST scheme from $H = 15$ dB to $H = 25$ dB which is inside the no energy cooperation region of the EC-ST scheme, as shown in Fig. 4.4. Outside this region, the EC-ST scheme outperforms by applying energy cooperation. Furthermore, the idealistic Tx ST scheme is consistently the worst performer.

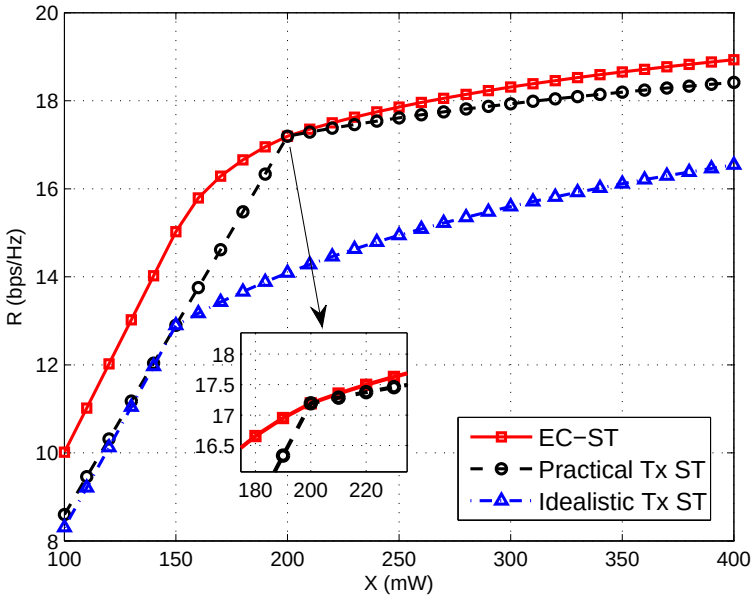

Figure 4.5: Normalized throughput in AWGN channels as a function of the energy arrival rate X, with $\alpha = 0.75$ and $H = 60$ dB.

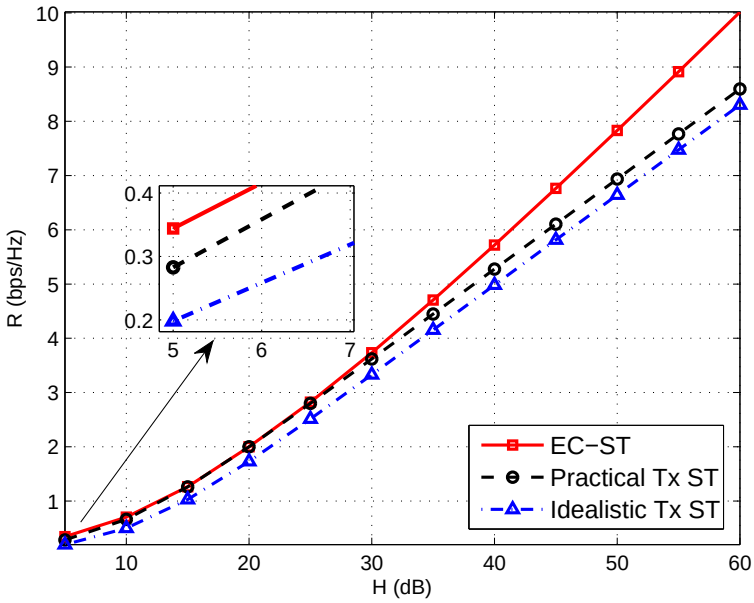

Figure 4.6: Normalized throughput in AWGN channels as a function of the normalized channel power gain H, with $\alpha = 0.75$ and $X = 100$ mW.

4.4.2 Simulation Results for the Rayleigh Channel Case

In Rayleigh block fading channel condition, the target communications rate for this system $\bar{R}$ is set to 1 bps/Hz, and energy transfer efficiency $\alpha = 0.75$. The optimal

energy cooperation power P_{rt} and P_{tr} are derived based on the different statistical characteristics of the random variables X and H according to the method in Section 4.4.2 (we use shape parameter $k = 1$ for the Gamma-distributed X in the simulation). Then the simulation are conducted by generating a large number of samples of X and H, and then examining the outage of the system.

Fig. 4.7 depicts how outage probability varies with ρ under the EC-ST, practical Tx ST, and idealistic Tx ST schemes. The means of the Gamma-distributed random variable X and the exponentially distributed H are $\lambda_X = 100$ mW, $\lambda_H = 30$ dB respectively. The optimal active-ratio ρ^* for these three schemes are approximately located from 20% to 30%. The idealistic Tx ST scheme leads to the larger outage probability than the others. When ρ exceeds 50%, the outage probabilities of the practical Tx ST and idealistic Tx ST schemes become extremely close, because the outage events for these two schemes are essentially the circuit outage at the receiver in this case, which depends on the same P_{rc} and λ_X. In addition, the EC-ST scheme achieves a lower optimal P_{out} than the other two schemes at $\rho^* \approx 22\%$. When $\rho > 50\%$, the EC-ST scheme can also reduce the outage probability by transferring energy from the transmitter to the receiver and prevent outage event at the receiver.

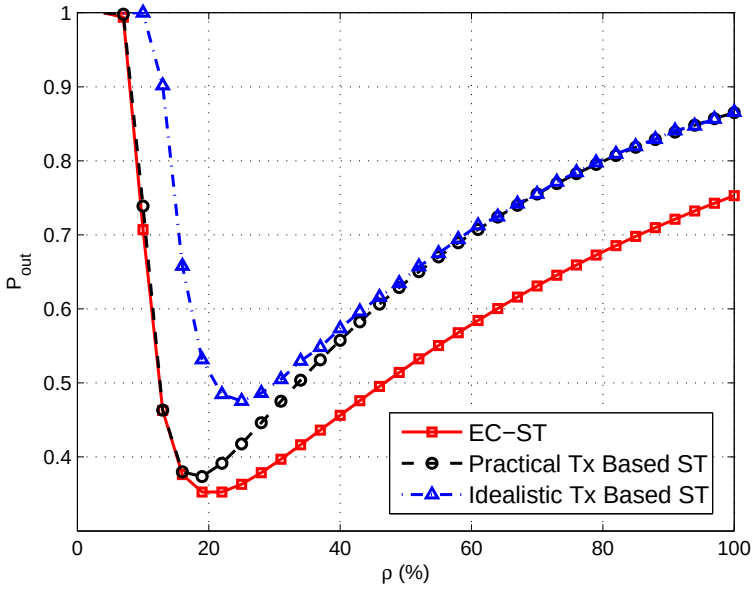

Figure 4.7: Outage probability in Rayleigh channels as a function of ρ.

Figs. 4.8 and 4.9 illustrate the outage performances with varying λ_X and λ_H respectively, under the EC-ST, practical Tx ST, and idealistic Tx ST schemes. In

Fig. 4.8, λ_H is fixed to 60 dB, we can further verify the performance improvement of the EC-ST scheme over the other two schemes. For the idealistic Tx ST scheme in this case, the outage probability begins to reduce more slowly at $\lambda_X = 150$ mW, with respect to the increasing λ_X. This transition point results from the more frequent circuit outage event at the transmitter due to the insufficiency of energy. In Fig. 4.9, the relative performance of the three schemes follows the same order as in previous figures. The overlapping part of the EC-ST scheme and the practical Tx ST scheme for $10 < \lambda_H < 20$ dB indicates that energy cooperation is ineffective ($P_{tr} = P_{rt} = 0$) under this condition. Similar to the result of Fig. 4.4, it is implied that the range of $10 < \lambda_H < 20$ dB is located in the no energy cooperation region in the Rayleigh block fading channel scenario.

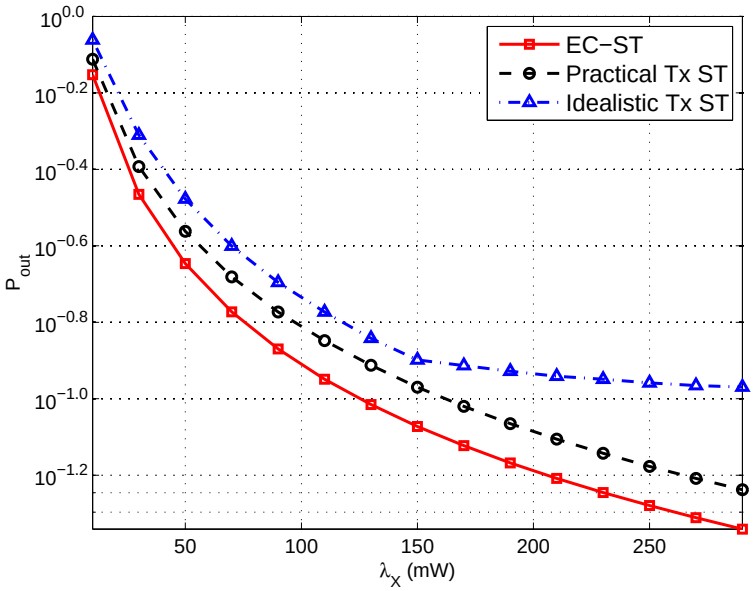

Figure 4.8: Outage probability in Rayleigh channels as a function of λ_X.

4.5 Summary

In this chapter, an energy cooperation save and transmit scheme has been designed to optimize the point-to-point wireless communication between a practical energy harvesting transmitter and receiver. The optimal normalized throughput and outage probability are analyzed respectively in additive white Gaussian noise and Rayleigh block fading channels. From the numerical and simulation results, we can see that, with a limited amount of energy, the communications performance does not only

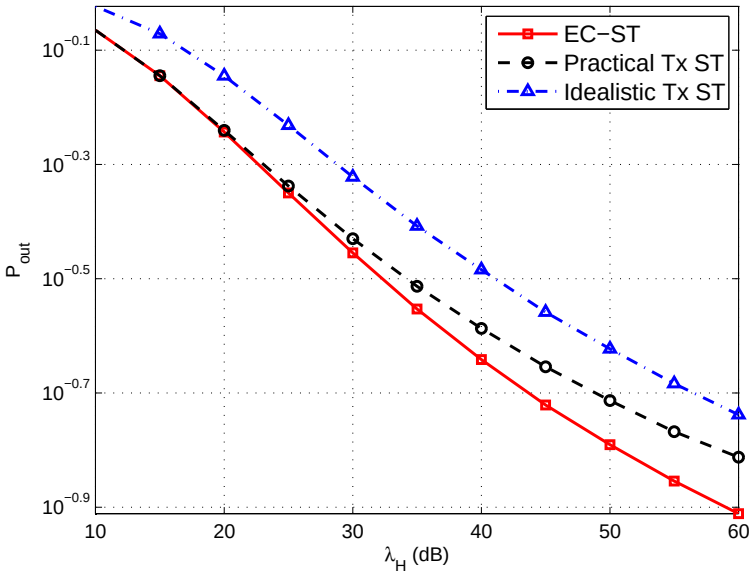

Figure 4.9: Outage probability in Rayleigh channels as a function of λ_H.

depend on the transmission power, but also the active communications intervals of the transmitter and receiver. One effective method for improving the communications performance between practical energy harvesting devices is to allow the energy flow between the devices, and then find an optimal tradeoff between the transmission power and the active communications intervals.

Chapter 5

Conclusions & Future Work

5.1 Conclusions

This thesis focuses on the practical implementation issues of the massive MIMO and energy harvesting systems, aiming to obtain high spectral efficiency and energy efficiency performance. To reduce the implementation cost of the massive MIMO systems, the hybrid processing structure has been utilized in both single-user and multiple-user scenarios. In the single-user scenario, the hybrid RF and baseband precoder/combiner are designed by directly decomposing the pre-designed digital precoder/combiner of a large dimension which is enabled by the the alternating optimization technique. The performance of the MD-HP scheme has been shown to be near-optimal compared to the SVD based full-complexity processing.

In the multiple-user scenario, a low-complexity Hy-BD scheme has been developed for the downlink communication of a massive MU-MIMO system. We aim to harvest the large array gain through the phase-only RF precoding and combining and then BD processing is performed on the equivalent baseband channel. It has been demonstrated that the Hy-BD scheme, with a lower implementation and computational complexity, achieves a capacity performance approaching that of the traditional high-dimensional baseband BD processing.

To achieve the goal of improving energy efficiency, we propose the energy cooperation assisted energy harvesting communication between the practical transmitter and receiver, whose hardware circuits consume non-zero power when active. The EC-ST scheme optimizes the active time ratio and energy cooperation power for the maximum throughput under additive white Gaussian channels and the minimum outage

probability under block Rayleigh fading channels. It has been shown that one effective method for improving the communications performance between energy harvesting devices is to allow the energy flow between the devices, and then find an optimal tradeoff between the transmission power and the active time ratio.

5.2 Future Work

We believe the hybrid processing structure will lead the main trend of the massive MIMO communications in the future 5G wireless communication system due to its satisfying performance as well as the relatively low hardware complexity. In this thesis, the hybrid processing schemes are based on the perfect CSI assumption while CSI can only be acquired by channel estimation. In the massive MIMO scenario, the computation complexity of estimating the channel matrix is very high since the dimension of the channel matrix is going to be large. The future work on hybrid processing will focus on the massive MIMO channel estimation with the hybrid processing structure implemented on all ends, and design a training and an estimation method with low overhead and low computation complexity for practical implementation.

Besides, the energy cooperation based energy harvesting wireless communication between the practical transmitter and receiver is now only considered in the P2P scenario. As an extension to the current P2P setting, the harvested energy may be allowed to flow among many devices in a network to increase the overall network throughput by adjusting the active-ratio and transmit power of each device. This can also be the future work of this thesis.

Bibliography

[1] J. G. Andrews, S. Buzzi, C. Wan, S. V. Hanly, A. Lozano, A. C. K. Soong, and J. C. Zhang, "What Will 5G Be," *IEEE Journal on Selected Areas in Commun.*, vol. 32, pp. 1065–1082, June 2014.

[2] T. L. Marzetta, "Noncooperative cellular wireless with unlimited numbers of base station antennas," *IEEE Trans. on Wireless Commun.*, vol. 9, pp. 3590–3600, Nov. 2010.

[3] F. Rusek, D. Persson, B. K. Lau, E. G. Larsson, T. L. Marzetta, O. Edfors, and F. Tufvesson, "Scaling up MIMO: Opportunities and challenges with very large arrays," *IEEE Sig. Process. Mag.*, vol. 30, pp. 4060, Jan. 2013.

[4] E. G. Larsson, O. Edfors, F. Tufvesson, and T. L. Marzetta, "Massive MIMO for next generation wireless systems," *IEEE Commun. Mag.*, pp. 186195, vol. 52, no. 2, Feb. 2014.

[5] U. Erez, S. Shamai and R. Zamir, "Capacity and lattice strategies for canceling known interference," *IEEE Trans. on Info. Theory*, vol. 51, pp. 3820–3833, Nov. 2005.

[6] H. Q. Ngo, E. G. Larsson and T. L. Marzetta, "Energy and Spectral Efficiency of Very Large Multiuser MIMO Systems," *IEEE Trans. on Commun.*, vol. 61, pp. 1436–1449, Apr. 2013.

[7] P. J. Smith, C. Neil, M. Shafi and P. A. Dmochowski, "On the convergence of massive MIMO systems," in *Proc. IEEE Intl. Conf. on Commun. (ICC)*, pp. 5191–5196, June 2014.

[8] L. Liang, W. Xu and X. Dong, "Low-Complexity Hybrid Precoding in Massive Multiuser MIMO Systems," in *arXiv:1410.3947*, Oct. 2014.

[9] X. Zhang, A. F. Molisch, and S. Y. Kung, "Variable-phase-shift-based RF-baseband codesign for MIMO antenna selection," *IEEE Trans. on Sig. Process.*, vol. 53, pp. 40914103, Nov. 2005.

[10] D. J. Love and R. W. Heath, "Equal gain transmission in multiple-input multiple-output wireless systems," *IEEE Trans. on Commun.*, vol. 51, pp. 11021110, July 2003.

[11] X. Zheng, Y. Xie, J. Li, and P. Stoica, "MIMO transmit beamforming under uniform elemental power constraint," *IEEE Trans. on Sig. Process.*, vol. 55, pp. 53955406, Nov. 2007.

[12] A. Liu, and V. Lau, "Phase only RF precoding for massive MIMO systems with limited RF chains," *IEEE Trans. on Sig. Process.*, vol. 62, pp. 4505–4515, Sept. 2014.

[13] O. E. Ayach, R. W. Heath, S. Abu-Surra, S. Rajagopal and Z. Pi, "The capacity optimality of beam steering in large millimeter wave MIMO systems," in *Proc. IEEE 13th Intl. Workshop on Sig. Process. Advances in Wireless Commun. (SPAWC)*, pp. 100–104, June 2012.

[14] O. E. Ayach, S. Rajagopal, S. Abu-Surra, Z. Pi and R. W. Heath, "Spatially sparse precoding in millimeter wave MIMO systems," *IEEE Trans. on Wireless Commun.*, vol. 13, pp. 14991513, Mar. 2014.

[15] C. Kim, T. Kim and J.-Y. Seol, "Multi-beam transmission diversity with hybrid beamforming for MIMO-OFDM systems," *IEEE Globecom Workshops*, pp. 61-65, Dec. 2013.

[16] A. Sayeed and J. Brady, "Beamspace MIMO for high-dimensional multiuser communication at millimeter-wave frequencies," in *Proc. IEEE Global Commun. Conf. (GLOBECOM)*, pp. 3679–3684, Dec. 2013.

[17] R. A. Stirling-Gallacher and Md. S. Rahman, "Linear MU-MIMO pre-coding algorithms for a millimeter wave communication system using hybrid beamforming," in *Proc. IEEE Intl. Conf. on Commun. (ICC)*, pp. 5449–5454, June 2014.

[18] A. J. Duly, T. Kim, D. J. Love and J. V. Krogmeier, "Closed-Loop beam alignment for massive MIMO channel estimation," *IEEE Commun. Letters*, vol. 18, pp. 1439–1442, Aug. 2014.

[19] S. L. H. Nguyen and A. Ghrayeb, "Compressive sensing-based channel estimation for massive multiuser MIMO systems," in *Proc. IEEE Wireless Commun. and Network. Conf. (WCNC)*, pp. 2890-2895, Apr. 2013.

[20] D. Ramasamy, S. Venkateswaran and U. Madhow, "Compressive adaptation of large steerable arrays," in *Proc. Info. Theory and App. Workshop (ITA)*, pp. 234–239, Feb. 2012.

[21] A. Alkhateeb, O. E. Ayach, G. Leus and R. W. Heath, "Channel estimation and hybrid precoding for millimeter wave cellular systems," *IEEE Journal of Selected Topics in Sig. Process.*, vol. 8, pp. 831–846, Oct. 2014.

[22] Q. H. Spencer, B. D. Jeffs, M. A. Jensen and A. L. Swindlehurst, "Modeling the statistical time and angle of arrival characteristics of an indoor multipath channel," *IEEE Journal on Selected Areas in Commun.*, vol. 18, pp. 347–360, Mar. 2000.

[23] R. Escalante and M. Raydan, "Alternating projection methods", *Society for Industrial and Applied Mathematics*, vol. 8, 2011.

[24] H. Kim and H. Park, "Nonnegative Matrix Factorization Based on Alternating Nonnegativity Constrained Least Squares and Active Set Method", *Society for Industrial and Applied Mathematics*, vol. 30, July 2008.

[25] S. Boyd and L. Vandenberghe, "*Convex optimization*," Cambridge University Press, 2004.

[26] T. Kailath, A. H Sayed and B. Hassibi, *Linear estimation*, Prentice Hall, vol. 1, 2000.

[27] D. Tse and P. Viswanath, "*Fundamentals of wireless communication*," Cambridge University Press, May 2005.

[28] Q. H. Spencer, A. L. Swindlehurst, and M. Haardt, "Zero-forcing methods for downlink spatial multiplexing in multiuser MIMO channels," *IEEE Trans. on Sig. Process.*, vol. 52, pp. 461–471, Feb. 2004.

[29] S. Priya and D. J. Inman, *Energy harvesting technologies*, New York, USA: Springer Science+Business Media, 2009.

[30] T. J. Kazmierski and S. Beeby, *Energy harvesting systems*, New York, USA: Springer Science+Business Media, 2011.

[31] O. Ozel and S. Ulukus, "Information-theoretic analysis of an energy harvesting communication system," *IEEE 21st Intl. Symp. PIMRC Workshop*, pp. 330–3335, Sept. 2010.

[32] C. Huang, R. Zhang and S. Cui, "Optimal power allocation for outage probability minimization in fading channels with energy harvesting constraints," *IEEE Trans. Wireless Communications*, vol. 13, pp. 1074–1087, Feb. 2014.

[33] C. K. Ho and R. Zhang, "Optimal energy allocation for wireless communications with energy harvesting constraints," *IEEE Trans. Signal Processing*, pp. 4808–4818, Sept. 2012.

[34] L. R. Varshney, "Transporting information and energy simultaneously," *IEEE Intl. Symp. ISIT*, pp. 1612–1616, July 2008.

[35] L. Liu, R. Zhang and K. C. Chua, "Wireless information and power transfer: a dynamic power splitting approach," *IEEE Trans. Communications*, pp. 3990–4001, July 2013.

[36] L. Liu, R. Zhang and K. C. Chua, "Wireless information transfer with opportunistic energy harvesting," *IEEE Trans. Wireless Communications*, pp. 288–300, Jan. 2013.

[37] R. Zhang and K. C. Chua, "MIMO broadcasting for simultaneous wireless information and power transfer," *IEEE Trans. Wireless Communications*, pp. 1989–2001, Mar. 2013.

[38] S. Lee, R. Zhang, and K. Huang, "Opportunistic wireless energy harvesting in cognitive radio networks," *IEEE Trans. Wireless Communications*, pp. 4788–4799, Sept. 2013.

[39] A. Nasir, X. Zhou and S. Durrani, "Relaying protocols for wireless energy harvesting and information processing," *IEEE Trans. Wireless Communications*, pp. 3622–3636, July 2013.

[40] Z. Ding, S. Perlaza, I. Esnaola and H. V. Poor, "Power allocation strategies in energy harvesting wireless cooperative networks," *IEEE Trans. Wireless Communications*, pp. 846–860, Jan. 2014.

[41] V. Liu, A. Parks, V. Talla, S. Gollakota, D. Wetherall and J. R. Smith, "Ambient backscatter: wireless communication out of thin air," in *Proc. of the ACM SIGCOMM*, pp. 39–50, Oct. 2013.

[42] J. R. Smith, A. P. Sample, P. S. Powledge, A. Mamishev and S. Roy, "A wirelessly-powered platform for sensing and computation," in *UbiComp, Lecture Notes in Computer Science*, vol. 4206, pp. 495–506, 2006.

[43] H. Nishimoto, Y. Kawahara and T. Asami, "Prototype implementation of ambient RF energy harvesting wireless sensor networks," *Sensors, IEEE*, pp. 1282–1287, Nov. 2010.

[44] W. C. Brown, "The history of power transmission by radio waves," *IEEE Trans. Microwave Theory and Techniques*, pp. 1230–1242, Sept. 1984.

[45] B. Gurakan, O. Ozel, J. Yang and S. Ulukus, "Two-way and multiple-access energy harvesting systems with energy cooperation," in *Conference Record of the 46th ASILOMAR*, pp. 58–62, 2012.

[46] B. Gurakan, O. Ozel, J. Yang and S. Ulukus, "Energy cooperation in energy harvesting communications," *IEEE Trans. on Communications*, pp. 4884–4898, Dec. 2013.

[47] K. Ishibashi, H. Ochiai and V. Tarokh, "Energy harvesting cooperative communications," *IEEE 23rd Intl. Symp. PIMRC*, pp. 1819–1823, 2012.

[48] H. Ju and R. Zhang, "Throughput maximization in wireless powered communication networks," *IEEE Trans. Wireless Communications*, vol. 13, pp. 418–428, Jan. 2014.

[49] K. Tutuncuoglu and A. Yener, "Multiple access and two-way channels with energy harvesting and bi-directional energy cooperation," in *Information Theory and Applications Workshop (ITA)*, pp. 1–8, 2013.

[50] J. Xu and R. Zhang, "CoMP meets smart grid: a new communication and energy cooperation paradigm," *IEEE Trans. Vehicular Tech.*, Aug. 2014.

[51] Y. K. Chia, S. Sun and R. Zhang, "Energy cooperation in cellular networks with renewable powered base stations," *IEEE Trans. on Wireless Communications*, Aug. 2014.

[52] J. Xu and R. Zhang, "Throughput optimal policies for energy harvesting wireless transmitters with non-ideal circuit power," *IEEE J. Sel. Areas Commun.*, vol. 32, pp. 322–332, Feb. 2014.

[53] S. Luo, R. Zhang and T. J. Lim, "Optimal save-then-transmit protocol for energy harvesting wireless transmitters," *IEEE Trans. Wireless Communications*, pp. 1196–1207, Mar. 2013.

[54] S. Yin, E. Zhang, J. Li, L. Yin and S. Li, "Throughput optimization for self-powered wireless communications with variable energy harvesting rate,", in *Proc. of IEEE WCNC: MAC*, pp. 830–835, Apr. 2013.

[55] 2.4 GHZ ZIGBEE RF TRANSCEIVER CC2520 DATASHEET, [Online]. Available: "http://www.ti.com/lit/ds/symlink/cc2520.pdf."

[56] R. M. Corless, G. H. Gonnet, D. E. G. Hare, D. J. Jeffrey and D. E. Knuth, "On the lambert w function," in *Advances in Computational Mathematics*, pp. 329–359, 1996.

[57] J. Garnica, R. A. Chinga and J. Lin, "Wireless power transmission: from far field to near field," in *Proceedings of the IEEE*, pp. 1321–1331, Apr. 2013.

[58] W. Ni and X. Dong, "Near-Optimal Hybrid Processing for Massive MIMO Systems via Matrix Decomposition." *arXiv:1504.03777.*

[59] W. Ni and X. Dong, "Hybrid Block Diagonalization for Massive Multiuser MIMO Systems." *arXiv:1504.02081.*

[60] W. Ni and X. Dong, "Energy Harvesting Wireless Communications with Energy Cooperation between Transmitter and Receiver," *IEEE Trans. on Commun.*, vol. 63, pp. 1457–1469, Feb. 2015.